Technische Universität Braunschweig
Leichtweiß-Institut für Wasserbau
Abteilung Hydromechanik und Küsteningenieurwesen
Prof. Dr.-Ing. Hocine Oumeraci

Applying Laser Ranging for the Monitoring of Water Waves in the new Deltares Delta Flume Facility

Maximilian Streicher, B.Sc.
Matrikelnummer 2963532

Prüfer:
Prof. Dr.-Ing. H. Oumeraci

Betreut durch:
Dr. Bas Hofland (Deltares)
Dr. Roderik Lindenbergh (TU Delft)
Dr.-Ing. A. Kortenhaus (TU Braunschweig)

Braunschweig, April 2013

ACKNOWLEDGEMENT

During the master thesis project I have been supported by many people and I would like to use the opportunity to thank them all.

It was a great challenge and pleasure to work at Deltares company, department for hydraulic engineering and to be supported by the expertise of Dr. Bas Hofland at any time. I also want to thank Rob Hoffmann, Paul Meys and Bas Blok for their technical support.

I appreciated the close cooperation with TU Delft and especially with the institute for optical and laser remote sensing. Here, I would like to thank Dr. Roderik Lindenbergh for his professional support.

Many thanks to Wim Uijttewaal for providing the TU Delft wave flume facility to conduct experiments. It was a great help to have Sander de Vrede and Jaap van Duin providing their technical support during experiments. In this context I also want to thank Raoul Panday and Henk Wijengaard from SICK company for providing the TLS device and sharing their knowledge. When conducting the experiments the help from Manuel Diaz and Jinhu Wang was highly appreciated.

Provided by data sets from earlier TLS based measurements of water waves, I was able to analyze different set-ups and TLS devices. Thanks to Bas Hofland, Roderik Lindenbergh, Gerben Ruessink, Chris Blenkinsopp and Dan Howe for sharing their work.

I would like to thank the LWI Braunschweig and the department for hydrodynamics under the leadership of Prof. Oumeraci. I have been supported in every step during the project. Especially I would like to thank Dr. Andreas Kortenhaus for the scientific and Mike Lieske for the organizational support.

Since it was a new experience for me to live in the Netherlands I am very happy to have met a number of friends and good willing people. Especially I would like to thank Dorothea Kaste and Andreas Burzel for their support in the new situation.

Last but not least I would like to thank my family and closest friends, because they would always be there.

ABSTRACT

The need of protection against flooding is a crucial issue in the Netherlands and other low lying countries in the world. Floods may be induced by storm surges over the North Sea which then result in both high water levels and large waves loading the coastal defense structures. To test the impact of waves on different coastal defense structures and materials, Deltares operates the Delta Flume facility, which is one of the largest wave flume facilities in the world. Currently a new Delta Flume (length = 230 m, width = 5 m, depth = 9 m) is constructed in Delft. Hydraulic experiments near to full scale conditions can be conducted and waves with significant heights of $H_s = 2$ are generated.

Together with the new facility, a modernized measurement/monitoring equipment will be installed. One of the potential sensor techniques is Terrestrial Laser Scanner (TLS) based range measurements of water waves. A TLS device emits laser pulses in short time intervals. These energy pulses are reflected by the target surface, recorded by the device and a range calculation based on the travel time is carried out. TLS based range measurements are considered a very fast and accurate method (for solid surfaces), providing a temporal and spatial continuous profile measurement. The post processing is kept very simple compared to related methods, e.g. stereo image photogrammetry. The wave parameters (Height, Period, Length) are extracted, as well as wave breaking, wave run-up and swash zone characteristics analyzed. TLS based range measurements have been adapted to hydraulic modeling in the green water of a small wave flume by Allis et al. (2011) and Blenkinsopp et al. (2012).

Relevant parameters influencing TLS based range measurements from water waves are the TLS parameters (e.g. scanning frequency, spectral resolution, receiver resolution, measurement principle, laser power), the geometry/atmosphere parameters (e.g. height above water surface, incidence angle, footprint size, influence of rain and light) and the water parameters (e.g. turbidity, surface roughness, wave steepness). In this study the influencing parameters are investigated, to explore possibilities of applying TLS based range measurements of water wave in the new Delta Flume facility.

Data sets obtained with a Faro, SICK and Riegl TLS device are analyzed with the purpose of wave field reconstruction and quality assessment of the results. Afterwards preliminary experiments with a SICK TLS device are conducted in the small wave flume facility of the TU Delft. Processing of the data gives insight in the possibilities and expected problems of the new measurement method. It reveals which filtering, averaging and correction steps are necessary to reconstruct a wave field from the obtained data. Also, accuracy issues (e.g. the simultaneous movement of waves and laser beam will introduce an error to the measurements) are researched in this study.

Finally, the gained knowledge is transferred to the Delta Flume facility and an optimized TLS based measurement set-up from water waves for future experiments is proposed.

Keywords: TLS, Delta Flume, Wave Measurement Device

TABLE OF CONTENTS

LIST OF SYMBOLS

c = Wave celerity [m/s]

D_{50} = Grain size [mm]

H_s = Significant wave height [m]

H_{m0} = Spectral wave height [m]

h = Water depth [m]

L = Water wave wavelength [m]

L_0 = Deep water wave wavelength [m]

T = Wave period [s]

α = Incidence angle [°]

β = Total horizontal error due to parallel movement of wave and TLS [m]

λ = Laser beam wavelength [nm]

ξ_0 = Surf similarity parameter [-]

ρ = Density [kg/m³]

σ = Range standard deviation [m]

LIST OF ABBREVIATIONS

ALS	Airborne Laser Scanning
AM	Amplitude Modulation
CW	Continuous Wave
DSM	Digital Surface Model
DEM	Digital Elevation Model
DTM	Digital Terrain Mapping
EMR	Electro Magnetic Radiation
FFT	Fast Fourier Transformation
FM	Frequency Modulation
FOV	Field of View
IR	Infrared
LASER	Light Amplification by Stimulated Emission of Radiation
LIDAR	Light Detection and Ranging
LIF	Laser Induced Fluorescence
LWG	LiDAR Wave Gauge
MWL	Mean Water Level
NASA	National Aeronautics and Space Administration
NTU	Nephelometric Turbidity Units
PIV	Particle Image Velocimetry
PS	Phase- Shift
RADAR	Radio Detection and Ranging
SHOALS	Scanning Hydrographic Operational Airborne LiDAR Survey
SNR	Signal to Noise Ratio
TLS	Terrestrial Laser Scanner
TOF	Time- of- Flight
USACE	US Army Corps of Engineers

LIST OF FIGURES

LIST OF TABLES

1 Introduction

The need of protection against flooding is a crucial issue in the Netherlands and other low lying countries in the world. Floods may be induced by storm surges over the North Sea which then result in both high water levels and large waves loading the coastal defense structures. To test the impact of waves on different coastal defense structures and materials, Deltares operates the Delta Flume facility. This is one of the largest wave flume facilities in the world. Hydraulic experiments near to full scale conditions can be conducted and waves with significant heights up to 2.2 m and periods up to 12 s can be generated. Currently a new Delta Flume (length =230 m, width = 5 m, depth = 9 m) is constructed in Delft. Together with the new facility, a modernized measurement/monitoring equipment will be installed. One of the potential sensor techniques is Terrestrial Laser Scanner (TLS) based range measurements of water waves. A TLS device emits laser pulses during short time intervals. These energy pulses are reflected by the target surface, recorded by the TLS device and a range calculation based on the travel time is carried out.

Compared to conventional laboratory wave measurement devices (e.g. resistance wave probes), TLS based range measurements are considered nonintrusive 1D measurements. Nonintrusive means that there is no disturbance of the wave due to physical penetration of the water. Instead of a measurement at a single point, a whole profile measurement is possible, resulting in a temporally and spatially continuous signal of the water surface. TLS based range measurements for solid surfaces are considered to be a very fast and accurate method. The post processing is kept very simple compared to related methods, e.g. stereo image photogrammetry. The wave parameters, height, length and period are extracted as well as wave breaking and swash characteristics analyzed. The obtained profiles could also serve for the validation of numerical models.

1.1 Key Objectives and Research Questions

The ultimate goal is the application of TLS based range measurements to water waves conditions. The application will result in a totally new sensor device technology in hydraulic modeling. However, considering the optimum configuration of TLS, water and geometrical set-up parameters, still some unresolved questions remain.

The main objective of this work is to explore possibilities to apply TLS based range measurements of water waves in the new Delta Flume facility.

More specifically, the following research questions can be formulated:

(1) What are the parameters that influence TLS based range measurements of waves?
(2) How is it possible to extract the necessary information from the obtained signal to finally derive a wave field reconstruction? What are the problems and which steps for filtering, correction, averaging and interpolation are necessary?
(3) What are the accuracies in wave measurements using a TLS device?
(4) How does an optimized measurement set-up for the new Delta Flume facility look like?

1.2 Methodology and Outline

This section provides an overview of how the thesis is structured to finally answer the research questions formulated in section 1.1. A summary of the methodology is given in Fig. 1. First, a literature study is conducted to understand water sensor devices, wave properties, the TLS mechanism and the reflection characteristics of waves (section 2). Also, results from earlier experiments with TLS devices are included. All findings are collected in the parameter inventory (section 2.7). There, all parameters which have an influence on TLS based range measurements of water waves are summarized. Available data sets obtained with Faro, SICK and Riegl TLS devices from the run-up zone and green water area are analyzed with the purpose of wave field reconstruction and quality assessment of the results. Processing of the data gives insight in the possibilities and expected problems of the new method. A most suitable TLS device and its set-up, as well as the required water parameters are determined (section 3.1).

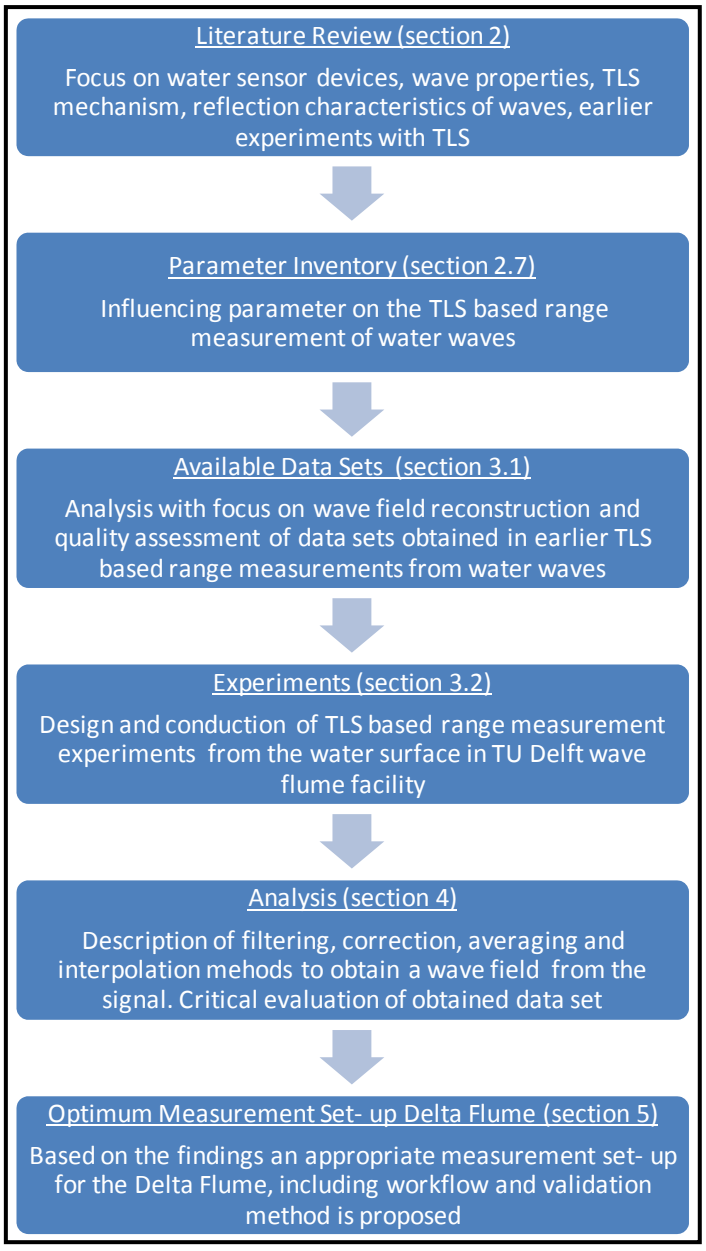

Fig. 1: Methodology flow chart for the work

Preliminary experiments are conducted in the small-scale wave flume facility of the TU Delft. The purpose is to get a working TLS based measurement set-up for water waves. This set-up can be adapted to the large dimensions of the Delta Flume facility. The configuration and set-up of the experiment is based on the results from parameter inventory and the analysis of available data sets (section 3.2).

The problems of reconstructing a wave field from the signal as well as the necessary filtering, correction, averaging and interpolation steps are described. This is followed by a critical evaluation of the results (section 4).

Finally, all the gained knowledge is transferred to the new Delta Flume facility and an optimized TLS based measurement set-up for future experiments is proposed. Additionally a possible workflow and validation methods are described (section 5).

2 Theoretical Background

In this section available knowledge about water sensor devices, wave properties, the TLS mechanism and the reflection characteristics of waves is presented. Also, results from earlier experiments with TLS devices are included. In detail, the Delta Flume facility operated by Deltares is described in section 2.1. Hydrodynamic parameters, such as wave height, period, celerity and wave breaking are introduced in section 2.2. Turbidity and the presence of foam on the surface, influencing the water characteristics are presented in section 2.3. Available knowledge about the background of existing water sensor devices is presented in section 2.4. A more detailed description about the principles of LASERs and especially about Terrestrial Laser Scanner (TLS) based range measurements is given in section 2.5. Existing knowledge about the application of TLS devices to water wave measurements is given in section 2.6. The gained knowledge about influencing parameters on TLS based range measurements from water waves is summarized in the parameter inventory (section 2.7).

2.1 Delta Flume

The Delta Flume is an experimental test facility for coastal engineering purpose, where physical models near to the prototype scale are tested under wave conditions. The flume is crucial for the physical modeling of coastal structures and the assessment of its safety against major wave attack, storm surges and flooding for the Netherlands.

The old Delta Flume (Fig. 2) is placed in the Nordoostpolder, approximately 200 km away from the Deltares headquarter in Delft.

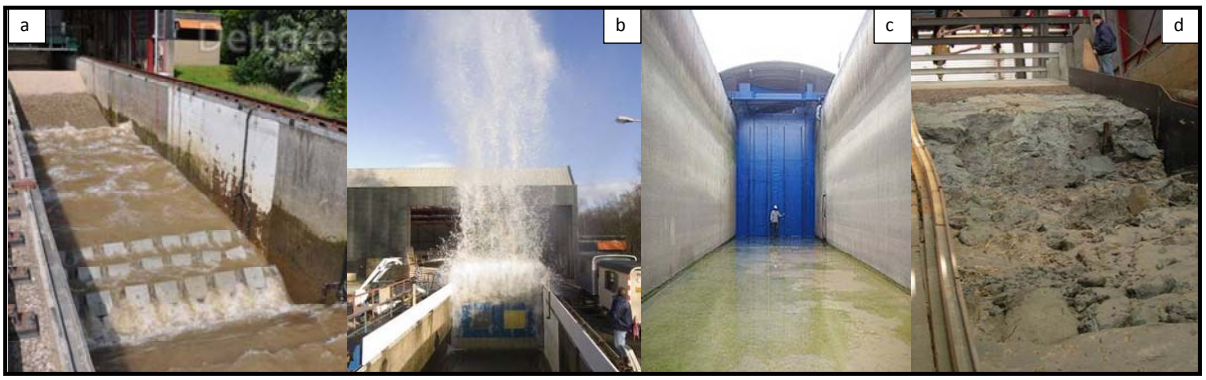

Fig. 2: a.Dike revetment with concrete blocks, b.Wave impact on a vertical wall, c.Wave paddle in empty flume, d.Dune after erosion test

It has a length of 240 m, a width of 5 m and a depth of 7 m. Maximum regular waves with a height of H_{max} = 3.1 m and periods between 1 s and 12 s are generated. Irregular waves with a significant wave height of H_s = 1.6m can be generated. It contains a reflection compensation mechanism at the wave paddle, to minimize the influence of re- reflecting waves. The flume parameters are compared to the new Delta Flume parameters, currently under construction on the Deltares ground (Delft) in Fig. 3.

The new Delta Flume (Fig. 3) is 9.5 m deep on the first 183 m, followed by a 7 m deep and 75 m long section. The width is 5 m and the same compared to the old Delta Flume. The maximum wave height is H_{max} = 4.1 m and the maximum significant wave height H_s = 2 m. The

flume is optimized for the spectral wave height H_{m0} = 2.2 m, according water depth h = 6.9 m and wave period T_p = 9.4 s. Additionally the filling discharge is ten times higher compared to the old Delta Flume, allowing for a fast watering of the test facility. Since it is placed in Delft it will be easily accessible for the researchers at Deltares. It is the aim to equip the flume with the most advanced water sensor devices. Additionally the new flume will be equipped with a measurement vehicle and an installation crane installed on tracks at the side of the Delta Flume. Hence, easy measurement and installation of the physical models is possible. The estimated opening is in November 2013.

	Old Flume	New Flume
Total Depth	7m	9.5m
Length	220m	258m
Width	5m	5M
Max. Hs	1.5m	2m
Max. H	3.1m	4.1m
Filling discharge	0.1m³/s	1m³/s

Comparison old and new Deltaflume

Picture taken: 13.01.2013

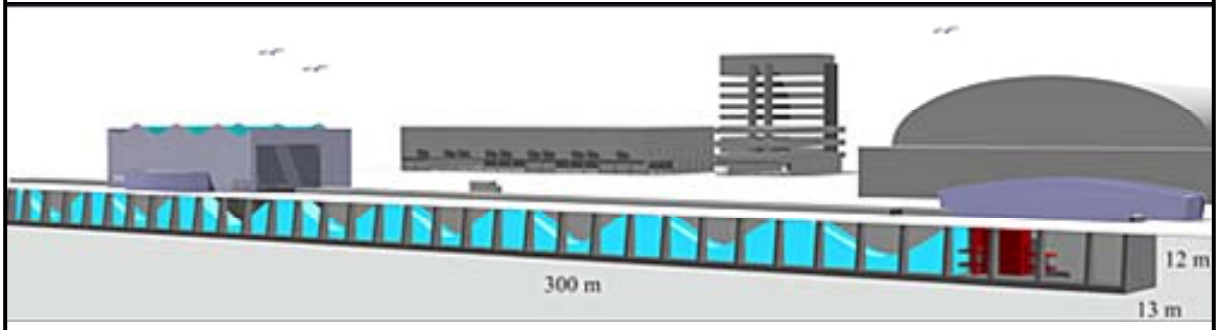

New Deltaflume

Fig. 3: New Delta Flume currently under construction and comparison with old Delta Flume

2.2 Water Wave Characteristics

In this section the characteristics of water waves are presented. For simplification the term water waves substitutes the physical correct term water surface elevation in this thesis.

First the wave characteristics, such as height, period and celerity are discussed. An introduction to wave breaking characteristics follows.

2.2.1 Wave Height

The height of a wave H is defined as the distance between the lowest point in the wave trough to the topmost point at the wave crest.

Most of the waves in the sea are wind generated. When wind is arising small ripples and capillary waves (with heights of a few centimeters) are formed on the surface. The water particles are accelerated by wind induced shear stress. Regarding fully developed waves a wind field with a certain fetch length, which is the length along which the water particles experience shear stress, and a certain wind speed need to be present.

There are many possibilities to calculate a wave height from a single point measurement (section 2.4.). Time based $H_{1/3}$ and frequency based calculation of the wave height H_{m0} are distinguished (EAK (2002)).

The parameter $H_{1/3}$ is derived from the time based examination of the wave height signal. The average value of the 33.3% highest waves in this specific time interval is calculated.

$$H_{1/3} = \frac{\sum 33.3\% \text{ highest wave heights}}{\text{number of waves}} \qquad [1]$$

$H_{1/3}$ corresponds to the significant wave height H_s.

The spectral wave height H_{m0} is derived from a frequency based examination of the single point wave height measurement (section 2.4.2). After frequency analysis (Fourier Analysis) of the measured time series a possible frequency spectrum is generated and a spectral energy distribution is calculated. The area underneath the spectral energy distribution function is the total energy of the wave field m_0, the zero order moment of the spectrum as described by Bendat (1986). H_{m0} approximately corresponds to $H_{1/3}$ in deep water conditions and is defined as:

$$H_{m0} = 4\sqrt{m_0} \approx H_{1/3} \qquad [2]$$

Although there is a theoretically difference between $H_{1/3}$ and H_{m0} it is common practice in engineering to assume that $H_{1/3} = H_{m0} = H_s$ (EAK (2002)).

The root mean square wave height H_{rms} is derived with:

$$H_{rms} = \sqrt{\frac{\sum_{i}^{n} H_i^2}{n}} \quad [3]$$

Where;

H_i = Wave height [m]

n = Number of waves [-].

2.2.2 Wave Period

The according wave periods $T_{1/3}$ and Tm are derived from a measured wave signal (EAK (2002)). The time based wave period $T_{1/3}$ is the sum of the 33.3% wave periods which belong to the 33.3% peak values of $H_{1/3}$, divided by the number of waves.

$$T_{1/3} = \frac{\sum T(H>H_{1/3})}{N/3} \quad [4]$$

Where,

$H_{1/3}$ = 33.3% of highest waves.

An example of a frequency based wave period is T_m (or T_{01}). This is derived with help of the zero and first order moment of the spectral energy distribution m_0 and m1.

$$T_m = \frac{m_0}{m_1} \quad [5]$$

Where;

m_n = n_{th} moment of spectral energy spectrum [m²]

S(f) = Spectral energy density function [m²s]

Δf_i = f_2-f_1 [1/s].

2.2.3 Wave Celerity

Wave celerity describes the movement of the local disruption in the water surface (identified as wave). It is not a current but only the movement of the wave shape on the water surface. Based on the ratio h/L wave celerity is calculated:

$$c = \frac{L}{T} \rightarrow h/L \leq 0.05 \quad [6]$$

$$c = \sqrt{\sqrt{\frac{g*L}{2*\pi}} * \tan(\frac{2*\pi*h}{L})} \rightarrow 0.05 \lhd h/L \lhd 0.5 \quad [7]$$

$$c = \frac{g*T}{2*\pi} \rightarrow h/L \geq 0.5 \quad [8]$$

Where;

L = Water wave wavelength [m]

T = Water wave period [s]

h = Water depth [m]

g = Acceleration due to gravity [m/s].

2.2.4 Wave Breaking

Another important wave parameter is the wave breaking. If the wave front becomes too steep, due to interaction between wave and bottom, interaction between waves, currents or wind, the wave breaks. The water particles at the top of the wave are faster than the water particles in the through because the wave celerity is dependent on the water depth. At a certain point the top part of the wave reaches out too far, resulting in breaking. This critical steepness found by Stokes (1880) is considered to be 120°. During breaking the wave loses a major part of their energy. This is why the wave height is lowered after breaking.

The maximum steepness in transition zone before the wave start to break is defined by Miche (1944):

$$(\frac{H}{L})_{gr} = 0.142 * \tanh*(\frac{2*\pi*h}{L}) \quad [9]$$

Where;

H = Height of the Breaking Wave [m]

L = Wavelength [m]

h = Water Depth [m].

Different types of wave breaking, based on the surf- similarity- parameter, are divided. The surf similarity parameter ξ_0 is given in EAK (2002):

$$\xi_0 = \frac{\tan\alpha}{\sqrt{\frac{H}{L_0}}} \qquad [10]$$

Where;

tanα = Beach slope [°]

H = Wave height [m]

L_0 = Deep water wave length [m].

Depending on the beach slope, wave height and deep water wave length spilling, plunging and surging breaker are distinguished:

$$\begin{aligned} &\xi_0 < 0.5 && \text{Spilling breaker} \\ &0.5 < \xi_0 < 3.3 && \text{Plunging breaker} \\ &\xi_0 > 3.3 && \text{Surging breaker} \end{aligned} \qquad [11]$$

For spilling breaker the crest cascades down the shoreward side of the wave (Fig. 4). Plunging wave breaking is even more turbulent and the crest curls down and splashes into the wave bottom. In surging wave breaking the wave crest remains nearly unbroken and only at the end of the wave run-up zone small breaking is observed (Kusterle (2007)).

During breaking turbulence is introduced to the wave, leading to increased foam production (section 2.3.1).

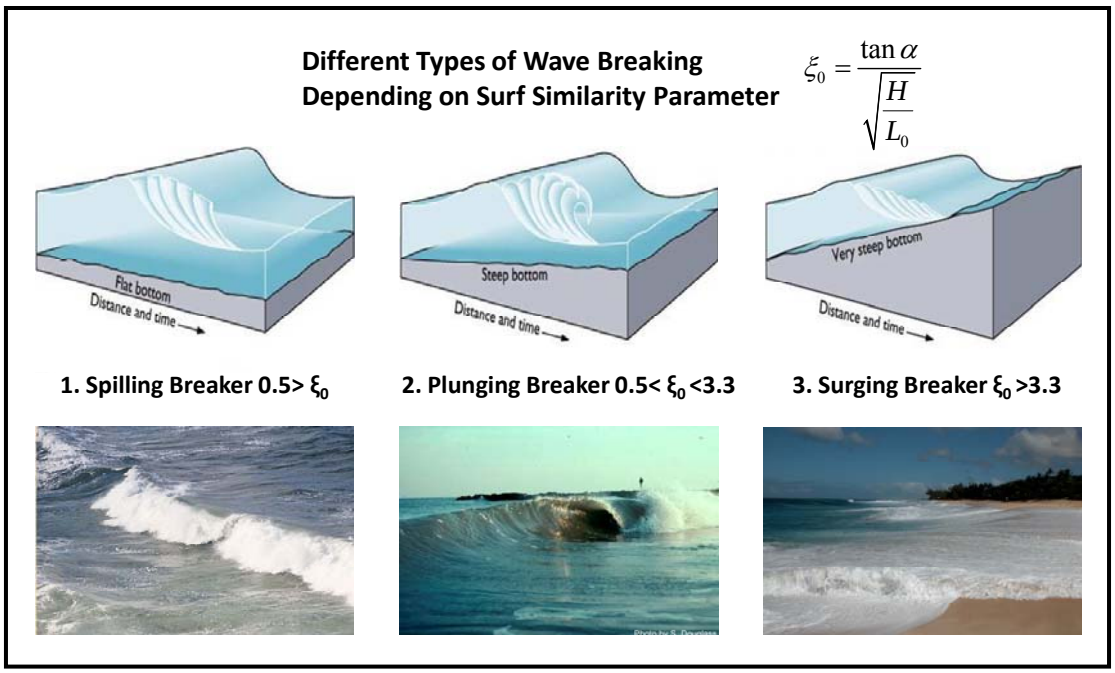

Fig. 4: Different types of wave breaking depending on surf similarity parameter ξ0(http://www.fhwa.dot.gov, http://geology.uprm.edu/, http://www.nature.com, http://clasfaculty.ucdenver.edu)

2.3 Water Characteristics

In this section the water characteristics such as foam on the surface and turbidity are presented.

2.3.1 Foam

The high amount of turbulence during wave breaking inserts air bubbles in the water, producing foam at the water surface (section 2.2.4).

Advanced foam production can occur in seas, due to a mixing of water, organic materials, strong wind and turbulent waves. Nevertheless this is a rather rare incident and normally foam production only takes place in limited amounts during wave breaking.

Different types of foam along the coastal zone are shown in Fig. 5.

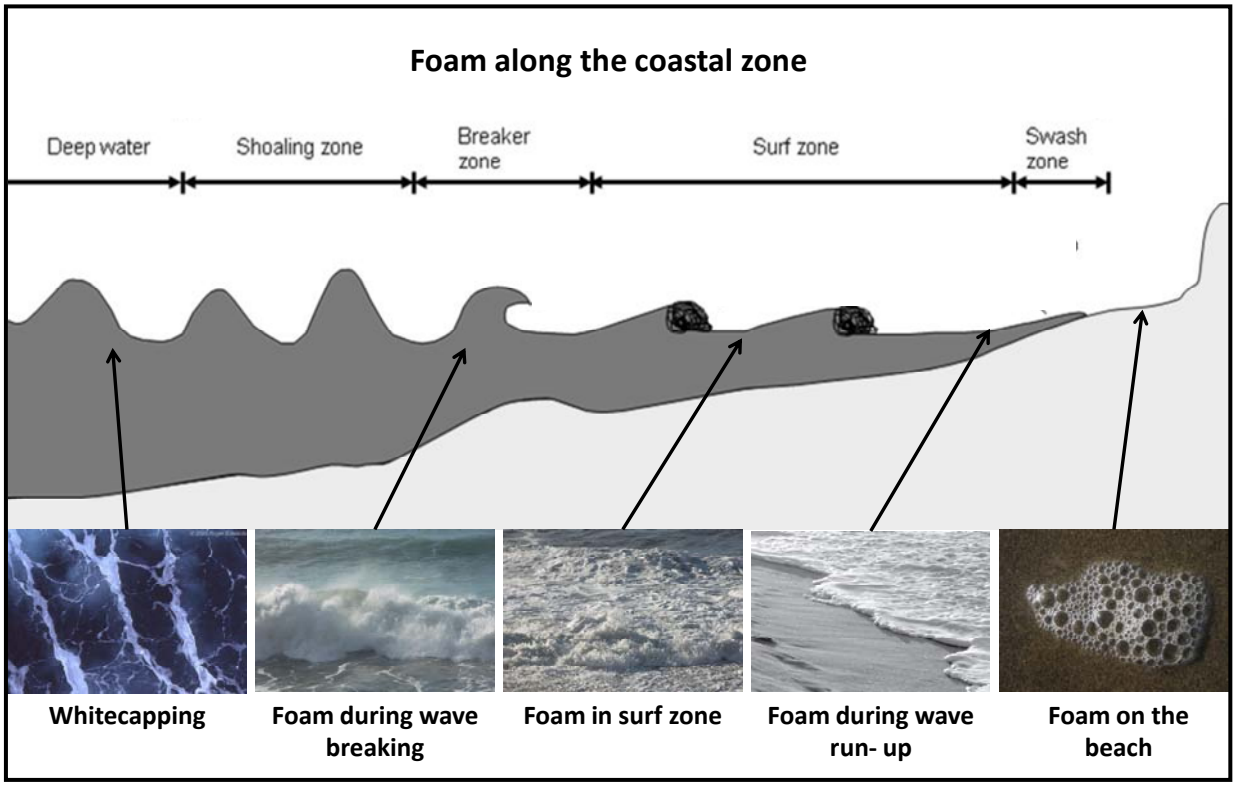

Fig. 5: Existence of foam along the coastal zone: whitecapping (www.stormeyes.org), during wave breaking (www.cepolina.com), in the surf zone (www.cepolina.com), during run-up (http://njscuba.net), on the beach (http://commons.wikimedia.org)

2.3.2 Turbidity

Fully developed water waves show an oscillating movement over depth, introducing a current in the water. If the oscillating movement of the wave experience bottom contact, they mobilize sand particles from the bottom into suspension. Hence the turbidity of the water increases.

Turbidity is created by small particles suspended within the water and the scattering characteristics (reflection, refraction, absorption, transmission) of these particles determine the turbidity. The particles are divided by size, shape and density and the amount of suspended particles is given in mg/l. The same amount of suspended particles does not necessarily lead to the same turbidity since it is dependent on the particles light scattering characteristics.

Turbidity gradients in estuaries, northeast Irish sea

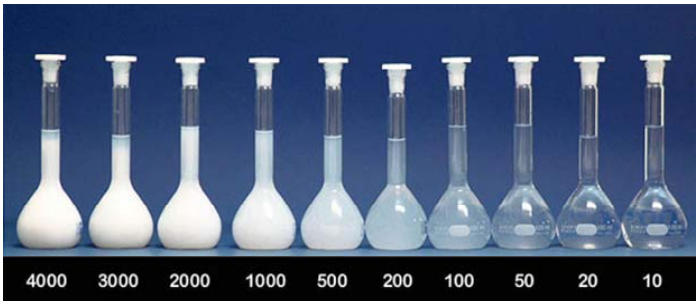

Different NTU's (suspended Formazin)

Secchi disk

Fig. 6: Turbidity in estuaries (Uncles et al. (2012)), and measurement methods: NTU (www.optek.com), Secchi disk (http://courses.washington.edu)

Turbidity of a liquid is given in several different units related to slightly different measuring methods, such as Nephelometric Turbidity Units (NTU), Formazin Turbidity Units (FTU), Jackson Turbidity Units (JTU) etc. The comparison between turbidity results should be handled carefully since all methods are referring to different methods or scales. Most common in laboratory measurement, the turbidity is given in Nephelometric Turbidity Units (NTU). White light is send into a transparent box with the investigated water and the intensity of the scattered light at an angle of 90° is measured. Particulate matter in the water will cause the light to scatter and not move straightly through. Particles which cause scattering are suspend-

ed solids such as silt, clay, algae, organic matter, various microorganisms, colloidal material and even large molecules (Sadar (2002)). A visualized result of NTU is shown in Fig. 6. The turbidity of drinking water should not be higher than 1 NTU. Rivers with a clear green color have usually less than 10 NTU (Swanson & Baldwin (1965)

If no laboratory derivation of turbidity is possible, e.g. in the field, the turbidity can be derived with a Secchi disk. A black and white disk attached to a cable is slowly lowered in the sea or lake and the depth in which the disk optically disappears for the viewer, is described as Secchi depth (Bruckner (2012)). This is true if the reflectance of the disk is equaled by the scattering of the water. The Secchi disc method is known for its low cost and easy handling, but difficulties appear in open, rough sea water and since testing and determination of Secchi depth is done manually, inaccuracies occur easily due to a degree of subjectivity.

2.4 Water Wave Sensor Devices in Hydraulic Modeling

Water wave sensors in hydraulic modeling are divided into intrusive and nonintrusive devices. Intrusive means the physical distortion of the measured water surface and nonintrusive describes every noncontact measurement from above or below the water surface. Again the nonintrusive methods are divided into active and passive remote sensing devices. Within active remote sensing an electromagnetic signal is send to the measured target and its reflection determined. Passive remote sensing methods are simply collecting signals within the optical spectral range.

The measurement devices are also classified into the spatial area they can cover while measuring. Basically, how many coordinates are needed to describe a point measured within this area. 0D are temporal point measurements, 1D are temporal profile measurements (helical mode) and 2D are temporal measurements which cover a whole field.

A first classification of water surface sensor devices based on these parameters is given in Tab 1. This section presents an overview on existing water wave sensor devices and enables the reader to better understand the context of TLS based range measurements from water waves. A short description with the most important definitions of Accuracy, Precision and Error is given in section 2.4.1. These terms are fundamental for the quality comparison between different devices.

This study is focused on the application of laser ranging to the monitoring of water waves. Since short range (< 400 m) Terrestrial Laser Scanner (TLS) (Heritage & Large (2009)) are used for this purpose the term TLS will be used in this report. TLS devices belong to the group of active (no natural light, but stimulated electromagnetic light source) remote sensing (non- contact) devices (Vosselmann & Maas (2010).

2.4.1 Systematical and Statistical Error

The systematical error is often related to the measurement device itself. Possible reasons are bad calibration of the instrument or influencing parameters from outside (e.g. thermal, radiation) during the measurement. If the measured values tend to change in a certain direction during measurements the error is called drift.

If the systematic error remains stable it is hard to detect and it reduces the accuracy of the measurement. Accuracy describes how near a measured value comes to its true value.

Statistical errors are due to random statistical distribution of the measured values. If the measurement is repeated for a sufficient number of times and the mean value calculated, the statistical error is reduced and the precision improved. Precision describes how near a second measurement of the same event would come to the already measured value.

2.4.2 Capacitance and Resistance Type of Wave Probe

The conventional method to measure water waves in the laboratory is intrusive and surface penetrating. Capacitance or resistance wave probes are used as a temporal 0D measurement (section 2.4).

The capacitance wave probe, as described by Whittenbury et al. (1959), consists of two parallel wires or rods. The construction is fixed partly immersed and the two wires are isolated and act, together with the water medium in between, like a capacitor. The plus and minus pole in the two wires is switched constantly, leading to a constant reorientation of the water ions towards the opposite pole. Based on the immersion the wires will have a variable capacity. The produced output voltage is linearly dependant on the wave height or the immersion of the wires and is large enough to be recorded with standard electronic recording devices (Foote & Horn (2002)). Limitations are that adhesive water particles attached to the wire, when the wave height is decreasing, lead to a deteriorated signal.

For resistance type of wave probes two conductive parallel wires produce an electronic circuit together with the water. Resistance changes with varying immersion of the wires into water, resulting in a difference in output voltage. The difference in conductivity of the water due to salinity, stratification and temperature is adopted with calibration or the use of a reference electrode, as developed by Deltares.

The resistance type of wave probes are most preferred in hydraulic modeling, because they show high reliability and accuracy in the order of at least 1% of the wave height. Shepherd (1997) even stated that capacitance and resistance type of wave probes provide accuracies less than 1mm, as shown in Tab. 1.

A standardized method is to place the capacitance or resistance type of wave probes in a row of at least four probes to eliminate errors during the measurement and to compensate for reflected wave effects.

Capacitance or resistance wave probes are also used in a different set-up as wave run up wires (Lange et al. (1982)). They are installed along the run up slope and are supposed to measure

the wave run up based on the same principle of variable capacity or resistance as described above.

The main limitation is that capacitance and resistance wave probes can only produce time varying output for a specific point, not allowing the study of whole wave fields. Besides, wires are vulnerable to manual or salt water damage and not easy to replace. Often they are installed near the wall and measuring also wall boundary effects of the wave.

2.4.3 Pressure Sensor

An nonintrusive and subsurface method to measure water waves in hydraulic modeling is the use of pressure sensors as described by Bishop & Donelan (1987). As the resistance and capacitance wave probes this is a temporally 0D measurement (section 2.4). Measuring the water pressure in a certain depth the current water surface elevation is derived via linear wave theory. In theory the pressure is transformed back into a water surface elevation by resolving the combination from hydrostatic and kinetic pressure in the Bernoulli theorem of the linear wave theory. The first use of pressure sensors for wave height determination dates back to 1947. Studies performed by Bishop & Donelan (1987) show that wave height accuracies for monochromatic and irregular waves are about 5% (Tab. 1) compared to standard capacitance wave probes (section 2.4.2). They found that linear wave theory is adoptable to derive wave heights from a pressure signal unless the pressure sensor is installed in very shallow waters. In this case extensions regarding currents or swash interaction are required in the linear wave theory.

2.4.4 Ultrasonic Altimeter

Ultrasonic altimeter are considered an nonintrusive, active remote sensing, temporal 0D measurement method (section 2.4). Two identical ultrasonic altimeters (transmitter and receiver) either located above or below the water surface are used for surface detection and ranging (Wang et al. (1991)). The acoustical signal above a frequency of 20 khz, which is out of the human hearing range, shows a very consistent motion pattern over long distances. For the measurement of water waves in the swash zone 95 khz is found to perform best (Blenkinsopp et al. (2012)). The transmitted acoustic signal is reflected at the air- water interface and the pulse echo is recorded by the receiver. The measured running time is converted into a distance. The combination of high frequencies and short wave lengths allow accuracies (section 2.4.1) of <1 mm as shown in Tab.1. Smooth and flat surfaces are even more accurate measured with an accuracy of 10 µm (Wang et al. (1991)). For water wave measurements, ultrasonic altimeters are usually placed in a height of approximately 0.8 m to 1 m above the water but its functional ability is tested to up to 10 m. As a low cost standard device ultrasonic altimeters are used by Blenkinsopp et al. (2010) for water wave measurements in the swash zone. Its applicability is widened by Houser & Barrett (2009) to the measurement of bed elevation changes in the swash zone. Investigations on the underwater adjustment of ultrasonic altimeters at the bottom of a ship testing tank are done by Stansberg et al. (2011). This application has the disadvantage that the measurement devices are exposed to corrosion. For application above and below the water surface it is true that the speed of the travelling signal is

very much temperature and humidity dependent. Hence the system need careful calibration (the new Delta Flume will be partly outside). Additionally the receiver is easily influenced by background noise and random electrical noise (Gillespie et al. (1982)) which may disturb echo signal from the measured surface.

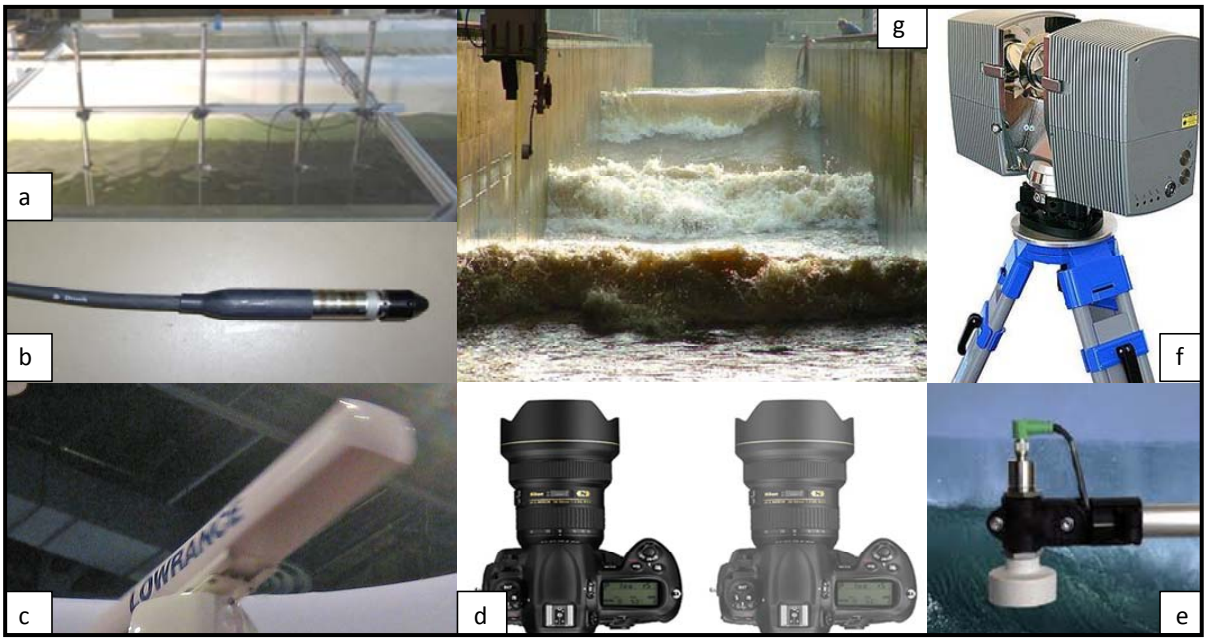

Fig. 7: Water surface measurement devices. a: wave probes (LWI Braunschweig), b: pressure meter (www.fs.fed.us), c: RADAR (www.panbo.com), d: stereo image photogrammetry (www.qwerty.com), e: ultrasonic altimeter (www.act-us.info), f: LIDAR (www.translationdirectory.com), g: waves in hydraulic measurement (Deltaflume, Deltares)

2.4.5 Video and Photography

As a standard nonintrusive measurement device digital video and photography are often used to qualitatively describe the water surface elevation. It is considered as a passive remote sensing method since it makes use of the optically visible electromagnetic range (section 2.5.1). It is categorized as a temporally 2D measurement. The main disadvantage is that without extensive post processing steps no quantitative water surface elevation is determined. These devices serve more as a qualitative control of differently identified water surface elevation. Since the standard measurement devices only produce punctual output, 2D video and photography allow for more detailed and qualitatively studying of the wave height and shape.

2.4.6 Stereo Image Photogrammetry

There are many names like two dimensional video technique, stereo photogrammetry, stereo vision, stereo video, stereoscopic images, stereo image sequence analysis, digital stereo images, describing the same principle of reconstructing the shape and location of objects with help of two different overlapping photographs. For simplification they are summarized under the generic term Stereo Image Photogrammetry. It operates in the optical electromagnetic range and is considered a nonintrusive and passive measurement method (section 2.4).

Basically it describes the retrieval of temporal 2D information from points in the image, using two overlapping pictures taken from at least two synchronized cameras placed at different locations. The visualized and reconstructed objects serves as input for mapping and generation of DTM and DSM purposes (Baltsavias (1999)). Stereo Image Photogrammetry is applied for water wave measurements in the nearshore and swash zone (Strybny et al. (2001)) as well as in hydraulic modeling (Vries et al. (2011)). They could validate their measurements obtained with Stereo Image Photogrammetry for low and high frequency waves in the inner surf and swash zone with conventional pressure sensors (section 2.4.3), resulting in a difference of water surface elevation of h_{rms} = 0.034 m (Tab. 1).

Further research using Stereo Image Photogrammetry in laboratory measurements of the water surface elevation are conducted by Foote & Horn (2002). With GIS methods they extracted hydrodynamic parameters, such as wave height, resulting in a 2D profile of the wave in the swash zone.

Laboratory implementation of Stereo Image Photogrammetry has been done by Piepmeier & Waters (2004). During their studies they needed to roughen the surface to increase the visibility.

Stereo Image Photogrammetry measurements are applied by Stansberg et al. (2011) for the measurement of ship waves in a laboratory basin. The importance of lighting, seeding and sufficient surface roughness are highlighted. Hence, Stereo Image Photogrammetry is a feasible method but in laboratory scale some additional efforts are necessary. Applying Stereo Image Photogrammetry to field studies of the swash zone, wind, ripples, waves, foam etc. make a more suitable surface for stereo imaging. Also the preferred diffuse lighting is naturally given in the field.

The Wavescan project, initiated by Schimmels et al. (2002), uses Stereo Image Photogrammetry information gathered in the swash zone at the coast of Norderney (200 square meter) for the calibration and validation of the phase based Boussinesq wave model Bowam2. They achieved an accuracy of 0.1 m at a sampling frequency of 10 Hz, validated against single wave buoys (Strybny et al. (2001)).

Holthuijsen (1983) investigated an airborne Stereo Image Photogrammetry method for the monitoring of ocean waves.

The high resolution measurement of temporal and spatial changes is the main advantage of these method compared to conventional punctual measurements (section 2.4.2).

Limitations considering the required synchronization of the two cameras and the motionless mounting, as well as the extensive data post processing steps to match the images and retrieve surface elevation are reported by Stansberg et al. (2011) and might complicate a routine workflow. Since it operates in the optical electromagnetic range it is highly dependent on lighting and illumination in order to prevent shadowing effects. Indirect encoding of 2D coordinates, raises the need for advanced manually post processing steps, not allowing for a high degree of automatisation, to registrate, match images and finally extract the coordinates. Mapping of surfaces with very little texture or surfaces below other surfaces is problematic, as well as the mapping of long features, where many pictures in a row need to be taken. Stereo Image Pho-

togrammetry also shows problems when handling with sharp discontinuities and small objects (Baltsavias (1999)).

2.4.7 Radio Detection and Ranging (RADAR)

Radar measurement devices produce a locally limited continuous signal of the water wave. They operate with wavelengths between 1mm and 100 km. Corresponding frequencies from 50 Hz to 300 GHz are used. Radar waves are reflected at the surface and the returned echo signal is detected with the receiver antenna. For the purpose of water wave measurements frequencies up to 10 Hz and approximately 30 cm footprint sizes are used (Rees & P.Pellika (2010)). Radar measurements are considered to be a nonintrusive and active remote sensing method (section 2.4). They are not affected by clouds, rain, fog etc. Limitations are spike phenomena, which is an oversaturated reflecting signal if the incident radar angle is perpendicular to water surface. Discontinuities in approximately 1% of the signal are measured during testing in the Deltares Delta Flume.

2.4.8 Particle Image Velocimetry (PIV)

Particle Image Velocimetry is considered a nonintrusive method to measure the kinetics of particles in a flowing fluid in hydraulic modeling. The fluid is seeded with tracer particles and with help of a laser they are illuminated. In two following scans the instantaneous displacement of the particles is measured and a velocity calculated (Raffel et al. (2007)). Besides the measurement of the velocity the possibility to estimate the water surface as well was evaluated by Peirson (1997). Particle image velocimetry is adopted for the instantaneous estimation of wave heights based on image segmentation methods. For that purpose particle velocimetry images of a hydraulic jump in a laboratory wave flume were used to estimate the air- water interface in post processing steps. The results are validated with a camera image taken from aside and the horizontal error between the processed PIV data and the validation image is 4 mm. This means a lower accuracy than in other water wave measurement methods (Tab. 1). Nevertheless the completely automated extraction process of the instantaneous water wave is an advantage (Misra et al. (2006)). It is up to discussion whether the seeding of particles in the water is considered as an intrusive act. In this thesis the PIV method is considered non-intrusive, since a very low influence of the particles on the water properties is expected.

2.4.9 Laser Induced Fluorescence (LIF)

This method is comparable to the Particle Image Velocimetry method with the main difference that the seeded dye particles are fluorescent (section 2.4.8). In comparison to PIV the particles absorb light of a specific wavelength and subsequently reemit light at a different wavelength, which is then detected by the receiver. Usually Laser Induced Fluorescence is used to indicate the flow in hydraulic modeling. It is applied to water wave measurement techniques by Peirson (1997).

2.4.10 Summary Water Wave Measurement Devices

Water wave measurement devices currently in use are given in Tab. 1. They are divided into intrusive and nonintrusive devices. With accuracy the difference between the measured and the true value is described (section 2.4.1). Time varying spatial dimension refer to the number of coordinates which are needed to describe a point within the measurement point/line/field. TLS applied for water wave measurement in the laboratory has the advantage that it measures a whole profile of the wave (section 2.6.3). Remaining methods are Video and Stereo Image Photogrammetry as well as PIV and LIF, which also produce line or field measurements. PIV and LIF are more suitable for velocity and current measurements. Compared to Video and Stereo Image Photogrammetry the use of TLS might have the advantage of an easier work-flow implementation, since it doesn´t need detailed registration and segmentations steps. Nevertheless the TLS high spatial resolution can´t compete with the accuracy of the low spatial resolution measurement devices such as resistance type of wave probes (section 2.4.2).

	Intrusive	Nonintrusive		Accuracy	Time Varying Dimension
		Additives	No Additives		
Capacitance Wave Probe	+		+	<1mm*[1]	0D
Resistance Wave Probe	+		+	<1mm*[2]	0D
Pressure Meter			+	5% *[3]	0D
Ultrasonic Altimeter			+	<1mm*[4]	0D
Video			+	-	2D
Photogrammetry		+	+	<34mm*[5]	2D
LIF		+		-	1D
PIV		+		<4mm*[6]	1D
Laser Ranging		+	+	<3.62mm*[7]	1D

*[1] Shepherd (1997)
*[2] Shepherd (1997)
*[3] Bishop & Donelan (1987), 5% of wave height
*[4] Wang et al. (1991)
*[5] Vries et al. (2011), compared to capacitance wave probe
*[6] Peirson (1997), compared to image
*[7] Allis et al. (2011), compared to capacitance wave probe

Tab. 1. Classification of water surface measurement devices

2.5 Principles of LASER and TLS Based Range Measurements

The use of TLS devices in hydraulic measurements is a new challenge for coastal engineers and often an uncovered topic during their studies. A simplified and relatively physical introduction about the principals of LASERs is given and its use in TLS based range measurements of water waves explained.

The spectral reflectance curves for seawater, foam and suspended solids in section 2.5.3 give a first overview of the expected reflectance during TLS based range measurements from water waves.

Since few research is carried out, this section is not only focused on TLS applied to hydraulic modeling (section 2.5.6) but also TLS based measurements from the field (section 2.5.5) and airborne LiDAR (section 2.5.4) are taken into account enlarging the available knowledge about TLS based range measurements of water waves.

2.5.1 Light Amplification by Stimulated Emission of Radiation (LASER)

Already in 1917 A. Einstein predicted that if enough energy is added to an atom the surrounding electrons are excited to a higher energy level (Williamson (2010)). The new position is highly instable for electrons and they will return to their former energy level position by emitting a photon at a certain wavelength. Since the energy levels within an atom are quantized the emitted wavelength is controllable. Based on this principle a first laser is constructed by Maiman (1960). It contains a ruby crystal to generate the stimulated emission for a visible laser ray wavelength of 694.3nm. Recently semi conductor, solid state, gas or fluorescent dye lasers with different wavelength spectra are constructed (Heritage & Large (2009))

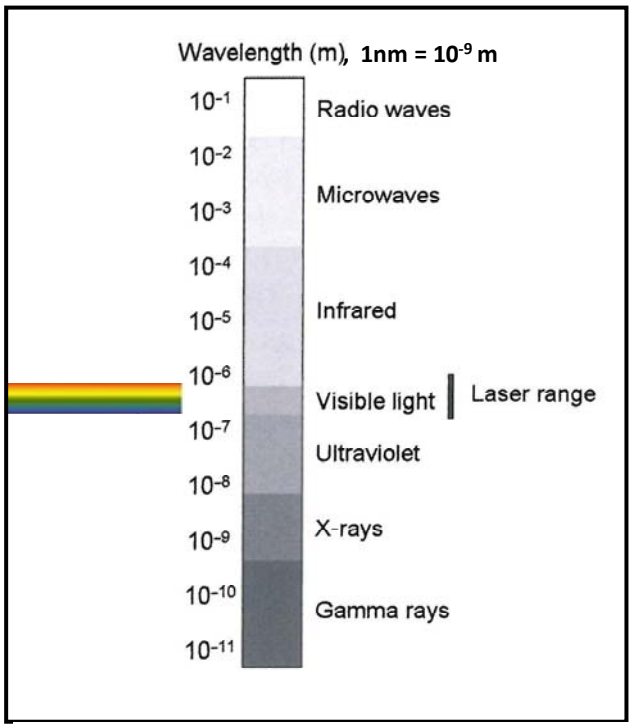

Fig. 8: Electromagnetic spectrum (Heritage & Large (2009))

A light source is employed to stimulate the laser material, leading to a higher but unstable state of the electrons, as described by Einstein. When returning to its original state the electrons emit energy as a photon at a specific wavelength. This photon again excites other atoms already in higher state and two or more photons are emitted from there with same wavelength and direction. Subsequent stimulation of further atoms causing even more photons to be emitted, lead to an amplified, highly coherent and low divergent light, which is allowed to travel through an opening out of the laser aperture (Heritage & Large (2009)). By coherence a laser beam with constant wavelength and amplitude, travelling in phase is described. This allows the laser beam to stay in a small spot when targeting distant objects. The coherence length in this context is the

speed of light divided by the spectral width of the laser source and is used to describe the purity of the beam (Vosselmann & Maas (2010)). The spectral width of a laser beam is very narrow and within the electromagnetic spectrum lasers are applied for the visible spectrum (~ 390 nm – 750 nm), but are reaching out in the ultraviolet (< 390 nm) and the infrared (> 750 nm) spectrum as well (Fig. 8). This part of the electromagnetic spectrum is called atmospheric window. It describes the spectral width, which is not reflected or absorbed but transmitted by the earth atmosphere and thus most common on earth surface. Most remote sensing techniques, including TLS based range measurements (section 2.5.2), operate within the spectral width of the atmospheric window (Rees & P.Pellika (2010)).

2.5.2 TLS Based Range Measurements

A laser beam is emitted by the TLS device and travels through the propagation medium until it hits a surface. During travel the once collimated laser beam experience diffraction. This results in spreading of the laser beam, called beam divergence as shown in Fig. 9.

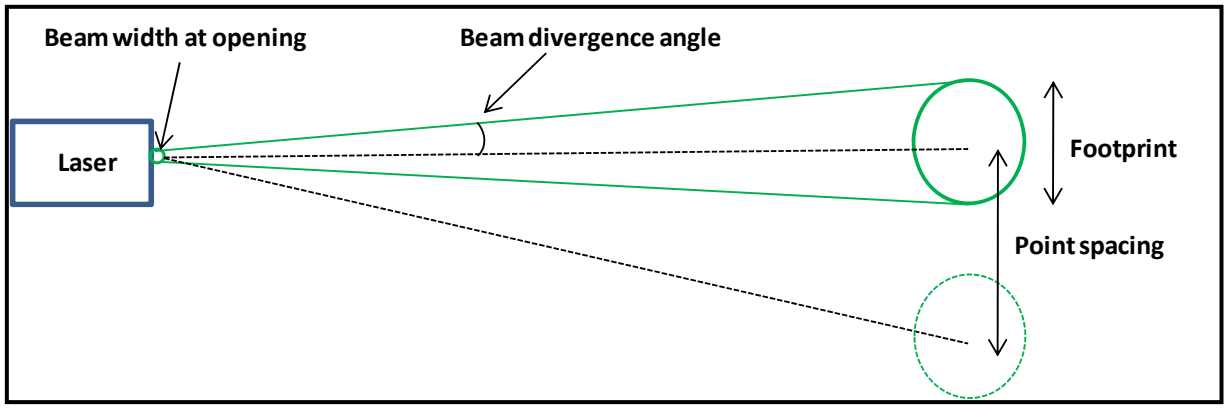

Fig. 9: Laser beam divergence, footprint and point spacing

The amount of beam divergence is dependent on initial beam radius at the focus lens, wavelength and refraction index of the propagation medium (Vosselmann & Maas (2010)). Since the radius of the beam is changing with distance, a footprint is introduced, describing the beam diameter at the distant target (Fig. 9). A non- perpendicular beam incidence leads to a distorted footprint and a broadened reflection.

Hitting a distant surface the laser beam is reflected, absorbed or transmitted, depending on the surface characteristics and wavelength of the laser beam. For remote sensing purposes the reflection is of major importance since the reflected beam carries the information about the surface and based on the travel time its range to the TLS device is calculated. The ratio of originally received and emitted radiance is called reflection.

For simplification specular and diffuse reflection are distinguished (Fig. 10).

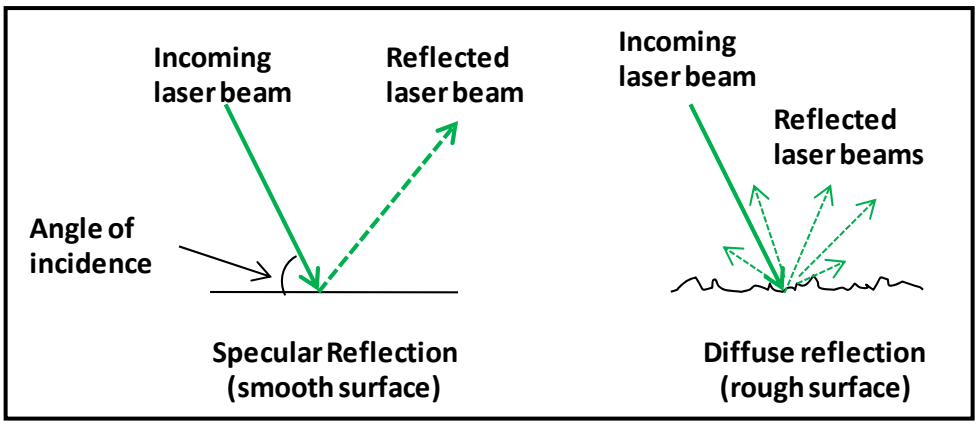

Fig. 10: Specular and diffuse reflection

Specular reflection occurs if the incident wavelength is larger than the surface roughness. In case of specular reflection either no reflected signal or a fully oversaturated signal (spike phenomena) is recorded, as for smooth water surfaces or glass. If the incidence angle is 0° an oversaturated reflection is expected (spike). With increasing incidence angle no signal at all is recorded, since the reflection is going in a different direction. The angle in the remaining direction is defined as slant angle (Fig. 11). Soudarissanane et al. (2009) found that the incidence angle has the highest influence on the quality of the recorded signal. With increasing

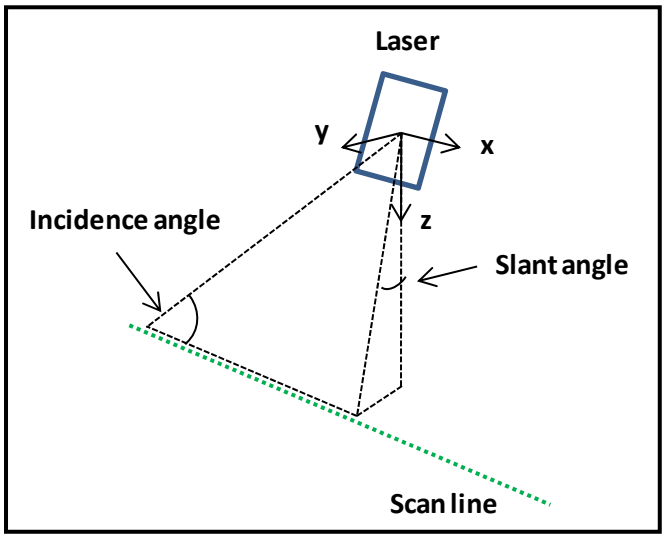

Fig. 11: Definition of incidence and slant angle

incidence angles the recorded signal will deteriorate.

Diffuse reflection is present if the wavelength of the incident beam is shorter than the geometrical inaccuracies on the surface. The incident laser beam is reflected by the geometrical inaccuracy of the surface in any direction, depending on the local orientation and shape of the surface.

For TLS based range measurements of water waves diffuse is the preferred type of reflection, since part of the incident laser beam is reflected back to the recording device.

The optimum reflection is expected for objects with opaque surfaces, diffusely reflecting and surroundings which don´t create spurious signals.

Laser light is used as an emission source because of its ability to stay relatively coherent and a minimum return signal can be detected from distant surfaces. This allows for determination of 3D coordinates of complex objects in a fast, high density and precise way. The TLS device emits either short pulses or a continuous wave (CW). The generated beam propagates at the speed of light and is reflected from the first obstacle, if not absorbed or transmitted. The return signal is recorded by the receiver. The propagation time is calculated and knowing the speed of light, the range is calculated.

In the transmitter aperture the stimulation and amplification (section 2.5.1) of laser light takes place, generating the laser beam. An opto-mechanical project mechanism, mostly a mirror, is used to deflect the light in the desired direction and move it over the target surface (Heritage & Large (2009)). The TLS may rotate in one or more planes. Often a horizontal rotation of the TLS device is combined with a vertical rotation of the mirror. Hence, precise angular changes are generated and a whole area is covered. The Palmer project mechanism (rotation axis and mirror don't form a 90°) is most common in terrestrial laser scanning. A combination of horizontal TLS and vertical mirror movement provides a 360° field of view. Standard TLS devices have an angular resolution of 0.04 mrad (Vosselmann & Maas (2010)). Limitations related to the mirror are wobble (deformation perpendicular to scan direction), jitter (deformation in scan direction) and dynamical deformation. If a variance in footprint is needed a beam expander or focus lens, to widen or narrow the laser beam is used.

The laser beam is then travelling through the propagation medium, hits the surface and is either reflected, absorbed or transmitted. The controlled laser beam parameters are affected by the reflecting surface and the return signal is measured by the receiver. The receiver records and evaluates the return signal. If combined with transmitter it is also called transceiver. P-n photodiodes, avalanche photodiodes and photomultipliers are used for photon detection. They measure the intensity of reflected laser light, which basically is the reflectivity of objects at a specific wavelength (section 2.5.1). Three peak detection methods are divided. Based on the implemented criterion the receiver records either the peak of the returning pulse (peak detection), or if the pulse exceeds a certain threshold (threshold edge detection), or if the returning pulse exceeds 50% of its maximum amplitude (constant fraction detection). Multiple echo measurements are possible do detect reflections from subsurfaces (e.g. sea and sea- bottom or trees and bottom).

Time- of- Flight (ToF) and Phase Shift (PS) measurement principals (Fig. 12), to calculate the distance between TLS device and reflecting surface, are distinguished (Vosselmann & Maas (2010)).

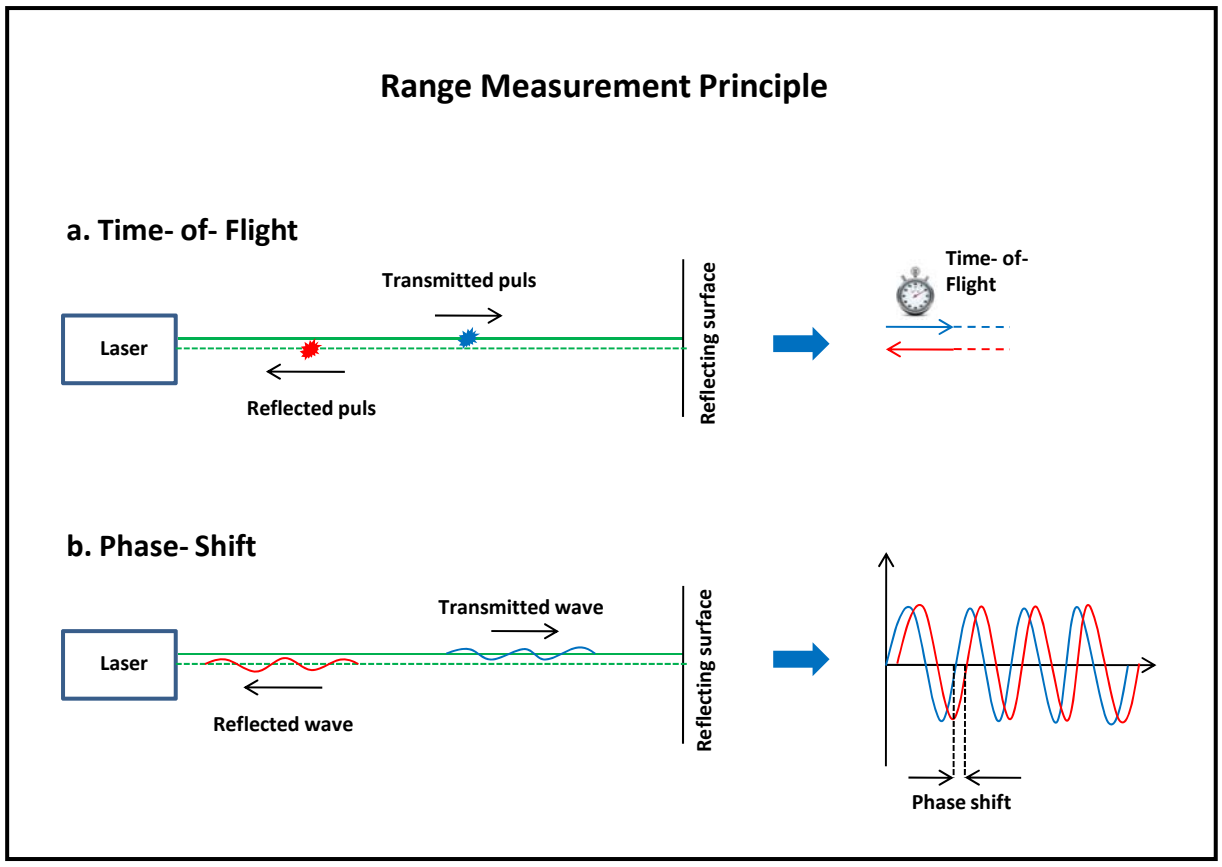

Fig. 12: Range measurement principle

Time- of- Flight devices emit high energy pulses in discrete units. The receiver measures the time until the reflected pulse is recorded again. Knowing the finite and constant velocity of a laser beam travelling through a propagation medium the range calculation is given by Heritage & Large (2009):

$$\rho = \frac{c * \tau}{n * 2} \qquad [12]$$

Where;

ρ = Range [m]

τ = Time delay for one round trip [s]

c = Speed of light (299792458 m/s in vacuum) [m/s]

n = Refractive index depending on propagation medium [-].

If it travels in air the refractive index is n = 1.00025. The maximum range is limited by the emission to record time. If the pulse is not returned before the next pulse is emitted it will not be recorded. Time- of Flight devices are used to measure larger ranges of 3 km with accuracies between 5 mm and 10 mm (Vosselmann & Maas (2010)).

Phase- Shift based measurements (Fig. 12) are an indirect Time- of- Flight measurement for a continuous laser pulse. The range measurement is based on the recorded phase difference between emitted and recorded laser beam wavelength. Since the range would be limited by the

time interval between two identical points on the wave, several modulated phases are used to accurately determine the range over long distances. The phase is either amplitude (AM) or frequency modulated (FM). Most phase- based TLS devices are developed for scan distances up to 80 m (Vosselmann & Maas (2010)). Phase- based TLS devices provide higher accuracies 1mm - 3mm and increased measurement velocity (Alonso et al. (2011).

The power of the recorded signal is calculated with laser range equation:

$$P_r = \frac{P_t * G_t}{4*\pi*R^2} * \frac{\sigma}{4*\pi*R^2} * \frac{\pi * D^2}{4} * \tau_{sys} * \tau_{atm} \qquad [13]$$

Where;

P_r = Received signal power [W]

P_t = Transmitted power [W]

G_t = Transmitter antenna gain [-]

σ = Effective target cross section [m²]

R = System range to target [m]

D = Aperture diameter [m]

τ_{atm} = Atmospheric transmission factor [-]

τ_{sys} = System transmission factor [-].

2.5.3 Spectral Curves Seawater, Foam, Suspended Solids

In Fig. 13 the spectral reflectance curve for sea water provided by NASA is shown. Most industrial LASERs are equipped with wavelengths between 0.4 µm and 1.5 µm. In this range the spectral reflectance of water is around 2%, decreasing towards near infrared (~ 800 nm to ~ 1500 nm). A striking peak of 4% reflection for laser beam wavelengths around 2500 nm is shown in Fig. 13. It is the question whether TLS devices with this spectral resolution exist.

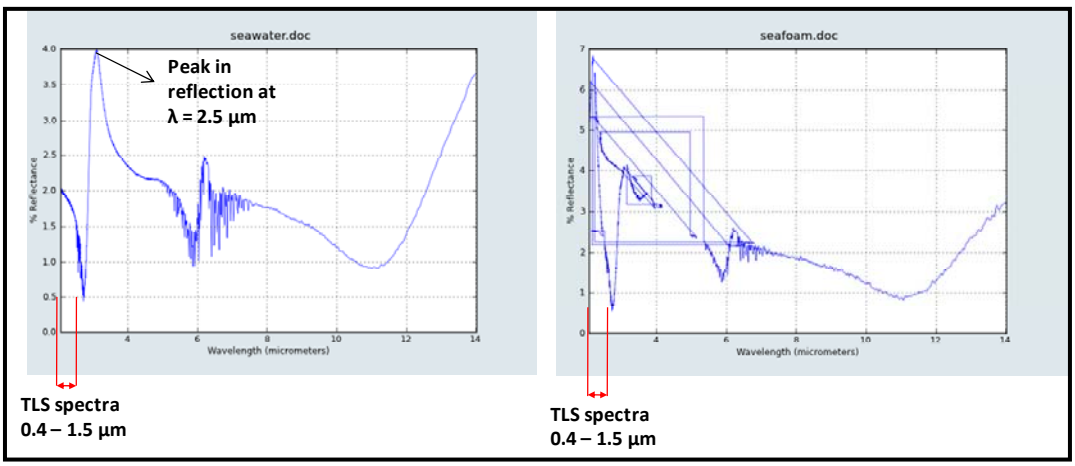

Fig. 13: Spectral reflectance seawater (left) and seafoam (right) (http://speclib.jpl.nasa.gov/)

Foam and enclosed bubbles increase the reflectivity of the water surface and are therefore helpful for LASER based measurements of water waves (section 2.3.1). Reflectivity in the visible spectral range is about 55% as observed by Whitlock et al. (1982). Spectral reflectivity of fresh, dense foam is better than the reflectivity of ordinary foam as observed by Koepke (1984). Their research is focused on the reflectivity of whitecaps on the free ocean surface in the visible spectral range. The reflectivity of whitecaps and foam in this range is found to be 22% (which is much lower than in the studies of Whitlock). The reflectivity is lowered towards infrared spectral range. Spectral foam reflectivity diagrams from NASA show the same tendency (Fig.13). Frouin et al. (1996) explains the decrease in reflectivity towards the near infrared spectrum. During wave breaking air bubbles are introduced in the water looking like white foam, but in fact there isn't a thin water layer dividing large air bubbles (like in fresh, dense foam) but a sufficiently large water layer in between leading to increased absorption towards the infrared spectrum. This seems reasonable since the amount of absorption in water increases also towards the near infrared.

Suspended particles in the water causing scattering of the light such as silt, clay, algae, organic matter, various microorganisms, colloidal material and even large molecules (Sadar (2002)) lead to a higher spectral reflectivity, as shown in Fig. 14. Also the maximum reflectance is shown for incidence laser beam wavelengths around 700 nm.

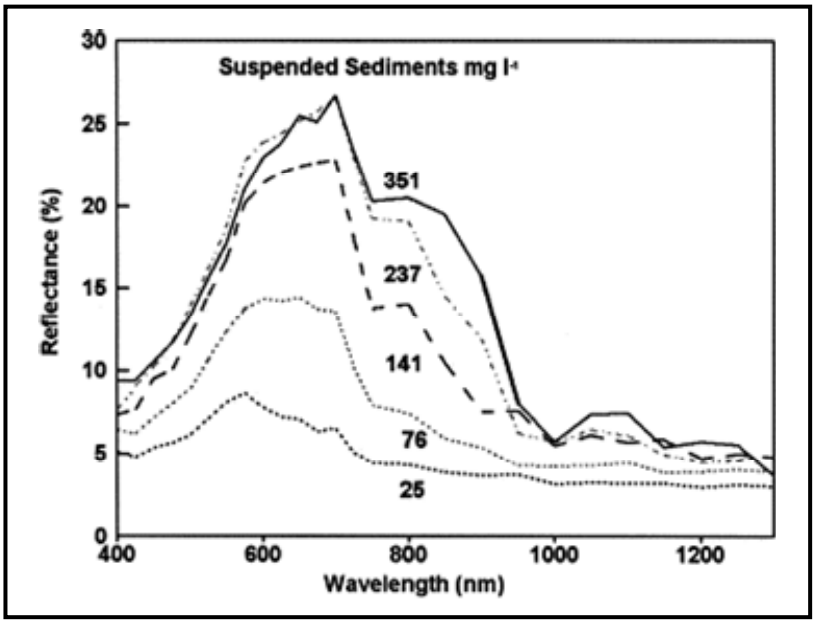

Fig. 14: Spectral reflectance of water with a varyied amount of suspended sediments (Schmugge et al. (2002))

2.6 TLS Based Range Measurement Applied to Wave Measurements

Only few TLS based range measurements of water waves have been done already. Hence not only experiences with TLS used in hydraulic modeling but also TLS used in the field and airborne LASER range measurements are presented in this chapter

2.6.1 Airborne Laser Range Measurements

In this case the term Light Detection and Ranging (LiDAR) will substitute the term TLS based range measurements.

Airborne LiDAR measurements are mainly applied to topographic measurement of landscapes, bottom detection and bathymetry measurements, but also for delineation and classification of the water- land boundary along rivers (Höfle et al. (2009)). Hydrographic fronts are detected with airborne LiDAR by Reuter et al. (1993) in the German north sea. Morphological measurements of the sea bed are conducted by Long et al. (2010) to derive sedimentological information about the formation and reflectivity of underwater dunes. Airborne LiDAR is also applied for the survey of shallow benthic environments, monitoring of coastal reefs and underwater ecological systems (Brock & Purkis (2009)). Applications of airborne LiDAR to oil film monitoring on the water surface, including thickness measurements of the oil film are reported by Fingas et al. (1997).

The main advantage of this method is the capability to obtain quantitative information about water waves for large areas in comparably short time.

The most common way to do so is the use of a collinear green laser pulse (532 nm) together with an infrared laser pulse (1064 nm). The green wavelength penetrates water the most and is less absorbed, resulting in a reflection from the sea bottom. Additionally it excites the water particles to emit a different wavelength, so called Raman scattering, which is also measured at the receiver and gives a first indication of the dimensions of the water column. The infrared wavelength is less water penetrating, resulting in a reflection from the water surface.

The airborne LiDAR system SHOALS, developed by the US Army Corps of Engineers and constructed by Optech operates this way and is well described (Guenther et al. (2000)).They found that depth penetration increases with higher pulse energies and that the maximum incidence angle is 20°. This is due to the high number of dropouts and low backscatter energy of the water. The author points out that the system limitations are water clarity and vertical accuracy. Validating their results to water depth values from USACE showed a standard deviation of 20 cm. The surface uncertainty problem describes the possibility that a recorded surface reflection might come from a particle slightly below the surface, representing not the true surface any longer. Difficulties when defining the beginning of the Raman scattering, because of a slow increase in Raman backscattering, are reported. Also, problems in shallow waters, because of overlaying bottom and surface reflection, are outlined. Nevertheless they declared it as an accurate, capable and cost- effective technique.

In most applications water surface elevation measurement is only a byproduct to calculate water depth, nevertheless it is the first attempt to really detect the water surface with LASER based measurement techniques.

Hwang et al. (1998) investigated even further and were able to compare airborne LIDAR measurements of a dissipating wave front with good agreement to an analytical approach for wave dissipation, taking into account bottom and wave breaking dissipation.

2.6.2 Shore-Based Terrestrial Laser Scanning (TLS)

Most of the TLS based measurement of water waves is carried out with shore-based TLS devices in the field. Although the accuracy in field tests is often not sufficient for laboratory experiments it gives knowledge about the principle and interesting phenomena observed, which are then adopted to the measurements in laboratory.

Fadeev et al. (1999) describe a basic set-up for a future coastal monitoring system and they include as one of three key measurement devices a shore- based TLS to obtain continuously temporal and spatial information about the water surface elevation, subsurface and if possible atmospheric parameters. He theoretically calculated that the achievement of longer scan distances is only dependant on the laser power and the quality of the detector. Due to his research the return factor decreases with the square of the distance. The angle of incidence is of minor importance in sea conditions since waves provide a sufficiently reflective surface. It is assumed to scan distances up to 1000 m, with incidence angles between 0.5° and 10°.The TLS recordings should include measurements from Raman backscattering and fluorescence material. In this way also changes in salinity and temperature could be detected. The possibility to detect oil films and estimate the thickness in variations of Raman backscattering is described. The author is quite enthusiastic about the possibility of wave field reconstruction from shore-based TLS measurements.

A Russian group of scientists (Maslov et al. (2000)) used a TLS for sea water surface monitoring (Russian Black Sea) to validate the theoretical approach of Fadeev et al. (1999). The experiments were conducted with a pulsed shore- based YAG-Nd TLS device. In a self build set-up they were able to use the three harmonics of the original wave length (534 nm, 355 nm, 266 nm) and a scanning frequency of 10 Hz for their experiments. The TLS device is mounted 10m above the water surface, measuring distances between 50 m and 80 m, resulting in incident angles between 13° and 21.4°. The 534 nm wave length excites the water particles to emit a different wavelength (650 nm), so called Raman scattering, which was measured during experiments. According to their findings there is a correlation between the laser pulse energy and the measured echo signal. The minimum laser pulse energy should be 10 mj to get a return signal from 50 m distance with this set-up. They predict a maximum measured distance of 1 km. The power of the laser can be increased by either higher pulse energy, higher scan frequency or a combined action. They also point out that this maximum distance can only be achieved because of the present waves. Due to geometrical reasons the reflective surface increases during high wave conditions (section 2.2.1). Hence, in the case of developed waves, the achievement of longer measuring distances is only dependant on the power of the laser and the sensitivity of the detector.

During the test of an autonomous robot vehicle equipped with a Velodyne HDL-64E the water surface on Langeoog has been measured by Vousdoukas et al. (2011). The scanner operates with near infrared 905 nm wave length and a sampling frequency of 15 Hz. The field of view is 360° and the maximum scanning range is 120 m. From the collected data waves,

breaking waves and swash motion were clearly visible. Qualitatively they declare it promising to apply TLS based range measurements to water waves.

Similar findings are reported by Harry et al. (2010). In their experiments they used a Riegl VZ-400 to acquire data from an elevated position at the beach. The laser is in the near infrared range and scans up to 120 lines per second. Recorded significant wave heights of 1.3 m were present. From the measured point cloud waves could be identified as well as shadowing effects behind the wave front. They were struggling with the horizontal movement of the TLS device and are suggesting a 1D profile scan only. During preliminary experiments they also found that white bubbles on the water surface will increase the reflectivity and improve the quality of the water surface measurement.

TLS based range measurement from water waves in the field are conducted by Park et al. (2011). They used a wave staff, installed in the breaking zone at Malippo Beach approximately 100 m from the coastline, to validate the measurements. The Optech Ilris HD device is mounted on a concrete platform at the beach. It is equipped with an infrared laser wavelength of 1535 nm. The purpose of the study is to measure the incoming waves and determine the wave height. They outline the advantage of TLS devices, to measure wave transformation processes continuously in a fast way with adequate accuracies (section 2.1.1). They found that using the infrared wave length they got only reflection from the bubbles and foam at the roughen surface. Another limitation they found is that only the forward side of the wave and most of the time not the fully trough was scanned because of geometrical shadowing effects. Since estimation of the wave height is based on the length between crest and trough, only crest height is compared to the video measurements at the wave staff, resulting in an RMS error of 5.3 cm. Spectral wave heights of $H_m = 1$ m were present. They could confirm that the recorded reflection decreases with longer measuring distances. A demand for advanced noise filtering techniques and an accuracy improvement of the measurement is stated. They are convinced that spatial and temporal resolution of the data is sufficient enough to investigate characteristics of breaking waves.

Another shore-based TLS experiment to measure water waves is conducted by Belmont et al. (2006). For data acquisition purpose a self build laser with a green wave length of 532 nm and a sampling rate of 20 kHz is used. They scanned a line of approximately 200 m consisting of 50 single points. The measurements are validated against a conventional capacitance wave probe resulting in a difference in a RMS error of 0.037 m. Inevitable with shore-based TLS devices, the incidence angle becomes very shallow. They found that it is very inconvenient for further data analysis to have geometrical shadowing at the rear side of the wave and non uniform sample spacing due to different angles between wave and laser beam. Signal post processing techniques taking into account this non uniform sampling are presented and also possibilities to reconstruct data values which are not recorded because of wave shadowing effects are introduced.

Point measurements using Laser technology for the extraction of directional wave properties are conducted by Irish et al. (2006) at the eastern US Coast. The motivation is to study wave breaking, wave current interaction in detail without using surface penetrating methods, which are easily destroyed in rough sea conditions. Four Optech SLX- 3A infrared, ToF (section 2.5.2) laser range finders with a sampling rate of 10 Hz are mounted on a fixed platform for coastal wave measurement. They are validated against the measurements of pressure sen-

sors (section 2.4.3). Each single laser has a footprint (section 2.5.2) of 7-12 cm and four devices together form a rectangular footprint of 0.6 m- 2 m. The RMS error in measured spectral wave height H_{m0} is 50 mm. Wave heights between 0.2 m and 1.5 m were present. The Laser devices were installed in heights between 6 m and 16 m above water surface (with the laser beam perpendicular to the still water surface). For this distance no influence of the set-up height on the quality of the signal was found. False elevation signals due to rain were not many in number and could be removed with spectral analysis. Also no influence of ambient light conditions is observed. Incidence angles above 10° resulted in poor signal. Also wind speeds above 5 m/s are required for the formation of capillary waves providing surface roughness which leads to sufficient back reflection of the laser signal.

The most recent TLS based range measurements of water waves in the swash zone with an industrial 1D TLS are conducted by Blenkinsopp et al. (2010). Interested in the swash motions (swash front gradient, backwash lens, swash- swash interaction) and the contour shape of the approaching wave a Sick LMS 200 TLS device with a pulsed laser wavelength of 905nm and a scanning frequency of 37.5 Hz is mounted 5m above the swash zone. The measured profile is approximately 12 m long. 35 cm apart from the measured profile 10 ultrasonic altimeters (section 2.4.4) are installed to validate the measurements. RMS error of 40 mm are measured. With a present significant wave height of $H_s = 0.58$ m. They state, that the main advantage is the continuous measured profile compared to the single point measurements of the ultrasonic altimeters. The original shape of the wave is represented in the recorded data (without uncertainties due to interpolation as present with single wave probes). They faced problems when scanning depths lower than 40 mm in the wave run-up zone. It was difficult to divide between wet and dry bed. Measurements of a smooth water surface caused problems, because of specular effects, low backscatter signal and spike phenomena (section 2.5.2). Furthermore a more consistent image is achieved with higher perturbation of the waves.

2.6.3 Terrestrial Laser Scanner (TLS) Applied to Hydraulic Modeling

Only few TLS based range measurements of water waves are conducted in the laboratory. The expected accuracies (section 2.4.1) in hydraulic modeling are higher than in the field, which is a challenge for every newly introduced measurement device. Still some promising results to measure the temporal and spatial varying free water surface elevation are obtained.

TLS based range measurement of the water waves from above in a hydraulic open channel flow model with a pulse- based Topcon GLS 1000 is done by Evans (2010). By adding tracer particles the water reflectivity is increased. The additives should be reflective and float on the surface, without clumping and pooling in eddies. Also they should be easily removable. The acquired data is analyzed and validated against conventional water wave measurements. According to the author the comparison of results show good agreement, but no quantitatively statement is given.

TLS based range measurements of water waves in hydraulic modeling are conducted by Allis et al. (2011). Experiments are performed in a 30 m*0.6 m*0.42 m dimensional wave flume and a SICK LMS 200 TLS device with 905 nm wavelength and 75 Hz scanning frequency is used to measure a 1D profile of water waves. The TLS device is mounted 2.1 m above MWL and the laser beam covers approximately a 6m profile in flume axis. The water surface eleva-

tion measurements are validated against 8 capacitance wave probes (section 2.4.2) placed slightly aside of the measured profile, to not disturb the TLS measurements. The RMS error between TLS and capacitance wave probe is 3.62 mm. The applied wave periods are $T_p = 0.3 – 0.8$ s with wave steepness between 0.05 and 0.2. During the measurements they were experimenting with the additive Kaolinite ($\rho = 2.65$ g/cm³, $D_{50} = 20$ µm) to increase the reflectivity of the water. If the turbidity exceeds 40 NTU (section 2.3.2) reliable results are obtained. By supplying Kaolinite maximum incidence angles (section 2.5.2) up to 55° are possible. In order to exclude spike phenomena (section 2.5.2) a slant angle of 4 degrees is recommended. The Matlab post processing steps consists of controlling data consistency, transformation from polar to cartesian coordinates, substitution of spurious results, linear interpolation to create a regular sample spacing and filtering of the signal. The filtering is done with Fast Fourier Forward and Backward Transformation. The author outlines the need for more sophisticated filtering techniques to remove noise.

Based on this research another series of experiments are conducted by Blenkinsopp et al. (2012). Since the SICK LMS 200 device performed well in previously experiments it is used again in a larger wave flume with water depths up to 1.05 m. Significant wave heights between 0.16 m and 0.3 m are tested. The TLS device is mounted 3.55 m above mean water level (MWL). A 1D profile of approximately 6m length was measured. Kaolinite ($\rho = 2.65$ g/cm³, $D_{50} = 20$ µm) was supplied to increase the reflectivity of the water. Additionally a slight slope was installed in the flume to apply TLS based measurements of water waves to the study of wave transformation and especially shoaling processes. For validation purpose four capacitance wave probes (section 2.4.2) are installed slightly beside the measured profile, resulting in a RMS error of 6.1 mm between TLS and wave probe. This 2% of the total wave height. To achieve better comparability between TLS and wave probe, the TLS data is interpolated into 20 mm intervals. The maximum incidence angle (section 2.5.2) is 61.5°. With larger incidence angles no valid signal return is recorded. A promising correlation between the TLS and capacitance wave probe measurements of the water wave were found. Additionally the continuous temporal and spatial information of the wave profile from the TLS data allows for very detailed research of the wave motions. They concluded that TLS based range measurements of water waves are ideal for the detailed and fast investigation of water wave motions and wave transformation processes with sufficient accuracy (section 2.4.1).

An overview about the above presented TLS devices applied to water wave measurement is given in Tab. 2. With RMS error the difference in water surface elevation between the TLS measurement and the validation measurement device is described.

	Field	Labor-atory	TLS Device	λ [nm]\ f [Hz]	Measurement Principle	Time Varying Dimension	Range [m]	Wave Height [m]/ Wave Period [s]	Validation Method	RMSE [cm]
Blenkinsopp et al. (2010)	+		SICK LMS 200- 30106	905/37.5	pulsed ToF	1D (line)	5- 8	$H_s = 0.58/T_p = 11$	ultrasonic altimeter	4.0
Allis et al. (2011)		+	SICK LMS 200- 30106	905/37.5	pulsed ToF	1D (line)	2- 4	$T_p = 0.3- 0.8$	capacitance probes	0.36
Evans (2010)		+	Topcon GLS 1000	-	pulsed ToF	2D (area)	-	-	-	-
Blenkinsopp et al. (2012)		+	SICK LMS 200- 30106	905/37.5	pulsed ToF	1D (line)	3- 5	Hs = 0.16- 0.3/ Tp = 1.02- 2.02	capacitance probes	0.61
Vousdoukas et al. (2011)	+		Velodyne HDL-64E 360	905/15	pulsed ToF	2D (area)	70	-	-	-
Belmont et al. (2006)	+		Self Build	532/20000	-	1D (line)	200	-	wave probes	3.7
Park et al. (2011)	+		Optech Ilris HD	1535/10000	pulsed ToF	2D (area)	100	$H_m = 1$	wave staff	5.3
Maslov et al. (2000)	+		Polyus RDI Nd:YAG	534, 355, 266 /10	-	1D (line)	-	-	-	-
Harry et al. (2010)	+		Riegl VZ400	nearinfrared	pulsed ToF	2D (area)	-	$H_s = 1.3/ T_z = 5.9$	-	-
Irish et al. (2006)	+		Optech SLX-3A	infrared/10	pulsed ToF	0D (point)	6- 16	$H_{mo} = 0.2- 1.5$	pressure meter	5.0
Guenther et al. (2000)	+		Optech Nd:YAG (SHOALS)	532, 1064 /200	pulsed ToF	2D (area)	200- 500	-	USACE data	20

Tab. 2: TLS based range measurement from water waves

2.7 Influencing Parameter on Scanning Water Waves

Soudarissanane et al. (2009) came up with a list of parameters influencing the quality of TLS scan points. Based on their classification the list is adapted to influencing parameters for TLS based range measurements from water waves. Since this is a relatively new measurement tool no such list is available yet.

The parameters are divided into three categories:

1. TLS parameter,

2. Geometry and atmosphere parameter

3. Water parameter

Additionally, combined parameter are described resulting from at least two of the above mentioned parameters. The influencing parameters are summarized in Tab. 3 to provide a full overview and better understanding of TLS based range measurements from water waves.

2.7.1 TLS Parameter

The TLS parameter influencing the measurement of water waves are presented in this section.

The LASER material inside the TLS device is stimulated to emit a LASER beam either in discrete pulses or as a continuous beam (section 2.5.2). This beam has a certain width at the focus lens. The beam divergence is dependent on the coherence of the light and the refraction factor of the propagation medium (section 2.5.2). The beam has a certain power which allows for different measuring distances and intensities of the reflected signal (section 2.5.2).

A whole set of TLS parameters are given in resolutions:

The spectral resolution describes the emitted wavelength of the LASER (section 2.5.1). If it is a bandwidth of wavelengths the spectral width describes the purity of the signal (section 2.5.1). The temporal resolution, specially scanning rate and sampling rate (section 2.5.2) determine the scanning speed of the device. The range resolution determines the depth accuracy of the measurements. Angular resolution describes the horizontal and vertical measurement step width, which results in a certain point density of the measurements at the distant target (section 2.5.2). With radiometric resolution the TLS ability to detect small changes in intensity is described.

In order to deflect the LASER beam in the desired direction an optomechanical device is used (section 2.5.2). Most of the TLS devices used for water wave measurement are provided with a rotating mirror (Palmer mirror, section 2.5.1).

Considering the measurement principle Time- of- Flight and Phase- Shift TLS devices are divided (section 2.5.2). Also different principles of peak detection are divided, maximum peak, average peak and multiple peak detection (section 2.5.2).

The accuracy and precision result in systematical and statistical errors of the TLS measurement (section 2.4.1).

Finally the TLS Software influences the quality of water wave measurements. Mostly, intensity thresholds are implemented in the TLS or filters adjusted and correction or interpolation methods applied which may influence the signal. Since water wave measurements show low reflection intensities, no thresholds or filters are desired, to not exclude valuable data by the TLS device itself.

2.7.2 Atmosphere/ Geometry Parameter

By atmospheric parameters all the influences on the measurement quality while the laser beam travels through the propagation medium are described. Influences by temperature and artificial or natural lighting are identified, as well as fog, cloud, rain and dust particles in the air (section 2.5.2).

Also the geometrical set-up of the TLS device and its distance to the target, as well as the resulting incidence angle, are of importance and influence the quality of the water wave measurements (section 2.5.2).

2.7.3 Water Parameter

In this section a summary of water parameter influencing the quality of water wave measurements is given. Surface roughness of the reflecting object is of major importance for the measurements. Small ripples and capillary waves of a few centimeters (section 2.2.1), the presence of foam (section 2.3.1) and turbulence, introduced to the water by breaking waves (section 2.2.4), will increase the surface roughness.

Natural turbidity created by small particles within the water as well as artificial turbidity, by adding particles to the water, is of influence for TLS based range measurements of water waves (section 2.3.2). Turbidity has an impact on the light scattering characteristics of the water.

Additionally the wave characteristics like water depth, wave height, period and length (section 2.2) resulting in different wave steepness influence the quality of water wave measurements.

Also wave celerity, as a dynamic parameter, may influence the quality of water scans.

2.7.4 Combined Effects

A certain number of combined effects, resulting from the combination of several parameters listed under section 2.7.1 to section 2.7.3 are identified.

The laser beam footprint (section 2.5.2) is a combination of the measuring distance, divergence and diameter of the laser beam.

Point spacing (section 2.5.2) is a function of the measuring distance and angular resolution.

Maximum incidence angle (section 2.5.2) is dependent on the set-up of the TLS device and the surface roughness of the water, as well as on the water turbidity.

Specular and diffuse reflection (section 2.5.2) are influenced by the surface roughness the incidence angle among others.

Spike phenomena (section 2.5.2) are due to the TLS device set-up, the measured distance and the water surface roughness.

With a disadvantageous TLS device set-up and dependent on the wave geometry, shadowing effects (section 2.5.2) may occur on the rear side of the wave crest.

Water surface ambiguity depends on the spectral resolution of the TLS device, water turbidity amongst others.

The parallel movement of wave and TLS device may also influence the quality of the measurements.

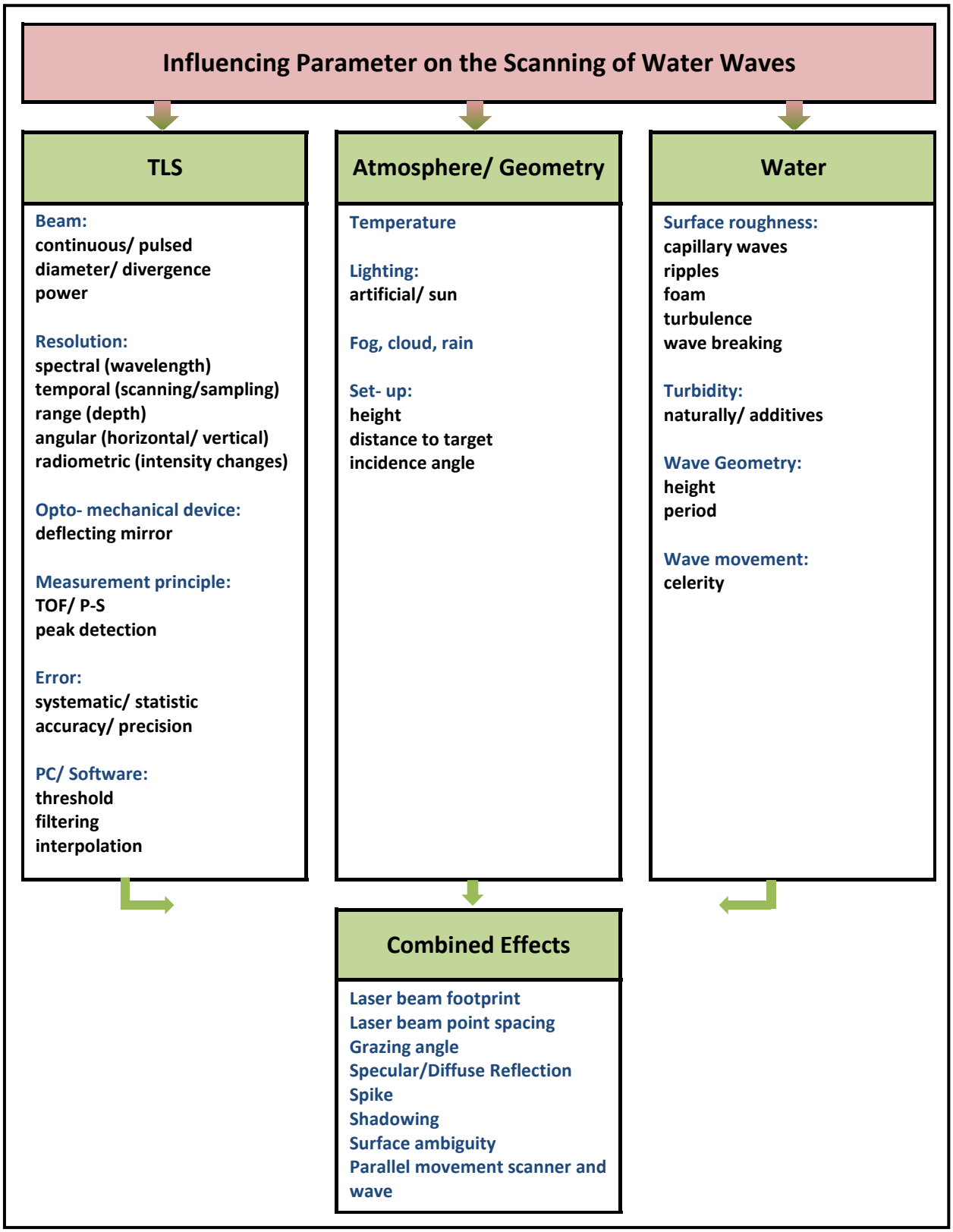

Tab. 3: Influencing parameter on TLS based range measurement of water waves

2.8 Summary and Conclusions

From literature review important influencing parameters on TLS based range measurements of water waves were identified and summarized in the parameter inventory. A basic distinction was made between TLS, geometry/atmosphere and water parameter, as well as combined parameters resulting from at least two of the above mentioned categories.

Also a basic overview about water waves and its reflection characteristics, the principles of TLS based measurements and water sensor devices in hydraulic modeling was given.

From spectral reflectance curves for seawater a striking peak at 2500 nm incidence wavelength was observed. Hence, TLS devices in this range should be investigated.

Most of the TLS devices applied to water wave measurements were operated in the near infrared spectrum (800 nm to 1500 nm) and with ToF measurement principle.

Foam and bubbles on the water surface as well as turbid water will increase the reflectivity.

TLS based range measurements from the water surface in hydraulic modeling were conducted by Allis et al. (2011) and Blenkinsopp et al. (2012). It is the purpose to set-up a working measurement in the TU Delft wave flume facility based on this experiments. This will also lead to a further understanding of the problems related to TLS based range measurements from water waves and the following wave field reconstruction. If this is working, the set-up can be transferred to the Delta Flume.

To provide a better understanding about TLS based range measurements from water waves available data sets from already conducted experiments will be analyzed and the wave field reconstructed and assessed.

3 Experimental Overview

Available data sets obtained with several TLS devices are presented in section 3.1 and its measurement quality and applicability for the Delta Flume discussed.

In a second step the detailed experimental set-up of a SICK LMS511 device in case A (green water of TU Delft wave flume facility) is given in section 3.2.

3.1 Available Water Surface Scan Data in Hydraulic Modeling

Several data sets from TLS based range measurement of water waves are available. In this section they are divided into case A to case F (section 3.1.1 to section 3.1.6). Each case contains a short description of the TLS device, the set-up and the water parameter. A first visualization, in order to determine the quality of the reconstructed wave field, is given.

In section 3.1.7 the cases are evaluated and based on the quality of the reconstructed wave field and its applicability to the Delta Flume preferred cases are selected for further analysis.

3.1.1 Case A: SICK LMS511 Pro SR Applied to Green Water in TU Delft Flume

In November 2012 experiments were conducted in the TU Delft Wave flume facility. A SICK LMS511 Pro SR was adjusted approximately 1.2 m above the water surface. The TLS, water and set-up parameter are given in Fig. 15 (more detailed in section 3.2).

A first visualization plot of the reconstructed wave field is shown in Fig. 15. Approximately 2 wave lengths are constantly visible from the reconstructed wave field.

A peak in nadir, changing with the moving wave face is clearly visible.

Since it is a rather small flume (l = 50 m, w = 0.8 m, h = 1.05 m) the dimensions are not comparable to the new Delta Flume (section 2.1).

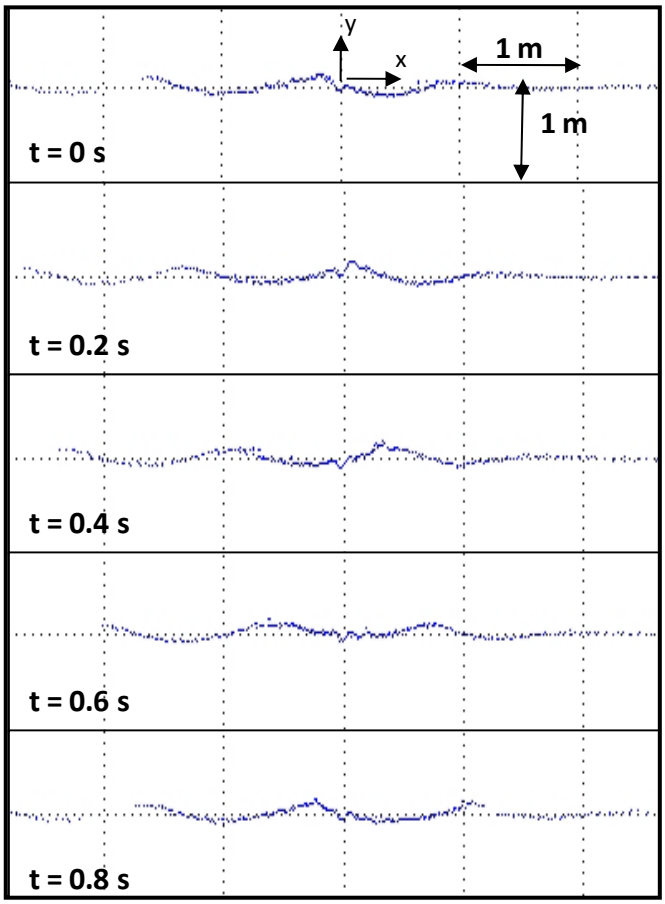

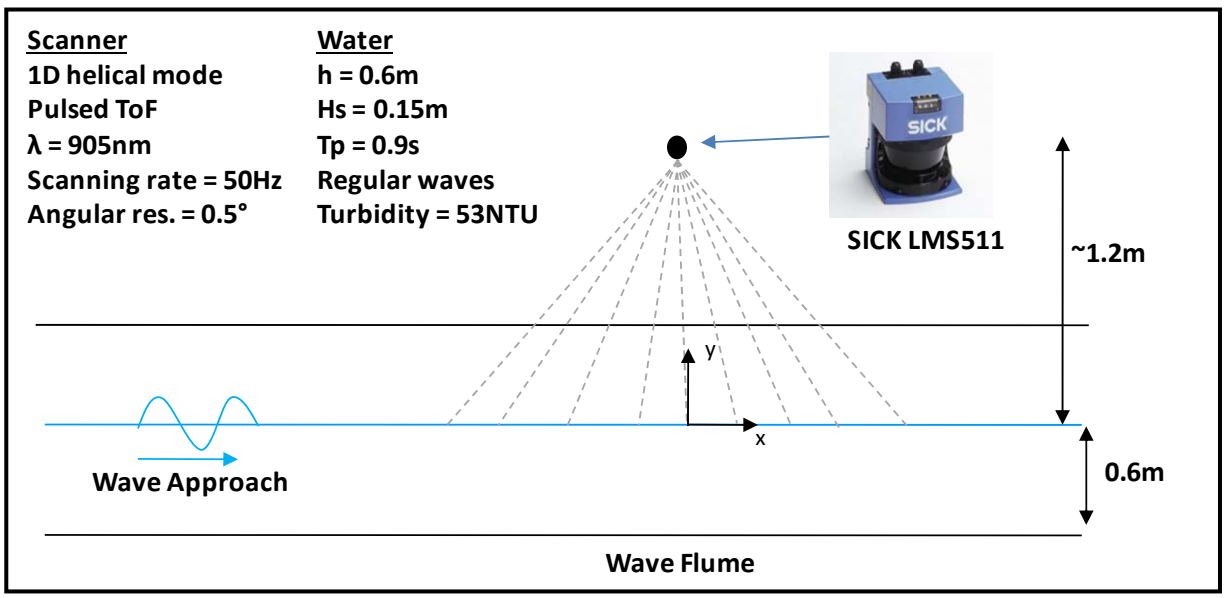

Fig. 15: Set-up case A (below) and reconstructed wave field (above)

3.1.2 Case B: Faro Photon 120 Applied to Green Water in TU Delft Flume

A Faro Photon 120 was applied in the same experiment described in section 3.1.1. The TLS was mounted approximately 1.5 m above the water surface scanning in an artificial helical mode (Fig. 16).

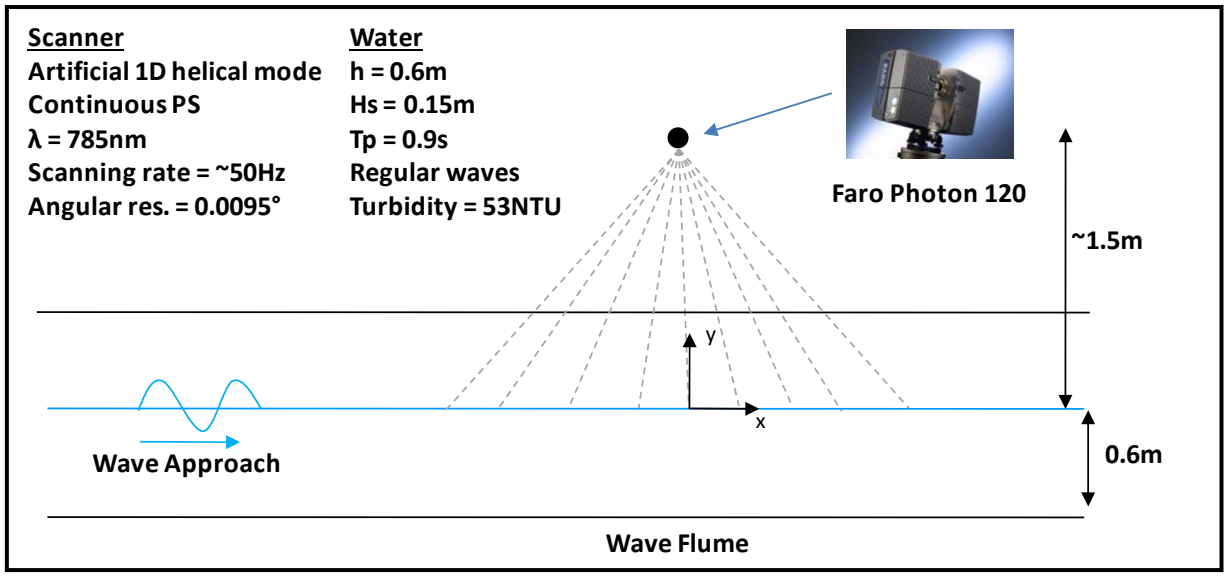

Fig. 16: Set-up case B

Usually measuring with the Faro Photon 120 includes a horizontal rotation as well. In this case only the TLS head (excluding the tripod) was placed on the measurement construction (Fig. 17). In this way the head of the TLS could not move horizontally and only the mounting at the bottom of the TLS device was rotating. This caused some problems when reconstructing a wave field from the data, since the TLS automatically assumes a horizontal rotation.

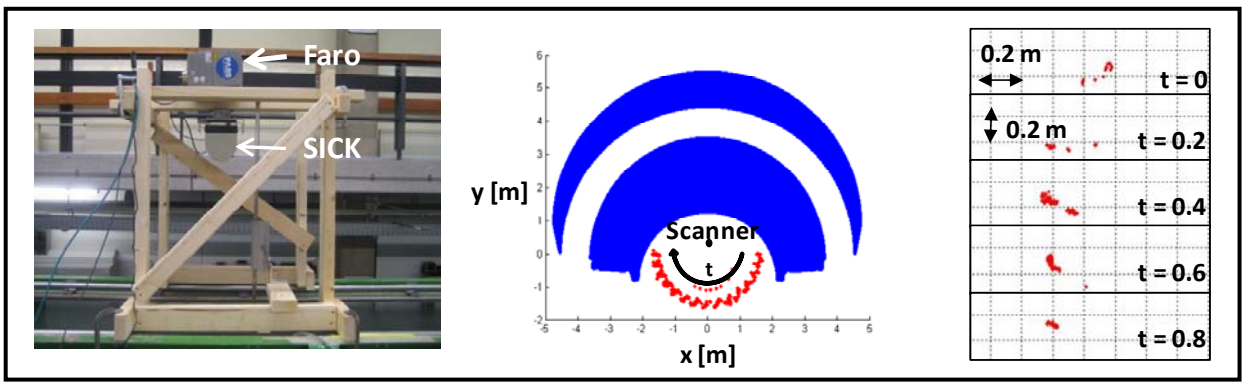

Fig. 17: TLS mounting construction (left), obtained point cloud = red points represent scan from wave (middle), reconstructed wave field (right)

In Fig. 17 a the reconstructed wave field is shown. Only the red points are points from the water surface (blue points from ceiling etc.). The results are of very poor quality and hardly any wave movement can be observed.

3.1.3 Case C: Riegl VZ-400 Applied to Green Water in Deltares Scheldegoot Flume

Experiments are conducted the 1. of May by Gerben Ruessink and Bas Hofland in the Deltares Scheldegoot wave flume facility with a Riegl VZ-400 TLS device.

The TLS was mounted above the wave flume (Fig. 18) in the green water area, where fully developed and unbroken waves are present. The measurement was performed in helical mode within a predefined area (50° to 80° incidence angle). Besides the steep angle of incidence, the reconstructed wave field shows that at least one full wave length is visible and a high amount of reflected points are present.

There is a problem of shadowing effects at the rear side of the wave. Since the angle of incidence is steep some parts behind the wave crest couldn´t be detected with the TLS device.

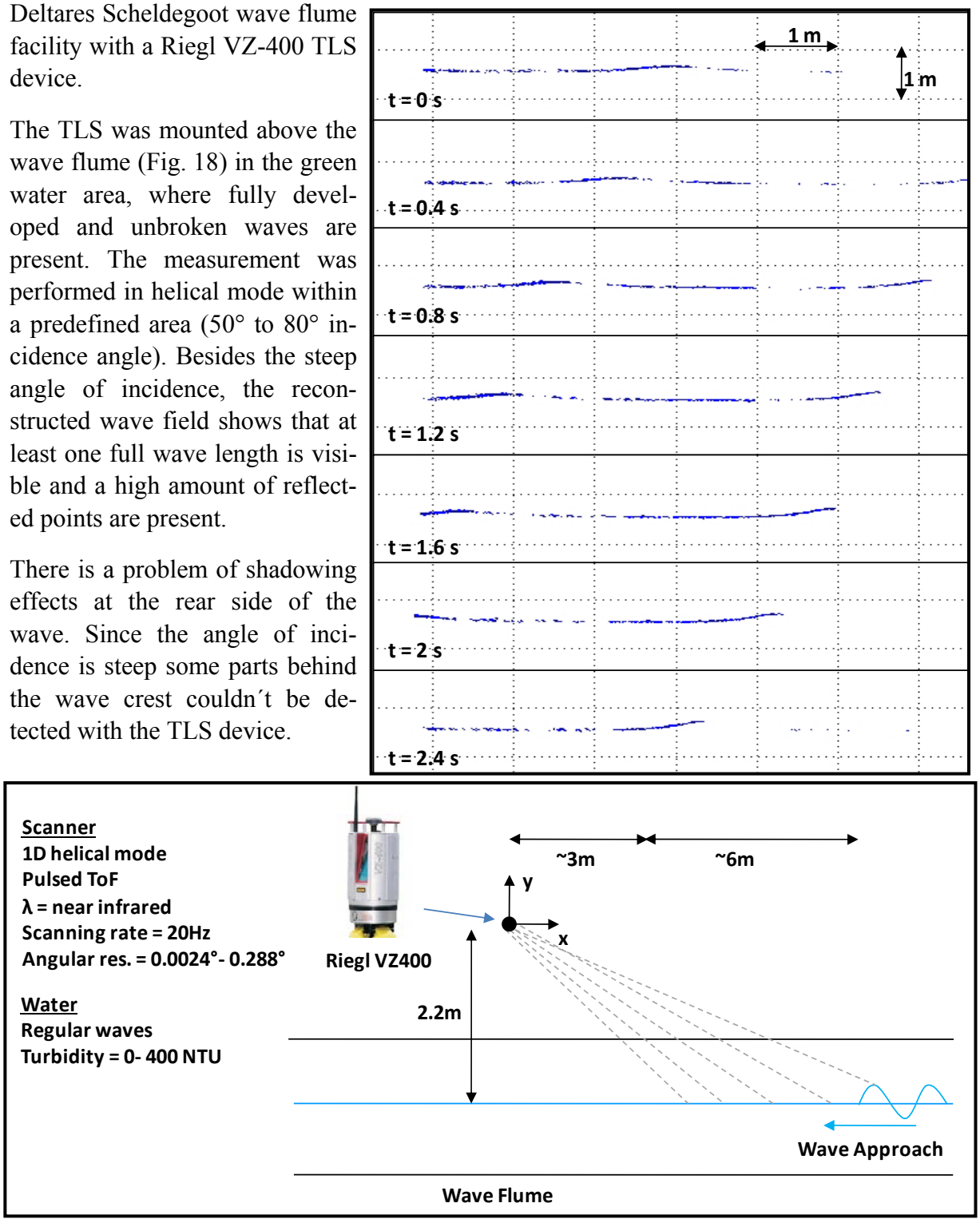

Fig. 18: Set-up case C (below), reconstructed wave field (above)

3.1.4 Case D: SICK LMS511 Applied to Run-up Zone in Delta Flume

In spring 2012 experiments with a SICK LMS511 were conducted by Chris Blenkinsopp and Dan Howe in the Delta Flume (section 2.1). It was part of the Bardex II experiments (Masselink et al. (2013)). The TLS device was mounted above the shoreline. The distance between TLS device and still water surface was approximately 4 m to 5m, as shown in Fig. 19.

A breaking wave, the change in shape and finally the run-up tongue are visible from the reconstructed wave field.

It was reported that up to 20 m distant waves were detected with this method. Here, it is an advantage that the breaking waves introduce a lot of foam and bubbles in the water surface resulting in improved reflection characteristics.

When using the same TLS device (in later experiments) in the green and still water of the Delta Flume, no good results were obtained.

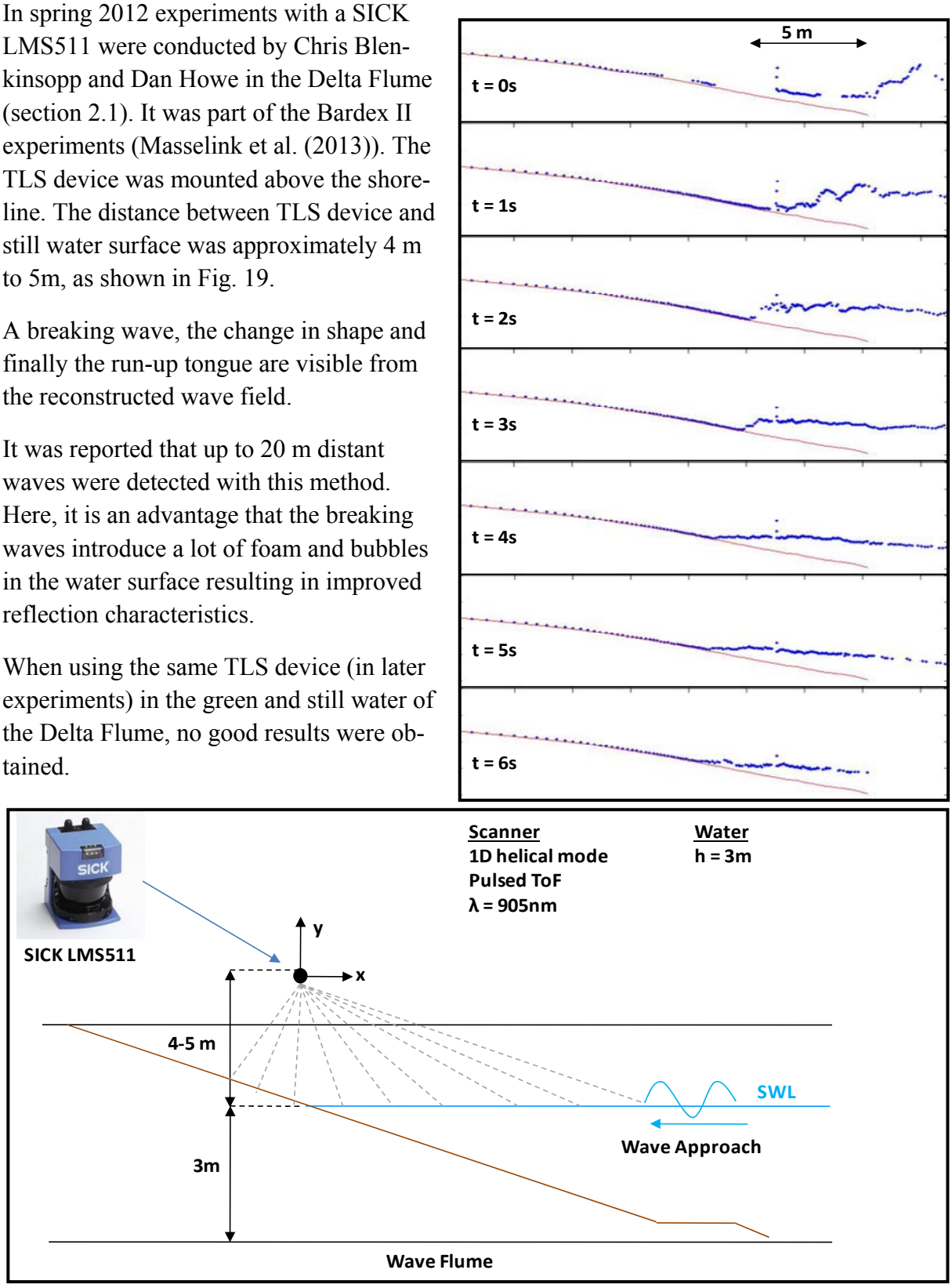

Fig. 19: Set-up case D (below) and reconstructed wave field (above)

3.1.5 Case E: Faro Photon 120 Applied to Run-up Zone in Delta Flume

From 10. to 19. of October 2011 experiments were conducted by Bas Hofland and Roderik Lindenbergh in the run-up zone of the Delta Flume (section 2.1).

The measurement from the run-up zone showed promising results. The set-up of measurement is given in Fig. 20 and the reconstructed wave field shows that the approaching and breaking wave front is clearly visible. After breaking, as well as at the top and back of the wave crest the measurements deteriorate.

Analyzing the intensities of the scan data might help to distinguish between water and bottom scan points in the run up zone. As it turns out that the water- land boundary was hard to detect from the dataset.

Addtionally measurements were taken in the green water of the Delta Flume, where fully developed and unbroken waves were present. The measurements from the green water turned out to be not useful, since no full waves were visible and the FoV has a maximum length of 0.3 m.

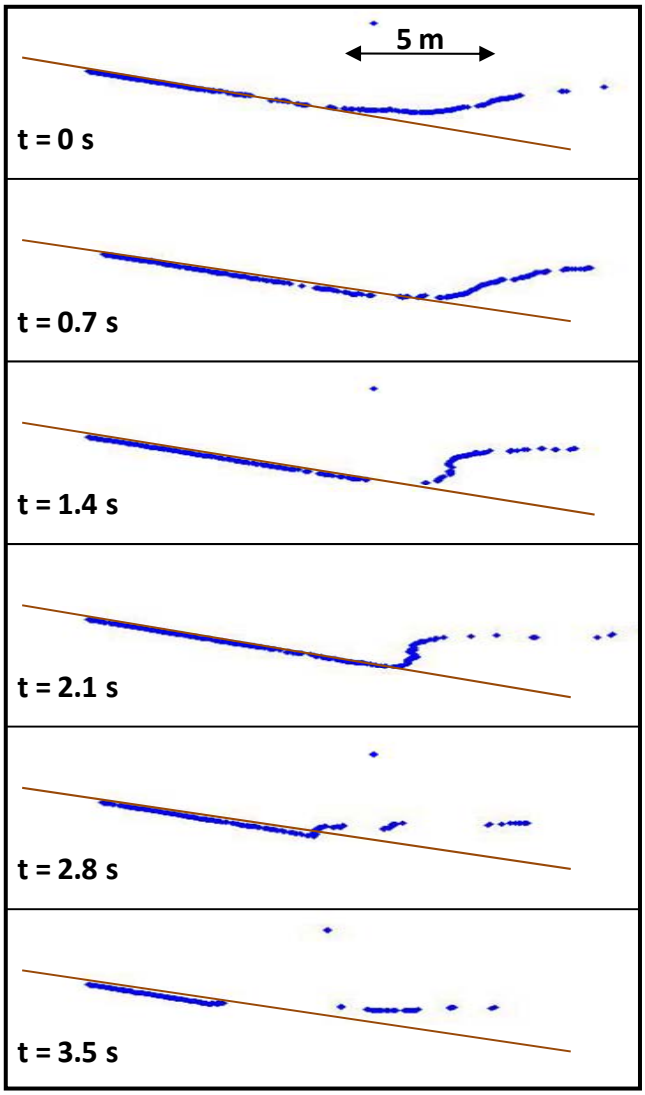

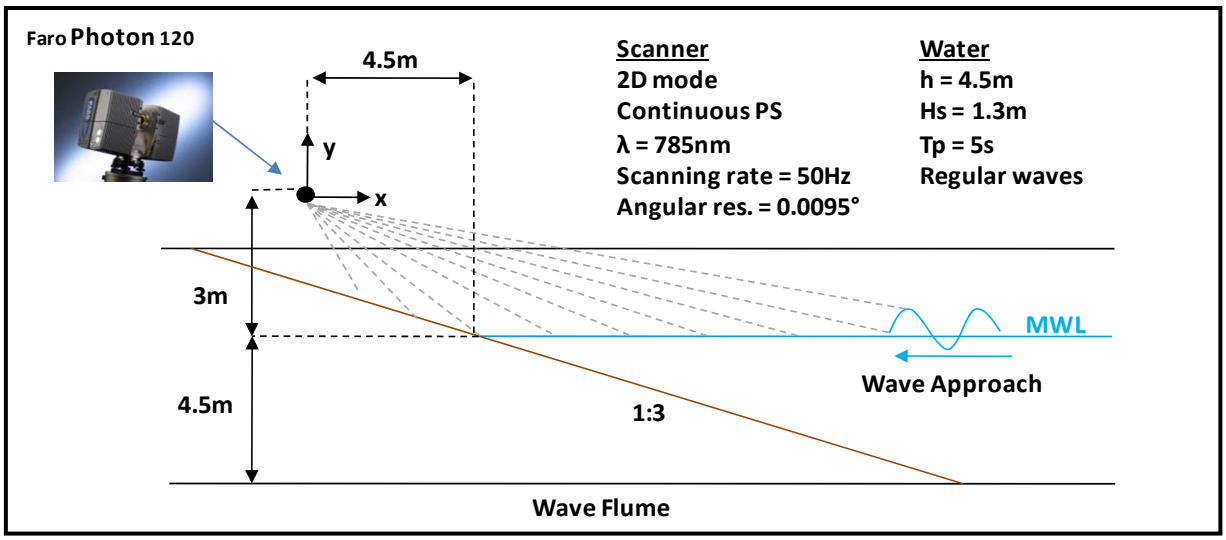

Fig. 20: Set-up case E (below) and reconstructed wave field (above)

3.1.6 Case F: SICK LMS511 Pro SR Applied to Different Heights Measurement

Since the SICK LMS511 worked well in the TU Delft flume (section 3.1.1) it's applicability for the Delta Flume was tested. It is the purpose to gather experience about the SICKs ability to measure from different heights. The location provides the possibility to scan from different heights into a basket of water (Fig. 21). Findings concerning the resolution, the measurement accuracy and noise level, dependant on the scanning height are obtained. The results for the scan heights of 0.5 m, 4 m, 10 m and 15m are visualized in Fig. 18. With increasing TLS height the resolution in horizontal direction is lowered.

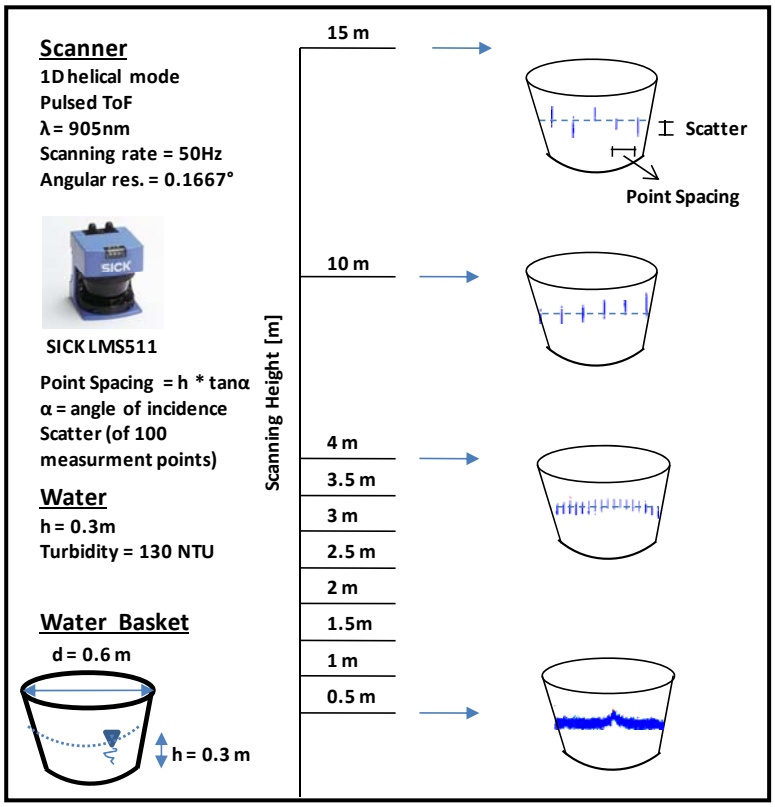

Fig. 21: Set-up case F, scanning from different heights in water basket (point density visible in accumulation of blue vertical lines in the basket)

3.1.7 Conclusion Case A- F

Case A, C and D show qualitatively good results, at least one full wave length is visible in the reconstructed wave field. Also the amount of recorded points is higher compared to the other cases. Analysis is focused on this three cases.

The simple measurement set-up and the wider FoV in case A allow for more complex analysis. Also good results with the TLS device from case A are reported by Blenkinsopp et al. (2012) and Allis et al. (2011). Hence, the experimental set-up is described in detail in section 3.2.

Case F is not a water wave measurement and is not taken into consideration. Still results might be of interest when scaling up the findings from case A to the Delta Flume dimensions (section 2.1). Since the same TLS as in case A is used and the measuring height is varied up to possible Delta Flume measurement heights (5 m- 15 m).

	Scanner	Facility	Scan Position	Quality	Further Research
Case A	SICK LMS 511 Pro SR/HR	TU Delft Flume	green water	good	✓
Case B	Faro Photon 120	TU Delft Flume	green water	bad	
Case C	Riegl VZ400	Deltares Scheldegoot	green water	good	✓
Case D	SICK LMS 511	Deltares Delta Flume	run- up zone	good	✓
Case E	Faro Photon 120	Deltares Delta Flume	run- up zone	middle	
Case F	SICK LMS511 SR	Deltares Zouthal	basket of water	good	

Tab. 4: Evaluation case A to F (case A, C and D selected for further research):

3.2 Experimental Set-up SICK LMS511 in case A (TU Delft Flume)

The experiments were conducted 1. and 2. November 2012 by Manuel Diaz, Jinhu Wang and Maximilian Streicher. In close cooperation with Wim Uijttewaal, Jaap van Duin, Sander de Vrede and Roderik Lindenbergh from TU Delft, Bas Hofland from Deltares and Henk Wijengaard and Raul Panday from SICK company.

Based on the findings from parameter inventory (section 2.7) the experimental set-up is divided in TLS, atmosphere/ geometry and water parameters.

3.2.1 TLS Parameters

During experiments several type of TLS devices were used. In case A only the SICK LMS511 Pro SR is described. It is equipped with a pulsed laser beam and ToF measurement principle (section 2.5.2). The laser beam has a spectral resolution of 905 nm. The beam diameter at the opening is 13.6 mm and the beam divergence is 11.9 mrad (Fig. 22). The TLS device is intended to measure in helical mode, resulting in a 1D profile (section 2.4).

A scanning rate of 50 Hz and an angular resolution of 0.5° are applied. The function to record multiple echoes is switched off as well as the fog (less sensitive in the near range < 7 m) correction. The fog filter would exclude valuable data from the low reflecting water.

In the specification sheet the sum of systematic and statistical error is about 31 mm for a range between 1 m and 10 m (Appendix B).

	SICK LMS511 Pro SR
Wavelength [nm]	905
Scan rate [Hz] [lines/s]	50
Range Meas. Principle	ToF (pulsed)
Beam Diameter at head [mm]	13.6
Beam Divergence [mrd]	11.9
Angular Resolution [°]	0.5
Systematic Error 1 -10m [mm]	25
Statistical Error 1- 10m [mm]	6

Fig. 22: SICK LMS511 Pro Standard Resolution

3.2.2 Geometry\ Atmosphere Parameters

Since the experiments were conducted inside the TU Delft laboratory artificial lighting from the ceiling was present. No influence of fog, cloud or rain could be observed and the indoor temperature was around 20° C.

A wooden mounting construction for the TLS device (Fig. 23) was adjusted on the sidewalls of the wave flume. The construction should allow for installation of the TLS in sufficient height above the water and a free field of view on the water surface, without bricks interrupting the laser beam. The final prototype had a height of 1 m, a width in flume direction of 0.8 m and a depth perpendicular to the flume axis of 0.8 m. Since the TLS device was mounted below the topmost brick, the source of the laser beam is approximately 0.2 m lower than the height of the mounting construction. This leads to a vertical distance towards the still water surface of approximately 1.2 m.

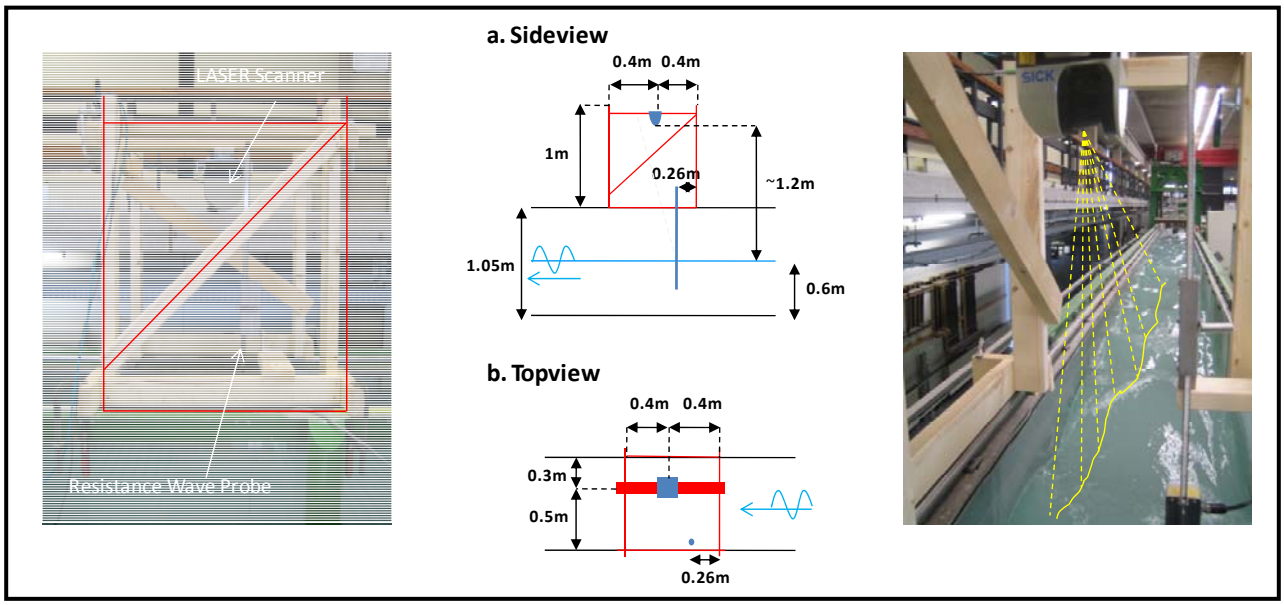

Fig. 23: TLS mounting construction

3.2.3 Wave Flume\ Water Parameters

The TU Delft Wave Flume facility is 50 m long, 0.8 m wide and 1.05 m high. During experiments a water level of 0.6 m was present, as shown in Fig. 24.

At the one end a wave maker was responsible to steer in the desired waves, defined in the internal software. On the other side a dissipative slope was installed to make sure that disturbing reflection phenomena were minimized. Approximately 20 m from the wave paddle the mounting construction for the TLS device (section 3.2.2) was applied.

The turbidity of the water was varied during experiments by using the additive Kaolinit ($\rho = 2.65$ g/cm³, D50 = 20 µm). In an extra basket the Kaolinit was given in suspension and then manually poured into the flume over a total length of approximately 8 m (4 m to each side of the TLS mounting construction). Stirring with a stick should optimize the equal distribution of Kaolinit. Then, a probe was taken below the TLS device and the turbidity was measured.

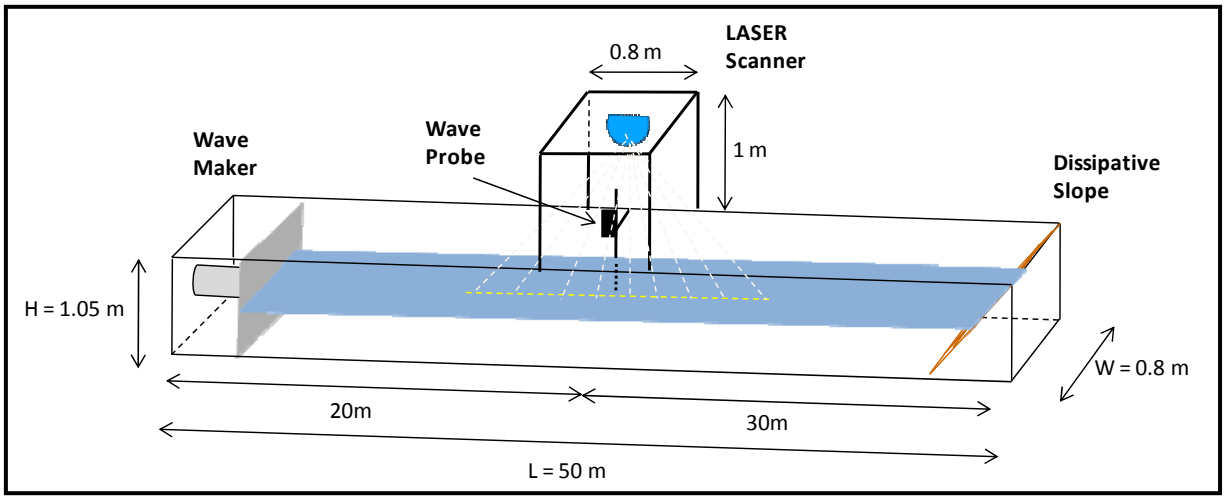

Fig. 24: TU Delft wave flume facility

As a second variable the wave characteristics were changed during experiments. Regular waves with wave heights H (section 2.2.1) between 0.05 m and 0.2 m were generated. Corresponding wave periods T (section 2.2.2) varied between 0.9 s and 1.7 s. The range of resulting wave steepness (H/L) varied from 0.03 to 0.12. An overview of the conducted tests is given in Tab. 5

Test Number	Date	Turbidity [NTU]	Wave Type	Wave Height H_s [m]	Wave Period T_p [s]	Wave Steepness H/L_0 [-]	Wave Breaking
1	1.11.12	2.13	regular	0.15	1.7	0.03	No
2	1.11.12	11.1	regular	0.15	1.7	0.03	No
3	1.11.12	25.1	regular	0.15	1.7	0.03	No
4	1.11.12	35.2	regular	0.15	1.7	0.03	No
5	1.11.12	33	regular	0.15	1.7	0.03	No
6	1.11.12	45.4	regular	0.15	1.7	0.03	No
7	1.11.12	89.5	regular	0.05	1	0.03	No
8	1.11.12	-	regular	0.1	0.9	0.08	No
9	1.11.12	-	regular	0.15	1.7	0.03	No
10	1.11.12	22	regular	0.15	1.7	0.03	No
11	1.11.12	33.5	regular	0.15	1.7	0.03	No
12	1.11.12	64.4	regular	0.15	1.7	0.03	No
13	1.11.12	42.1	irregular	0.15	0.9	0.1	No
14	1.11.12	53.3	regular	0.15	0.9	0.1	No
15	2.11.12	11.8	still water	-	-	-	No
16	2.11.12	20	still water	-	-	-	No
17	2.11.12	46	still water	-	-	-	No
18	2.11.12	66	still water	-	-	-	No
19	2.11.12	69	still water	-	-	-	No
20	2.11.12	60	still water/ floating particles	-	-	-	No
21	2.11.12	34.6	still water/ ventilator	-	-	-	No
22	2.11.12	29	irregular waves	0.15	1.2	0.1	No
23	2.11.12	-	irregular waves	0.2	1.2	0.1	No
24	2.11.12	19	irregular waves	0.25	1.2	0.1	Yes
25	2.11.12	18	regular waves	0.15	0.81	0.12	Yes
26	2.11.12	16	regular waves	0.2	0.81	0.12	Yes

Tab. 5: Test overview

In order to increase the turbulence in the wave field and to improve the reflectivity of the water, irregular (test 13, 22 - 24) and breaking (test 24 - 26) waves were tested as well.

As it was hard to estimate the 'true' water surface from the scan data and to validate the measurements afterwards a resistance type of wave probe was adjusted below the TLS and slightly beside the measured profile. Also, before each test a white piece of paper was put on the water surface in the area of the measured profile to give a first estimation of the 'true' water surface.

In test 20 small plastic particles floating on the surface were used. In test 21 a ventilator was applied below the TLS pointing towards the water surface, to generate capillary waves on the water surface (section 2.2.1).

Test 15, until test 21 were obtained during still water conditions.

3.2.4 Test Procedure

First the turbidity in the water was adjusted by adding a defined amount of Kaolinit. A probe below the TLS was taken and the turbidity measured.

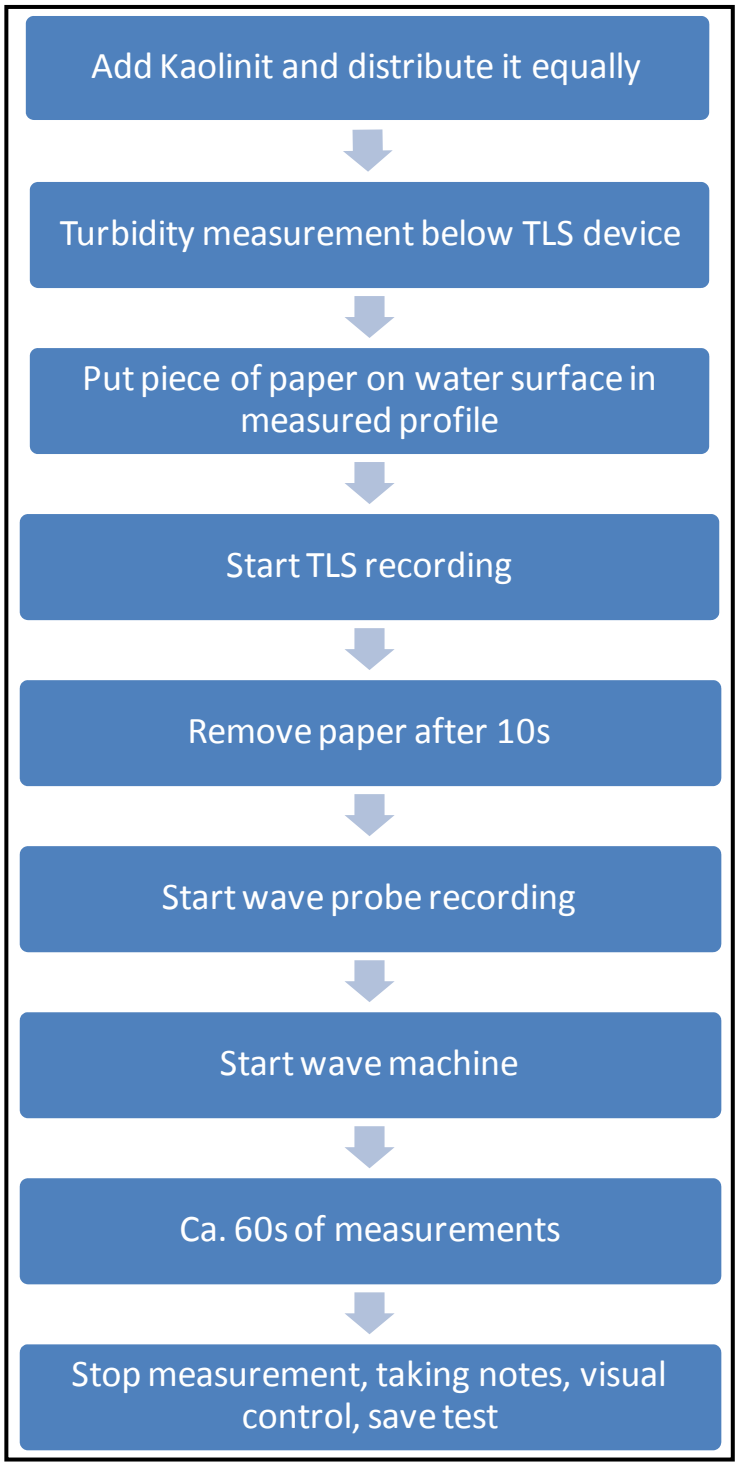

Fig. 25: Flow chart of test procedure

A piece of paper was put on the water approximately below the TLS and in the area of the measured profile. The recording of the TLS was started. After ca. 10 s of measurement, the piece of paper was removed and the wave probe recording started. As a next step the wave maker was switched on. The duration of each measurement, with waves present, was approximately 60 s. Afterwards, the TLS and wave gauges were switched off and finally the wave maker was stopped again.

A first visual quality check was performed and the test saved. A logbook of each test should guarantee for continuous and complete data sampling. Also observations and findings could be notated here. The full test procedure is given in Fig. 25.

4 Analysis of Scan Data From SICK LMS511

The simplified analysis of the still water surface profile (section 4.1) and its observed phenomena will lead to a more advanced understanding and analysis of water surface profile with present waves (section 4.2).

4.1 Still Water: Observed Phenomena

From the still water surface profile expected problems for TLS based range measurements can be detected and correction methods elaborated. Afterwards, the analysis can be applied to dynamic water wave conditions. In Fig. 26 several still water profiles are plotted in the same figure and observed phenomena highlighted.

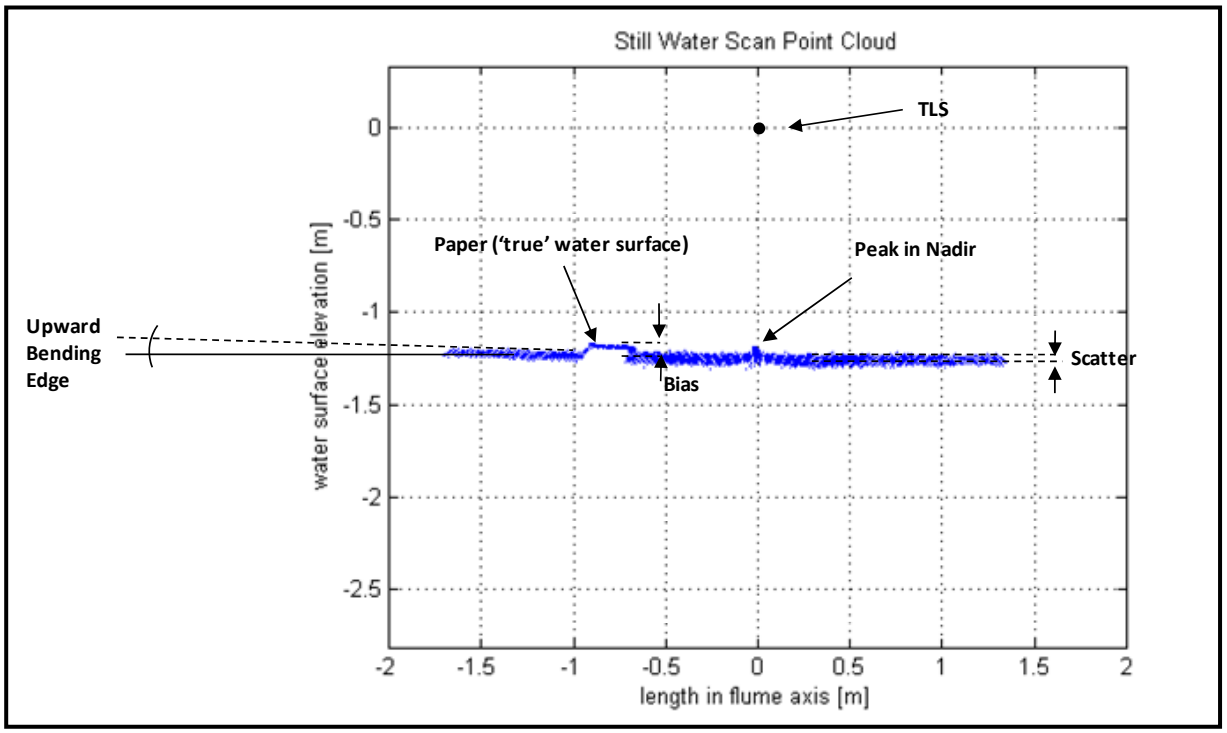

Fig. 26: Still water scan data (several profiles plotted in the same figure)

The recorded profile has a length of 1.3 m to the right and 1.7 m to the left of the TLS device.

In nadir (beam perpendicular to the water surface) a striking peak in water surface elevation is observed and analyzed in section 4.1.1. The peak is approximately of the same height as the water surface, indicated by a white piece of paper placed on the water surface, within the measured profile.

Also a bias between the water surface (= paper height) and the mean of the scan points is observed. This bias is decreasing towards the side, resulting in an upward bending of the obtained profile. At the far most end the height converges towards the water surface (= paper height). A physical explanation of the observed behavior is given and a possible correction method suggested in section 4.1.4.

A slight asymmetry in the profile is observed since the length on the left side (1.7 m) of the TLS and the according upwards bending towards this side is higher than on the right side (length 1.3 m) from the TLS.

Also variations in range measurement (scatter) along the water surface are observed. This deviation in the range measurements is researched in section 4.1.2.

4.1.1 Filtering, Interpolation and Averaging of Water Surface Profile

For further analysis, the obtained water surface profile is transformed from polar coordinates back to cartesian coordinates, a geometrical and reflection filter is applied and finally the scan points are interpolated as well as temporally and spatially averaged.

Polar and Cartesian Coordinates

Some parts of the analysis require the conversion of the scan points from one coordinate system into the other. Internal data collection of the TLS device is in polar coordinates. The transformation into Cartesian coordinates is shown in Fig. 27.

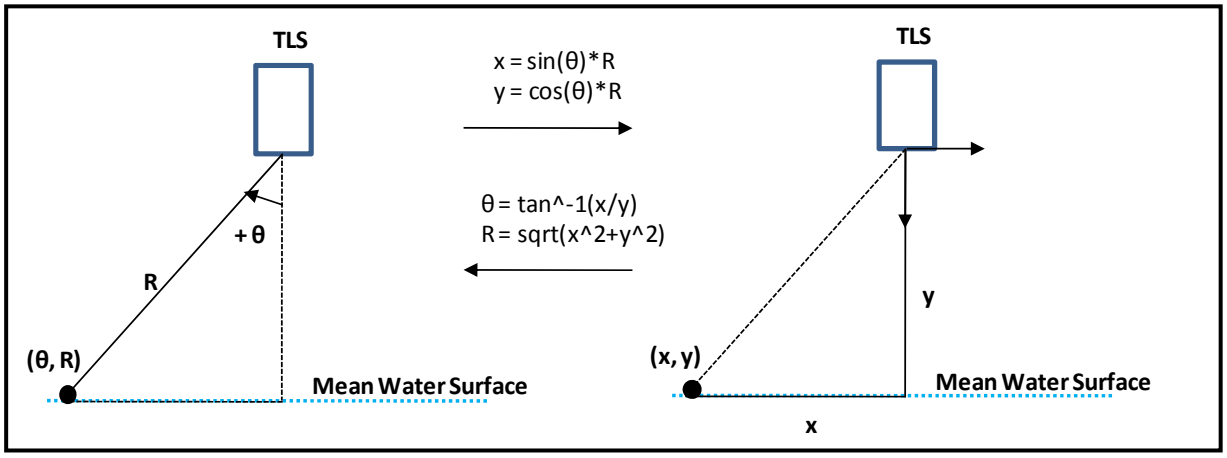

Fig. 27: Polar and cartesian coordinates

Geometrical Filter

Scan points taken from different locations but the water surface are excluded (e.g. points from the ceiling, the wave maker at the end of the flume or points from the bottom of the flume).

Since the vertical distance between TLS device and water surface is approximately 1.2 m, a buffer in vertical direction between 1 m and 1.5 m is applied. Only points within this y- range are selected.

A buffer in x- direction between +6 m to -6 m from the TLS device is chosen. Only points within this x- range are selected for further analysis.

Field of View (FoV) With 95% Reflection

A Field of View (FoV) is calculated to reduce the total number of scan points in the measured profile and to increase the quality of the remaining profile.

Based on the angular resolution of the TLS device scan points from the water surface are obtained in predefined steps. With increasing incidence angle and distance less points are recorded and the signal deteriorates. With coordinate transformation the x- point coordinates in flume axis for each incidence angle and range can be determined. The laser beam will pass by each x- point coordinate a predefined number of times during testing. Not every time a reflection will be recorded (due to low reflectivity of water, large incidence angle, etc.). The number of reflections for each x- point coordinate over the whole test duration is counted and compared to the theoretical number of possible reflections. The result is given as a percentage. If 100 scans are taken during testing and only 95 reflections measured for a specific x-point coordinate, 95% reflection are calculated. Each x- point coordinate in the profile will be analyzed and only x- point coordinates which exceed 95% reflection are used to determine the FoV. The FoV is then determined by the distance between the minimum and maximum x-point coordinate with at least 95% reflection, as shown in Fig. 28.

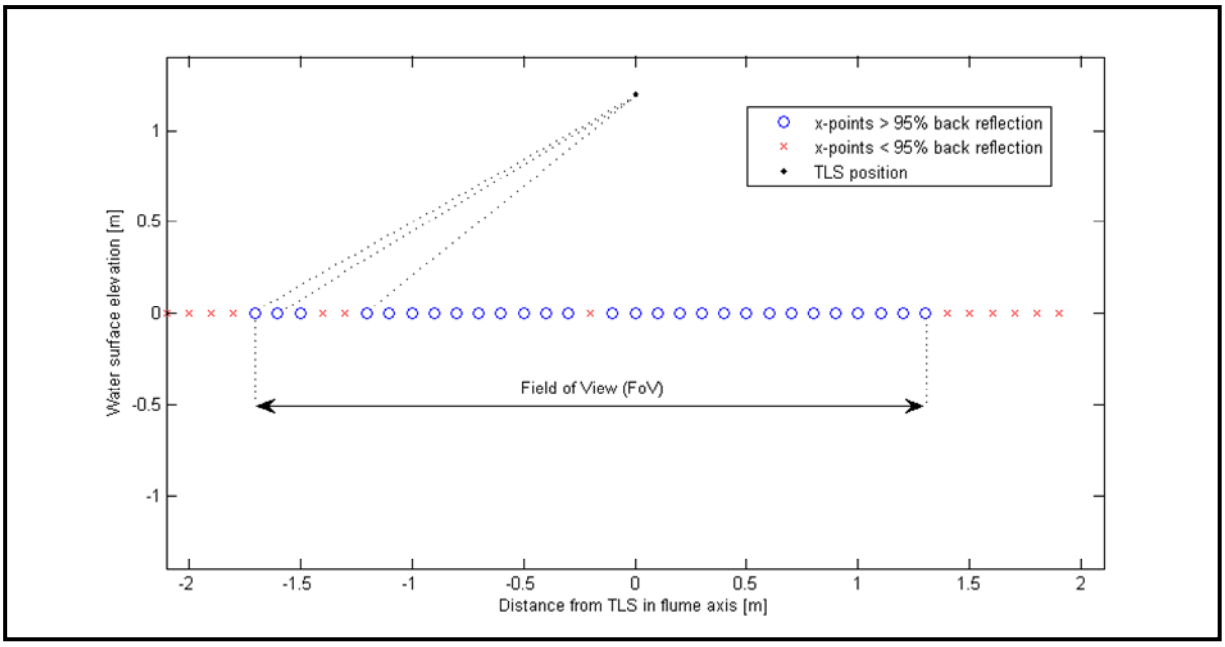

Fig. 28: Definition Field of View (FoV)

Also, in the area of the peak in nadir, single x- points didn't show 95% reflection, but points to the left and the right did so. These missing points are simply interpolated using two neighboring points. The same was true for x- points with less than 95% reflection near the edge of the profile.

Since no intensities of the reflection are considered it is also called a binary definition of reflectivity (either a reflecting signal is recorded or not).

Interpolation

The point spacing on the water surface is irregular due to increasing ranges with higher incidence angles (section 2.5.2). The height of the TLS above the water surface is 1.2 m and the angular resolution 0.5°. This results in a smallest point spacing in nadir, with approximately 0.01 m. The largest point spacing is at the edge of the profile with approximately 0.03 m. To provide an equally distribution, the scan points are interpolated in steps of 0.01 m over the whole profile.

Temporal Average

In still water conditions the temporal average of the range is calculated for each incidence angle.

Spatial Average

A moving window of 5 points is applied. This means that each point is averaged with the values from two points to the right, two points to the left and from the point itself. The fifth moving window (window size = 0.04m) is chosen because it gives a sufficient average without eliminating the peak in nadir and the small peaks in water surface elevation along the flume axis.

4.1.2 Peak in Nadir

As shown in section 4.1 the water surface profile obtained shows a striking peak in nadir, where the laser beam is approximately perpendicular to the water surface. Approximately 0.25 m to each side of nadir are influenced by the peak phenomena. In this area a comparably large scatter in the range measurement is observed.

The maximum height of the peak is approximately the same as the height of the paper on the water surface. This indicates that it is the true water surface which is measured in the peak and that it has something to do with the strength of the return signal. Still a proved physical explanation for the peak phenomena is missing.

It has been found that the peak could be eliminated by implementing a slant angle which results in a scan line shifted in transversal direction (section 2.5.2). A slant angle of 10° is recommended to eliminate the influence of the peak (section 4.1.3).

4.1.3 Range Precision

The range precision (section 2.4.1) describes the variation between repetitive range measurements for the same incidence angle and is given as the standard deviation from the mean.

In Fig. 29 the mean standard deviation for test 2 to test 7 and test 10 to test 19 and test 22 to test 26 are plotted against the according incidence angles (incidence angles from left and right side of nadir are summarized) The results are averaged in steps of 5°.

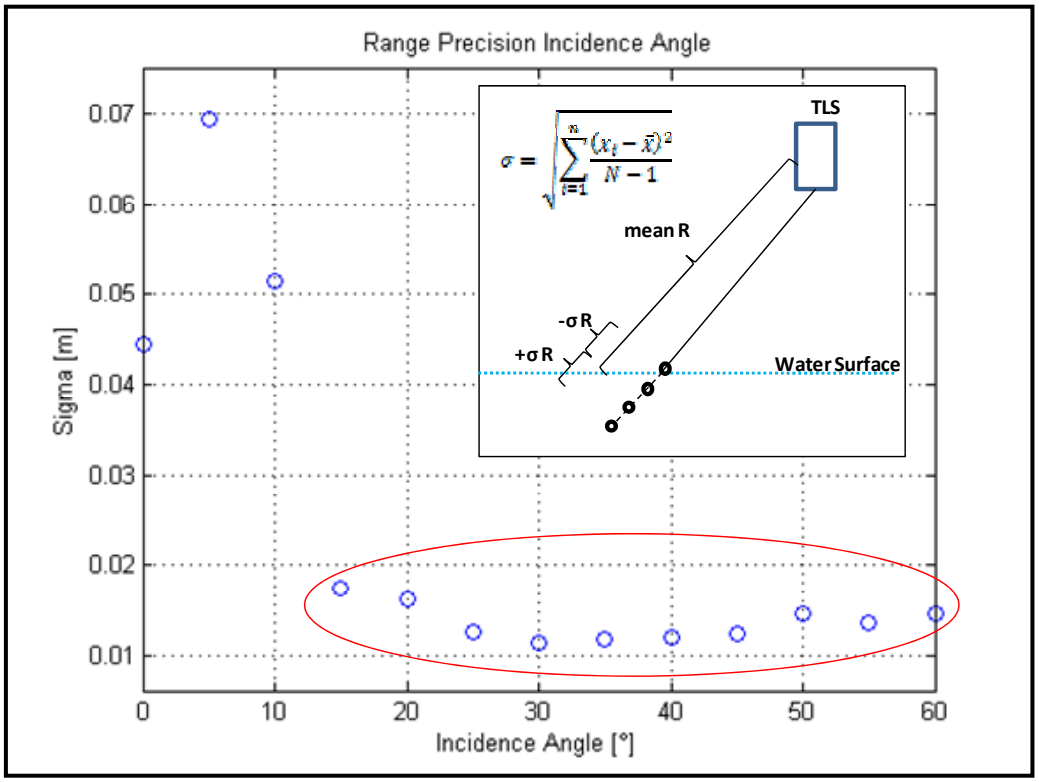

Fig. 29: Range precision against incidence angle (averaged over 5°)

Between 0° and 10° a comparably high standard deviation is found, which is related to the large scatter around the peak in nadir (section 4.1.2). Above 10° the standard deviation is comparably low between 0.01 m and 0.02 m. The minimum standard deviation of 0.011 m is calculated at 30° incidence angle. Above 30° the standard deviation shows a slightly increasing trend with increasing incidence angles. This is explained by the deterioration of the recorded signal with increasing incidence angles, as reported by Soudarissanane et al. (2009). The recorded signal is stretched due to an elongated footprint, not serving as a clear return signal for the detection mechanism any longer.

For further analysis incidence angles between 10° and 60° are considered. In Fig. 30 the averaged standard deviations for the above mentioned tests are plotted against the water turbidity.

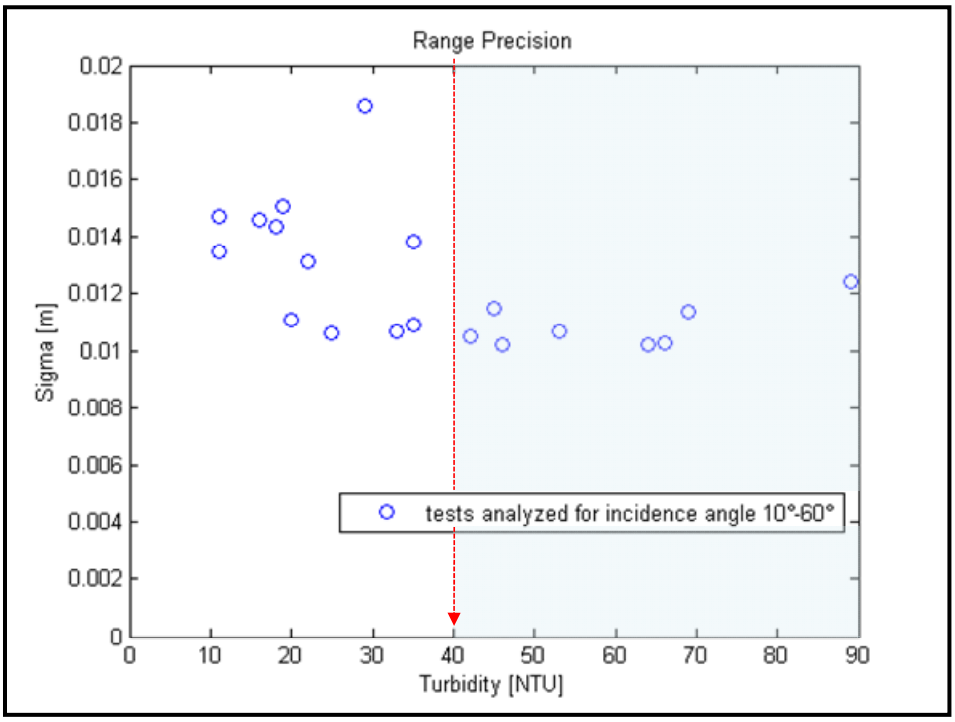

Fig. 30: Range precision against water turbidity (for incidence angles between 10° and 60°)

A tendency of decreasing range standard deviation with increasing water turbidity is shown in Fig. 30. For water turbidities above 40 NTU the range standard deviation is between 0.011 m and 0.0123 m. The scatter in range standard deviation is much less than for water turbidities below 40 NTU (between 0.011 m and 0.018 m). Hence, water turbidities above 40 NTU are required to guarantee for a low scatter in the range standard deviation.

The slight increase in standard deviation for turbidities 69 NTU and 89 NTU are related to the nonsufficient distribution of the Kaolinit along the flume axis, which may have led to unequally distributed turbidity along the flume (section 3.2.3).

Besides that, the results are in line with the findings of Allis et al. (2011), who also found a lowered scatter in range precision for water turbidities above 40 NTUs.

4.1.4 Refraction Correction

As outlined in Fig. 31 the obtained water surface profile is bending upwards with increasing incidence angles. It is assumed that the laser beam travels a certain distance B through the water column before being reflected by any particle. Hence, the laser beam experiences refraction and a decrease in velocity when entering the water column. For the range calculation the TLS assumes a constant velocity of the laser beam and a measurement which is on a straight line (Fig. 31). Therefore, the obtained results seem to be more distant and of higher elevation than in reality. To correct for this error a refraction correction method after Smith et al. (2011) is derived for this work.

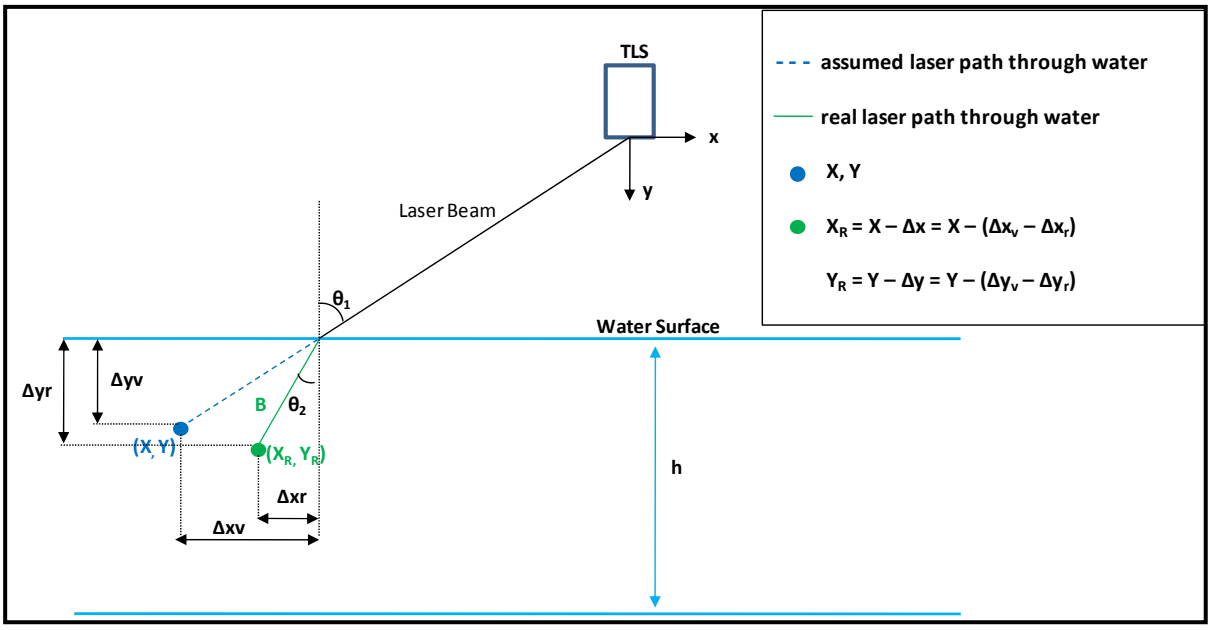

Fig. 31: Refraction of laser beam when entering the water column (after Smith et al. (2011))

The refractive index of water with an incidence laser wave length of 905nm is $n_{water} = 1.32699$ (Daimon & Masumura (2007)) and the refractive index of air is $n_{air} = 1.00027$. Knowing the incidence angle, the refractive angle is determined by Snells law:

$$\frac{\sin\theta_1}{\sin\theta_2} = \frac{n_2}{n_1} \qquad [14]$$

Where;

θ_1 = Incidence angle [°]

θ_2 = Refractive angle [°]

n_1 = Refractive index air [-]

n_2 = Refractive index water [-].

The refractive angle θ_2 is calculated using equation [14].

$$\theta_2 = \text{asin}(\sin\theta_1 * \frac{n1}{n2}) \qquad [15]$$

The refraction corrected horizontal distance Δx_r and vertical distance Δy_r (Fig. 31) of the refraction corrected coordinates are calculated with the sinus of refractive angle θ_2 multiplied by the distance B, the laser beam travels under water:

$$\Delta x_r = B * \sin\theta_1 * \frac{n1}{n2} \quad [16]$$

$$\Delta y_r = B * \cos(\text{asin}(\sin\theta_1 \frac{n1}{n2})) \quad [17]$$

The horizontal distance Δx_v and vertical distance Δy_v (Fig. 31) of the measured coordinates are calculated. The TLS device assumes no refraction, so the refractive angle is the same as the incidence angle and that the laser beam is travelling with the same velocity in water. Since in reality it is travelling slower in water, the length B must be multiplied with the quotient of the air- water refractive index:

$$\Delta x_v = B * \sin\theta_1 * \frac{n_2}{n_1} \quad [18]$$

$$\Delta y_v = B * \cos\theta_1 * \frac{n_2}{n_1} \quad [19]$$

The difference between the measured coordinates (Δx_v, Δy_v) and the refraction corrected coordinates (x_r, Δy_r) is calculated by subtracting the corrected from the measured distances:

$$\Delta x = \Delta x_v - \Delta x_r = B * \sin\theta_1 * (\frac{n_2}{n_1} - \frac{n_1}{n_2}) \quad [20]$$

$$\Delta y = \Delta y_v - \Delta y_r = B * (\cos\theta_1 * \frac{n_2}{n_1} - \cos(a\sin(\sin\theta_1 * \frac{n_1}{n_2}))) \quad [21]$$

Finally, refraction corrected coordinates (X_R,Y_R) are calculated from the originally measured water surface profile coordinates (X,Y).

The refraction corrected coordinates are a function of the distance B, the laser beam travels under water:

$$X_R = X - \Delta x = X - B * \cos\theta_1 * (\frac{n_2}{n_1} - \frac{n_1}{n_2}) \quad [22]$$

$$Y_R = Y - \Delta y = Y - B * (\cos\theta_1 * \frac{n_2}{n_1} - \cos(a\sin(\sin\theta_1 * \frac{n_1}{n_2}))) \quad [23]$$

Where;

B = Distance laser beam travels under water [m]

θ_1 = Incidence angle [°]

n_1 = Refractive index air [-]

n_2 = Refractive index water [-]

X,Y = Measured coordinates [m]

X_R,Y_R = Refraction corrected coordinates.

If the upwards bending of the water surface profile edges can be explained by the refraction of the laser beam and the slower velocity in water, the refraction correction should result in a most planar water surface profile. Hence, a backwards, iterative approach to determine B, which results in the most planar surface is chosen. It is assumed that for a given water turbidity, B is constant for all incidence angles. The root mean square error of the vertical part Δyr, of the refraction corrected coordinates, is calculated as a function of B:

$$Min(RMSE) = \frac{\sum_{i=1}^{n} (\Delta y_r(B) - \Delta y_{ri}(B))^2}{N} \quad [24]$$

The Δyr resulting in the minimum RMSE (most planar surface) is calculated. The according B is chosen for refraction correction.

In Fig. 32 a water surface profile before (blue dots) and after refraction correction (green dots) is shown.

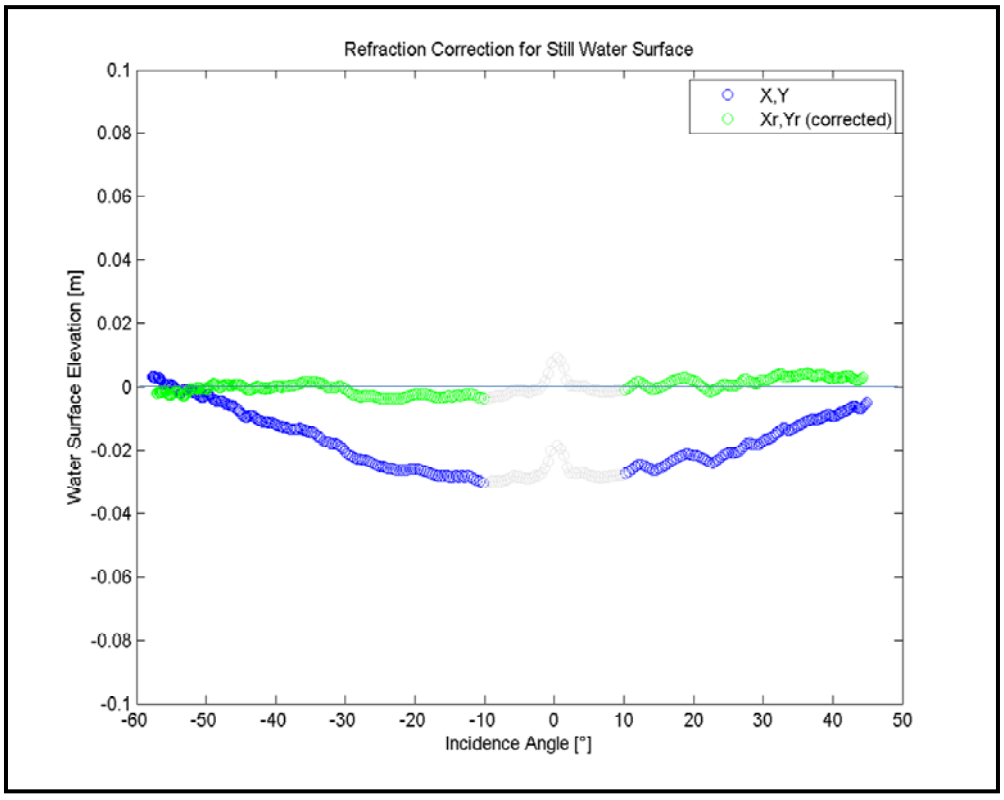

Fig. 32: Water surface before (blue dots) and after (green dots) refraction correction

Since only incidence angles between 10° and 60° are considered for the calculation (section 4.1.3) the missing points are highlighted in grey. The upwards bending of the edges is corrected and a rather horizontal water surface profile obtained. Refraction correction plots for each test are given in Appendix A.

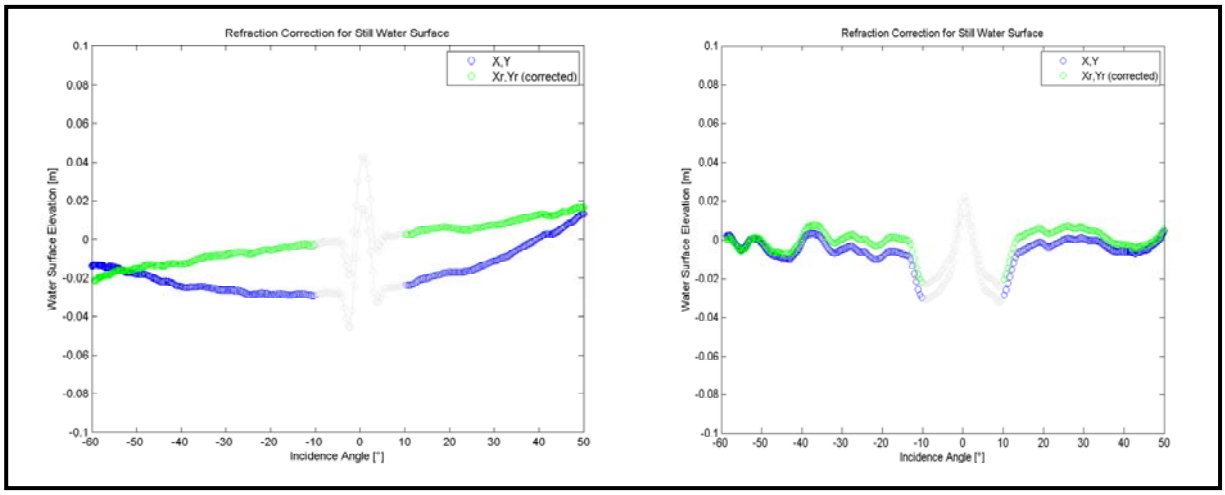

Fig. 33: Aslope water surface profile (left) and scattered water surface profile (right)

Two problems are observed which lead to difficulties when applying the refraction correction method. In Fig.33 on the left side, an aslope water surface profile is displayed. Since this is observed for each test conducted on the 1. of November, it is probably a systematic error and due to the aslope installation of the TLS device above the wave flume. Still, the refraction corrected water surface profile is much straighter and the upwards bending of the edges is corrected.

On the right figure, clearly unequally distributed Kaolinit (varying turbidity in flume axis) is the reason for the scatter in water surface elevation. In this case refraction correction is hardly possible. A more sophisticated steering of the additive is demanded to guarantee for an equally distribution of the turbidity along the flume axis.

In Fig. 33 the distance B, the laser beam travels through the water, is plotted against the turbidity. It is the expectation that B will decrease with increasing turbidity. With higher turbidity more Kaolinit particles are available serving for a sufficient reflection.

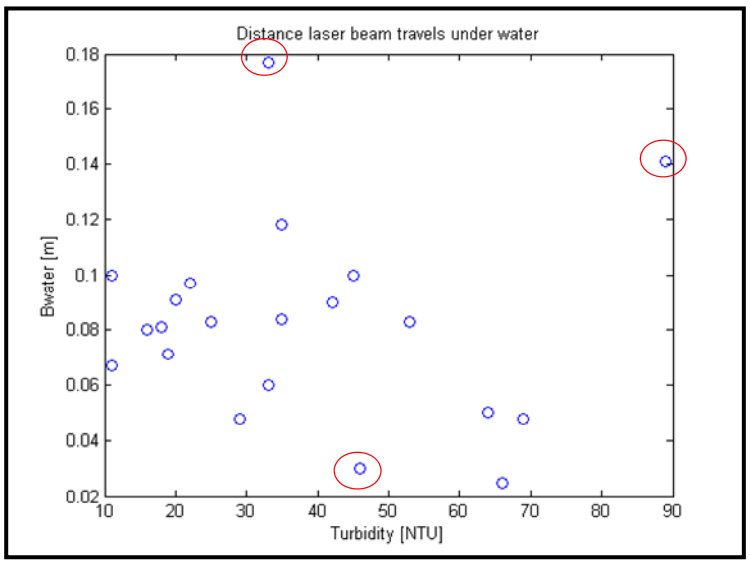

Fig. 34: Distance B laser beam travels under water, against water turbidity

The results are rather scattered and no clear trend can be recognized. If only turbidities above 40 NTU (section 4.1.3) are taken into account a trend towards decreasing B with increasing turbidities can be recognized. The outliers (marked in red circles) can be explained by the unequally distributed Kaolinit and its effect on the iteratively derived B.

Due to the above mentioned problems with the turbidity steering and aslope installation of the TLS it is not possible to prove yet that the distance B is dependent on the water turbidity. Further, improved experiments are required. Also, the error due to elongated footprint with higher incidence angles and its effect on the upwards bending of the obtained water surface profile has not been investigated.

Nevertheless, refraction correction with the above presented method can correct for the upwards bending of the edges.

An increasing phase shift in x- direction between the TLS and wave gauge measurements with increasing incidence angles is reported by Allis et al. (2011) and might be explained by the difference Δx (Equation [20]) derived in this section.

4.2 Water Waves

The phenomena described for still water (section 4.1) are true for dynamic wave conditions as well. The peak in nadir (section 4.1.2) is now moving with the changing wave face, always perpendicular to the water surface. The findings for range precision (section 4.1.3) and refraction (section 4.1.4) are assumed to be true for water waves as well. The Field of View (FoV) and maximum incidence angle are calculated in section 4.2.2. The error due to parallel TLS and wave movement is researched in section 4.2.3.

4.2.1 Filtering

The filtering done for water wave conditions is comparable to the still water filtering (section 4.1.1). The transformation from polar to Cartesian coordinates is followed by applying a geometrical filter. The FoV with 95% reflection is calculated the same way as in section 4.1.1.Interpolation, spatial and temporal averaging are not applied. Too many uncertainties concerning the optimum interpolation size and time step, as well as the optimum moving window remain. Spectral filtering is recommended in future research. Also, refraction correction is not applied to wave conditions. A reconstructed wave field is given in Fig. 35.

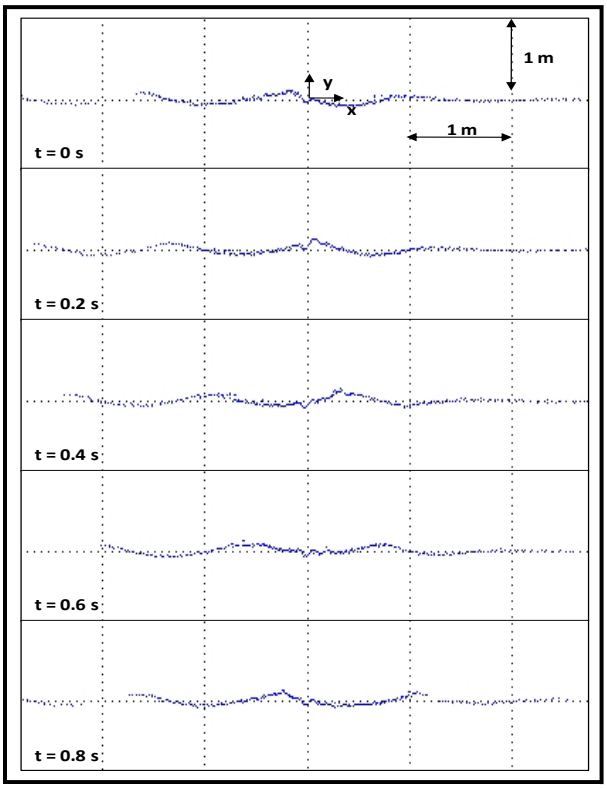

Fig. 35: Reconstructed wave field

4.2.2 Field of View (FoV) and Incidence Angle

The FoV for water waves with 95% reflecting points is calculated based on the method outlined in section 4.1.1. In Fig. 35 the obtained FoV for each test is plotted against the according turbidity (section 3.2.4).

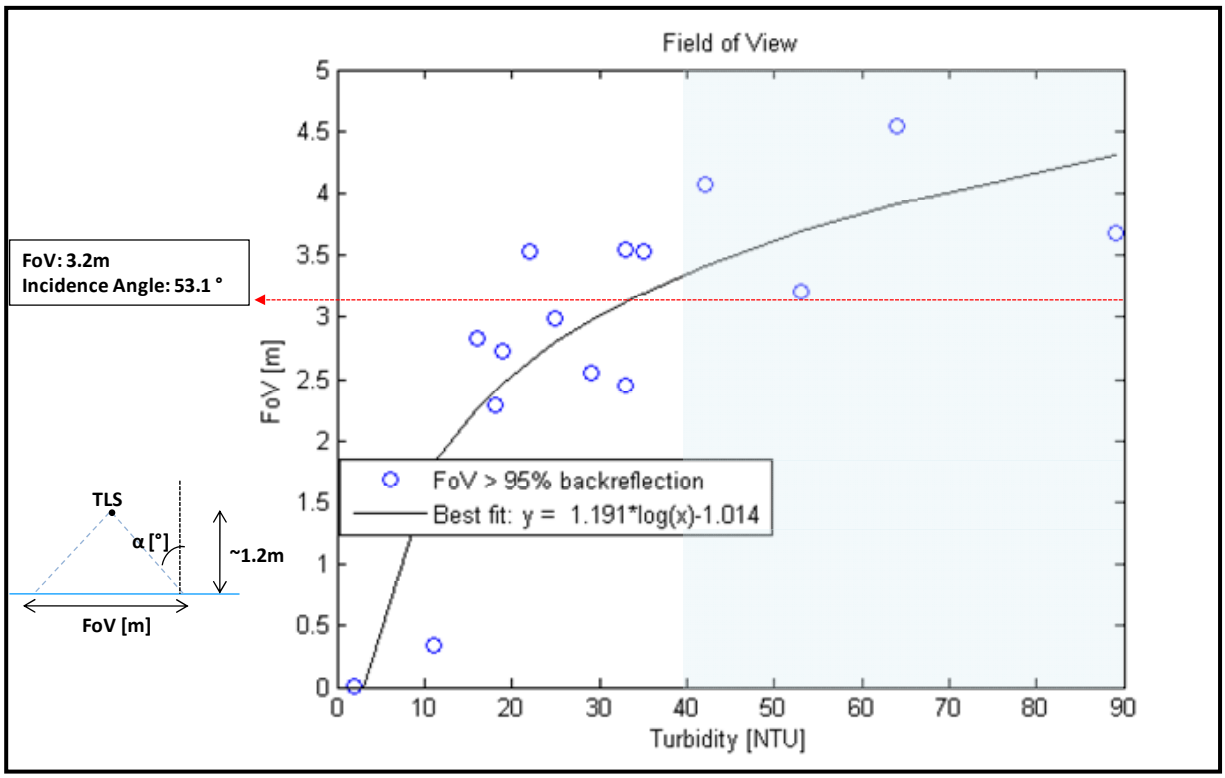

Fig. 36: Field of View for tests with waves and varying turbidities

It is shown that with increasing turbidities the FoV increases logarithmic. In this specific experimental set-up and for the recommended turbidities above 40 NTUs (section 4.1.3) a minimum FoV of 3.2 m width is expected to be always present. The according incidence angle is 53.1°.

This is lower compared to the maximum incidence angle of 55° found by Allis et al. (2011) and 61.5° found by Blenkinsopp et al. (2012). This could be related to the fact that in the present study the total number of reflected points is reduced to a FoV with sufficient reflection (95%). No such conservative FoV calculation is reported by Allis et al. (2011) and Blenkinsopp et al. (2012), resulting in larger maximum incidence angles in their case.

There is no 95% FoV for the turbidity of 2 NTU. Which leads to the assumption that what is actually giving the reflection in the water are not the water particles itself (Raman-, Mie- scattering) but the Kaolinit particles dissolved in the water.

4.2.3 Error due to Parallel Movement of Wave and TLS

In this section the error due to parallel movement of TLS device and water wave is calculated. By TLS movement the mirrors turnarounds, resulting in a deflection of the laser beam over the measured surface, is described. During testing the scanning frequency (section 2.5.2) was 50 Hz and the according period 0.02 s. Hence, 50 mirror turnarounds per second are present and for one turnaround 0.02 s are needed.

The required time Δt for one scan profile from the water surface is calculated with:

$$\Delta t = f * \frac{2 * \alpha}{360°} \quad [25]$$

Where;

f = Scanning frequency [Hz]

α = maximum incidence angle [°]

The maximum incidence angle for water turbidities above 40 NTU is 53.1° (section 4.2.2).

During the time Δt, the laser beam needs to move over the measured profile from the first measured water particle to the last one, the waves are moving with the wave celerity c (section 2.2.3). The total horizontal error due to parallel movement of wave and TLS device is then calculated with:

$$\Delta L = \Delta t * c \quad [26]$$

Where;

Δt = Required time for one measured water surface profile [s]

c = Wave celerity [m/s].

In relation to the water wave wavelength the error in percentage is:

$$\beta = \frac{\Delta L}{L} * 100 \quad [27]$$

Where;

ΔL = Error in horizontal direction [m]

L = Water wave wavelength [m]

Depending on whether the wave and mirror move in the same direction or not the water wavelength is compressed or decompressed respectively by ΔL. The water parameter, TLS parameter and resulting errors are given in Tab. 6. Since the movement of the wave (wave celerity) is a function of the wave period (section 2.2.3), only the periods used in the experiments (0.81 s, 0.9 s, 1 s, 1.7 s) are investigated.

Wave Period T [s]	Wave Height H_{mo} [m]	Wave Length L [m]	Water Depth h [m]	Wave Celerity c [m/s]	Scanning Frequency f [Hz]	Max. Incidence Angle α [°]	Required Time Δt [s]	Total Horizontal Error ΔL [m]	Horizontal Error β [%]
0.81	0.2	1.02	0.6	1.26	50	53.1	0.0049	0.0062	0.61
0.9	0.1	1.26	0.6	0.55	50	53.1	0.0049	0.0027	0.21
1	0.05	1.55	0.6	1.44	50	53.1	0.0049	0.0071	0.46
1.7	0.15	3.73	0.6	3.57	50	53.1	0.0049	0.015	0.4

Tab. 6: Horizontal error due to parallel movement of TLS device and water wave

The horizontal error β between 0.21% and 0.61% in relation to the wave length is acceptable for hydraulic measurements (approximately 1% required).

The error due to Doppler- effect, a change in frequency and measured distance due to the moving wave, is not further researched in this study.

4.3 Comparison SICK LMS511 vs. Riegl VZ-400

In this section the SICK LMS511 in case A (section 3.1.1) is compared to the Riegl VZ-400 in case C (section 3.1.3). For each device a test with approximately 60 NTU water turbidity was chosen for comparison. TLS-, water- and geometry parameter based on section 2.7 are distinguished and summarized in Tab. 7.

Comparison Riegl VZ-400 - SICK LMS511	SICK LMS511 Pro SR	Riegl VZ-400
		
Scanner parameter		
Wavelength [nm]	905	near infrared
Scan rate [Hz] [lines/s]	50	20
Range meas. principle	ToF (pulsed)	ToF (pulsed)
Beam diameter at head [mm]	13.6	-
Beam divergence [mrd]	11.9	0.3
Footprint [m]	0.0278	-
Angular resolution [°]	0.5	0.05
Systematic error 1 -10m [mm]	25	5
Statistical error 1- 10m [mm]	6	3
Laser power [mW]	3.79	-
Laser class (Eye- safety)	1	1
Geometry parameter		
Height above water [m]	1.2	2
Range [m]	1.2 - 2.5 (FoV 95%)	3.1 - 11.5
Incidence angle [°]	0 - 64 (FoV 95%)	50 - 80
Water parameter		
Wave type	regular	regular
Wave period [s]	1.7	-
Wave height [m]	0.15	-
Wave steepness [-]	0.03	-
Water depth [m]	0.6	~0.6
Water turbidity [NTU]	64.4	60.8

Tab. 7: Comparison between Riegl VZ- 400 and SICK LMS511

4.3.1 TLS Parameter

Scanning Frequency

The SICK LMS511 measured with 50 Hz and the Riegl VZ-400 with 20 Hz scanning frequency.

Spectral Resolution

SICK LMS 511 has a laser beam wavelength of 905 nm and the Riegl VZ-400 is stated to measure with nearinfrared laser beam wavelength, but no precise number is provided by the company.

Measurement principle

Both devices are equipped with a pulsed Time- of- Fligth (ToF) measurement principle.

Noise

The noise is calculated as the standard deviation of the still water signal for the incidence angle of 55°. At 55° incidence angle the according range is 2.1 m for the SICK LMS511 and 3.5 m for the Riegl VZ-400. The noise in the measurement is $\sigma = 0.0058$ m and $\sigma = 0.016$ m respectively. It is not clear whether the increase in noise for the Riegl VZ-400 device can only been explained by the larger range compared to the SICK LMS511 device.

Laser Power

The total laser power for the SICK LMS511 is P = 54 [W=J/s]. In order to calculate the laser power for one pulse, the total laser power must be divided by the pulse repetition rate. The pulse repetition rate (PRR) is calculated with:

$$PRR = f * \frac{1}{\alpha} * \beta = 50 * \frac{1}{0.5} * 360 = 36000 Hz \quad [28]$$

Where;

f = Scanning frequency [= 50 Hz]

α = Angular resolution [= 0.5°]

β = Area covered with laser pulses [= 360°].

Then, the laser power for one pulse (duration 3.7 ns) of the SICK LMS511 device is calculated with:

$$p = \frac{P}{PRR} = 0.015 = 15 \text{mJ/pulse} \quad [29]$$

Where;

P = Laser power [= 54 W]

PRR = Pulse repetition rate [= 36000 Hz]

The Riegl VZ-400 is classified in Laser Class 1 but no laser power is provided by the company.

Costs

Finally there is a difference in costs between ~5000 Euro for the SICK LMS511 and ~100000 Euro for the Riegl VZ-400.

4.3.2 Geometry/Atmosphere Parameter

Incidence Angle

For the Riegl VZ-400 the measurement area is preset to incidence angles between 50° and 80°. The SICK LMS511 measurement area is limited by the 95% FoV approach to incidence angles between 0° and 64°. Hence, the comparison is done for the overlapping incidence angles between 50° and 64°.

Range

The Riegl VZ-400 is installed approximately 2m above the water surface and the SICK LMS511 in 1.2 m height. In combination with the present incidence angles the measured ranges are between 3.1 m and 11.5 m for the Riegl VZ-400 and between 1.2 m and 2.7 m for the SICK LMS511. Hence, the Riegl VZ-400 is the preferred TLS device for measurements in the Delta Flume with larger ranges.

Footprint Size

The beam diameter for the SICK LMS511 at the head of the TLS is 0.0136 m and according beam divergence 0.0119 rad. The TLS is installed 1.2 m above the water surface. The footprint size on the water surface is then 0.0278 m. Since no beam diameter is provided by Riegl company, no footprint size could be calculated here.

4.3.3 Water Parameter

Turbidity

In both cases tests with similar turbidities (~60 NTUs) and regular waves are chosen for comparison.

4.4 Summary and Conclusions

Methods were described to extract a water surface profile from the recorded signal. First the coordinate transformation from polar to cartesian coordinates was performed. Then, a geometrical filter, to exclude points, different from the water surface, was applied. A FoV was defined with 95% reflecting points. After interpolation of the profile the scan points were temporally and spatially averaged. When reconstructing a wave field from the recorded signal, several problems were experienced (e.g. peak in nadir, upwards bending of the profile edges, scatter and bias in the measurements). These problems need to be solved for the simple case of still water (section 4.1) before being adapted to wave conditions (section 4.2). To correct for the upwards bending of the edges a refraction correction method was proposed. Based on the physical phenomena of refraction and the difference in velocity when the laser beam enters the air- water boundary the upwards bending is corrected. The distance B the laser beam travels under water was derived with a backwards iterative approach, resulting in the most planar surface. In furture experiments it might be possible to derive the distance B from the turbidity of the water and finally from the intensity of the reflected signal. It was found that the variance in range precision becomes low with water turbidities above 40 NTU. Also, the range precision beccame high for incidence angles between 0° and 10°. Hence, water turbidities above 40 NTU and a slant angle of 10° is recommended for future experiments.

In section 4.2 the analysis was adopted for wave conditions and a 95% FoV with present waves was calculated. Providing a water turbidity above 40 NTU a minimum 95% FoV of 3.2 m was obtained. The TLS height above the water was 1.2 m and the according maximum incidence angle 53.1°.

The error due to parallel movement of TLS device and water wave was calculated and found to be negligible (less than 1% related to the water wave wavelength) for scanning frequencies above 50 Hz.

In section 4.3 the SICK LMS511 was compared to a Riegl VZ-400 device in a slightly different set-up. The Riegl VZ-400 received a signal from the water surface for distances between 3 m and 10 m, which was larger compared to the SICK LMS511 (1.2 m to 4 m). Hence, the Riegl VZ-400 was the preferred device for the measurements in the Delta Flume.

As a next step the gained knowledge from section 2 to section 4 is used to design an optimized TLS based measurement set-up for the Delta Flume.

5 Application of TLS measurements to Delta Flume

In this section gained knowledge derived from the literature study (section 2) the experiments presented (section 3) and analyzed (section 4) is transformed to the use of TLS based range measurements from water waves in the new Delta Flume (section 2.1).

A possible monitoring set-up for the Delta Flume is given in section 5.1. The measurement workflow is discussed in section 5.2. Finally ideas are presented to validate the laser range measurements in section 5.3.

5.1 Monitoring Set-up Delta Flume

Based on the results from section 2.7, TLS-, geometry/ atmosphere- and water parameters are divided. In section 5.1.1 the TLS parameters are researched and their applicability discussed. The geometrical set-up and atmospheric influences are discussed in section 5.1.2. Two set-up locations are identified. Both placed in the new Delta Flume, one for green water and one for the wave run-up zone. In section 5.1.3 the water and wave parameters are discussed.

5.1.1 TLS Parameter

TLS Device

The Faro Photon 120 showed good results in the wave run-up zone of the Delta Flume with a very foamy and turbulent environment and measured ranges up to 10m. No results were obtained for the measurement of the green water in the Delta Flume as well as in the small flume (section 3.1.2).

The SICK LMS511 was found to give good results in the green water of the small flume (section 3.2 and section 4) with ranges between 1.2 m and 4 m. Also good results are reported by Blenkinsopp for the use in the wave run-up zone of the Delta Flume (section 3.1.4). Up to 20 m distance breaking waves were detected. When measuring still or green water in the Delta Flume with ranges between 4 m and 8 m no good results were obtained.

The Riegl VZ-400 was applied to still and green water conditions of the small flume with the largest measured ranges between 4 m and 10 m (section 3.1.4) under very shallow angle of inidence. Hence, it is assumed that the Riegl VZ-400 is the preferred TLS device for the Delta Flume. Still, its applicability has to be proved in future experiments.

Laser BeamWavelength

In the conducted experiments nearinfrared laser (~800 nm - ~1500 nm) were used (SICK:905 nm, Riegl:NR, Faro:785 nm). NASA spectral reflectance curves for water show an expected maximum reflection of 2% within this spectral range (section 2.5.3). The use of nearinfrared lasers for water surface detection is in line with the Optech Shoals approach for airborne LiDAR bathymetry measurements (section 2.6.1).

A striking peak in the spectral reflectance curve for seawater is found for laser beam wavelengths between 2500 nm and 4000 nm (section 2.5.3). A reflectance between 2.3% and 4% is

expected. If it exists, a laser beam wavelength in this range should improve TLS based range measurements from the water surface and could be investigated in future experiments.

Range Measurement Principle

Time- of- Flight (ToF) and Phase Shift (PS) measurement principle for TLS devices are distinguished in section 2.5.2.

In the conducted experiments TLS devices with pulsed ToF measurement principle (Riegl VZ-400 and SICK LMS511) provided better results. Additionally most reported TLS based range measurements from water waves are obtained with devices containing ToF measurement principle (section 2.6).

It was found that the laser beam enters the water to a certain distance before being reflected (section 4.1.4). When entering the water the laser beam experiences refraction and a slower propagation speed. The error in the measurements can be corrected easily for ToF based range measurements as outlined in section 4.1.4. It is not clear how refraction correction could work for PS measurement devices.

Guenther et al. (2000) reported, that during airborne LiDAR bathymetry Raman reflection from the water is measured. It is not clear what happens to the PS range measurements if a different wavelength (emitted by the water) than the incidence wavelength (emitted by the laser) is coming back to the device. Also, the Doppler effect due to a moving wave will influence the wavelength in the PS measurements. The error resulting from a change in wavelength has not been researched yet, but would only effect TLS devices with PS measurement principle.

Although there are more parameter influencing the quality of the measurements it is assumed that the ToF range measurement principle is more robust for water scanning purpose.

1D/2D/3D

The waves are assumed to have the same shape perpendicular to the Delta Flume axis. Hence, in the Delta Flume 1D measurements are preferable minimizing the amount of recorded data (compared to 2D measurements) and enabling a simplified post processing.

Filter

Water is a very low reflective surface. Therefore, Intensity filter (fog filter etc.), frequency filter or comparable internal TLS thresholds should have the possibility to be switched off. In this way as much data points as possible are obtained from the water surface. The TLS should offer the possibility to output the raw data without being handled internally.

If required, filtering of the point cloud can be done manually in post processing steps (section 4.1.1).

Scanning Frequency

The scanning frequency is recommended to be 50 Hz (section 2.4). Sufficient high scanning frequencies enable temporal averaging.

The error due to parallel movement of TLS device and water wave is typically lower than 1% in relation to the water wavelength (section 4.2.3). In hydraulic modeling often a maximum horizontal error of 1% is accepted. Hence, the scanning frequency of 50 Hz is sufficient.

These results are obtained for wave periods between 0.81 s and 1.7 s in the small flume. With larger wave periods, as present in the Delta Flume, the error will further decrease.

Peak Detection Method and Receiver

The laser beam shows a tendency to enter the water before being reflected (section 4.1.4). Based on the peak detection method, a predefined strength or shape (e.g. peak) of the reflected signal is required to trigger the measurement (section 2.5.2). This means that the first Kaolinit particle in the water giving a reflection is not sufficient but a certain number of reflections from several Kaolinit particles is required to trigger the measurement. It is assumed that the best method is to trigger the measurement as soon as possible, with the very first recorded reflection.

Very sensitive receivers with high radiometric resolution are required to measure the low intensity reflections and changes in intensity from the water surface.

5.1.2 Geometry-, Atmosphere Parameter

Measurement Location

Two different locations in the new Delta Flume (section 2.1) are identified for the TLS measurements. The first location is placed in the green water with generally unbroken waves. At this location wave profiles and the accompanying wave parameters are measured. A proposed measurement set-up for the green water location is given in Fig. 36.

The second location is placed in the wave run-up zone of the Delta Flume. Physical phenomena of the swash zone, wave breaking and wave run-up are not well understood yet and can not be measured with conventional measurement devices (section 2.4). Hence, it is important to also propose a measurement set-up for this location. The temporally and spatially continuous measurement of the wave will allow for a detailed study of breaking waves and swash motions. Additionally the foamy and turbulent environment of the breaking wave will provide better reflection for the TLS device. A proposed measurement set-up for the wave run-up location is given in Fig. 37.

The measurement location in flume axis should always be vertically above the area of interest (except for a slant angle). This way, errors due to high incidence angles, resulting in ellipsoidal footprints and signal deterioration (Sourarissanane et al. (2011)) are reduced.

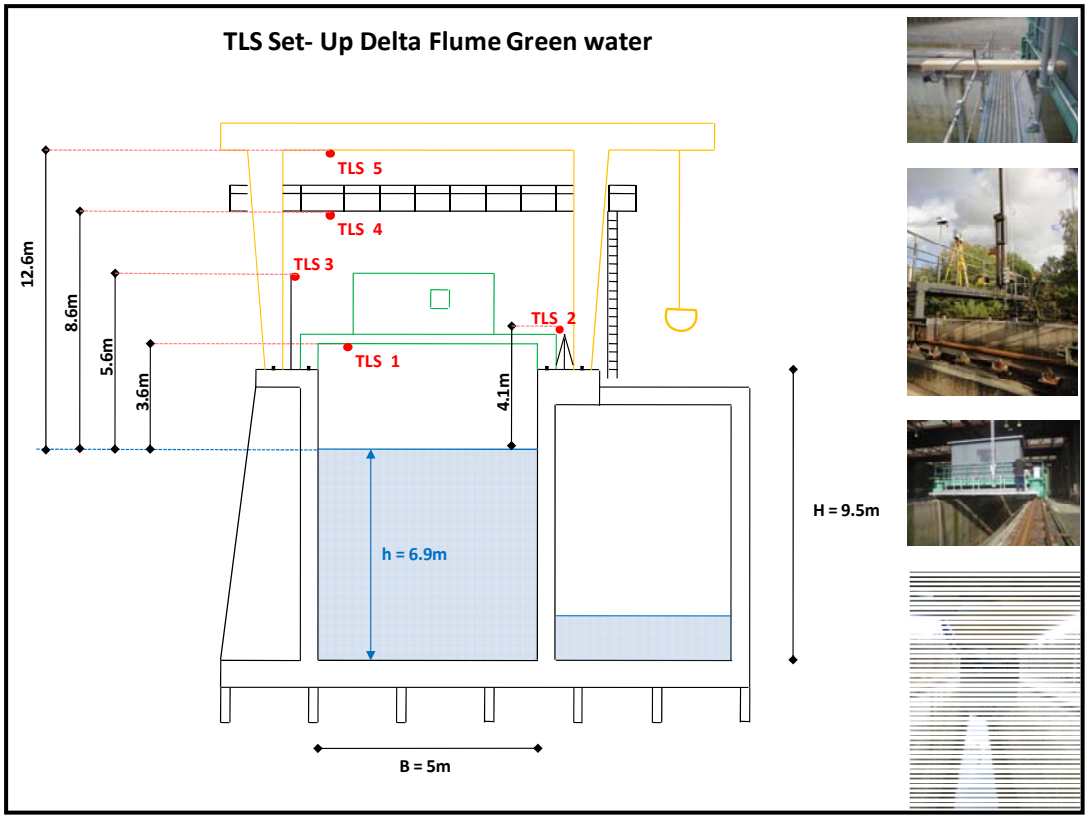

Fig. 36: Possible TLS set-up for green water in Delta Flume

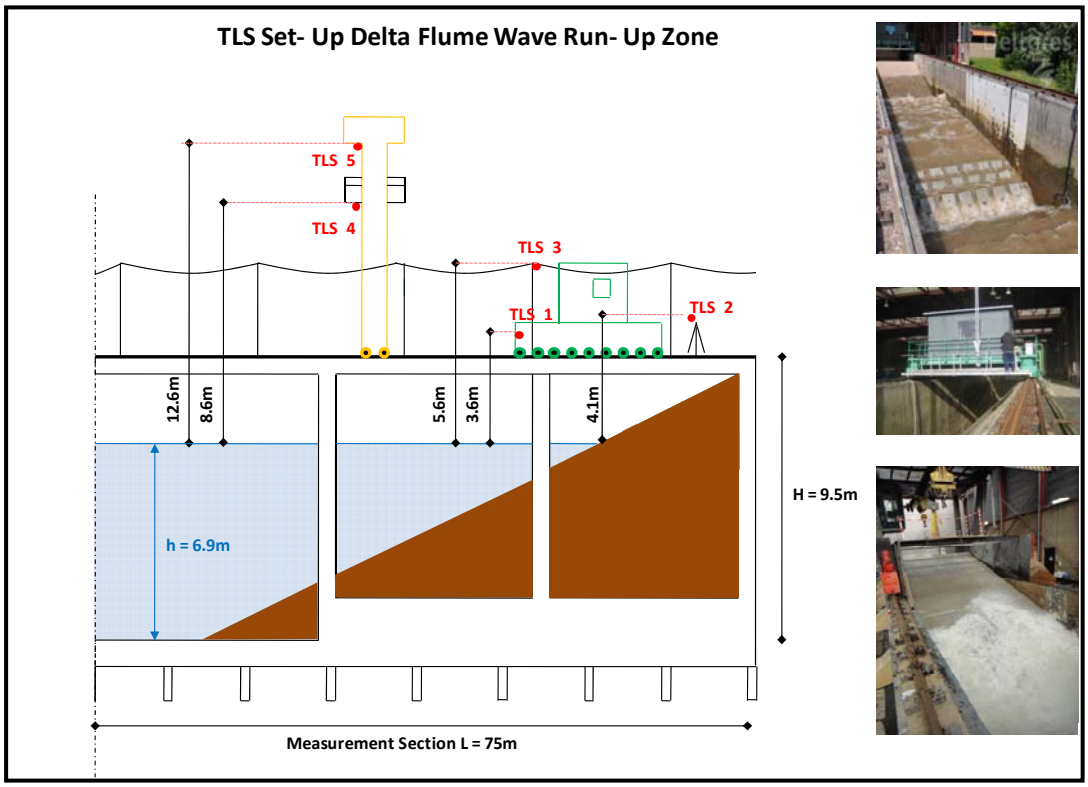

Fig. 37: Possible TLS set-up for wave run-up zone in Delta Flume

Height Above Water

Five different locations for the TLS are presented in Fig. 36 and Fig. 37. They are ordered according to their height above the water surface. The heights are given in Tab. 8 as well.

- TLS1
  The TLS is installed below the measurement platform. The moving platform would allow for varying measurement positions in flume axis. The scan data could be monitored in the housing of the measurement platform already equipped with the necessary hardware. If turned in cross flume axis the scanner could also be used as a profiler to measure the hydraulic models in the flume. Once the scanner is fixed and calibrated for this position it is considered a permanent solution. The height above the water (h = 6.9 m) is approximately 3.6 m.
- TLS2
  The TLS is installed on a conventional tripod beside the flume. The distance towards the water surface depends on the height of the tripod. It can be mounted anywhere beside the flume. It is considered a temporal solution, so the TLS could be also used for different purpose (e.g. scan of hydraulic model). New calibration would be necessary before each test.
  The height above the water (h = 6.9 m) is very dependent on the tripod and approximately 4.1 m.
- TLS3
  Next to the flume, pillars will be installed to carry the power supply cables. One pillar could be used for a permanent installation of a TLS device. The scanner is spatially limited to the flume area next to the attached pillar. It is considered a permanent solution with the advantage, that the calibration of the measurement device needs to be done only once. The higher elevation above the flume serves for a wider FoV.
  The height above the water (h = 6.9 m) is approximately 5.6 m.
- TLS4
  Comparable to TLS1 a moving crane platform will be installed, to easily rearrange the hydraulic models in the flume. The TLS is fixed below the installation platform, making it easily accessible for possible changes. The whole platform is spatially flexible and can be moved to the interested location along the flume axis. Interference with the measuring platform (TLS1) in lower elevation must be prevented. Since it is a crane used to transport heavy stuff, manual damage to the TLS must be prevented. The even higher elevation approximately 8.6 m above the water (h = 6.9 m) increases the possible FoV. Due to easy access, flexibility in flume axis and the largest distance to the water surface without interrupting objects, TLS4 is considered the most preferred measurement location.
- TLS5
  The measurement location is placed on the same moving crane as for TLS4, but on the topmost part of the installation crane. It becomes more difficult to access the TLS in this location and also the laser beam will interfere with the installation platform (TLS4) below.
  The height above the water (h = 6.9 m) is approximately 12.6 m.

Slant Angle

Each TLS location is slightly shifted from the middle of the flume, to easily implement a slant angle (section 2.5.2). A slant angle of 10° prevents the peak in nadir (section 4.1.2). When introducing a slant angle the laser beam will hit the water surface a certain distance apart from perpendicular, depending on the height of the TLS above the water surface. This offset in transverse direction is calculated and given in Tab. 8.

$$\text{Offset} = \tan(\alpha) * H \quad [30]$$

Where;

H = Height above water surface [m]

α = Slant angle [°].

The largest offset of 2.22 m is still lower than the total width (5 m) of the Delta Flume. Hence, a slant angle of 10° is geometrically possible for TLS location 1 to 5.

Field of View (FoV)

A maximum incidence angle of 53.1° was found in section 4.2.2 for TLS based measurements of the water surface with steep waves. Depending on the height of the TLS above the water surface a FoV is calculated for TLS location 1 to 5 and given in Tab. 8.

$$\text{FoV} = 2 * \tan(\alpha_{max}) * H \quad [31]$$

Where;

H = Height above water surface [m]

α_{max} = Max. Incidence angle [°].

The largest obtained FoV (9.59 m for TLS1) is still larger than one water depth (h = 6.9m). The local wavelength is L_0 = 73 m for the Delta Flume. Hence, TLS location 1 to 5 do not provide a sufficient FoV to detect at least one full wavelength. However, the highest locations (TLS4 and TLS5) will cover several water depths and a full wave peak or trough. Providing a 73m FoV the TLS need to be installed in 27 m height.

These values are rather hypothetical since it is not clear whether it is possible to simply scale up the FoV to the heights in the Delta Flume, by using the same incidence angle obtained in small flume experiments (section 4.2.2).

Footprint Size

The increase in footprint size will lead to more deterioration in the signal, especially when the footprint shape is elongated (Soudarissanane et al. 2009). Sufficient knowledge about an optimized footprint size for TLS base range measurements of the water surface is still missing. The obtained footprint diameter are calculated for location TLS1 to TLS5 and given in Tab. 8.

$$\text{Footprint} = d + 2 * \tan(\theta) * H \quad [32]$$

Where;

H = Height above water surface [m]

d = Beam diameter at focus lense [m]

θ = Beam divergence [mrad].

The beam diameter 13.6 mm and beam divergence = 11.9 mrd of the SICK LMS511 device (section 3.2) are used for the calculation.

Laser Power

The power of each laser pulse for the SICK LMS511 device is 15 mJ (section 4.3). When installing the TLS device in 1.2 m height good measurement results were obtained (section 3.2). Based on the laser range equation [13] the laser power can be scaled up for the measurement locations TLS1 to TLS5. It is assumed that the factor D^2/R^2 in the equation can be kept constant, so the received laser power decreases only quadratically with the range. The required laser pulse power is calculated and given in Tab. 8.

$$p_{\text{Delta Flume}} = p * \left(\frac{H}{1.2}\right)^2 \quad [33]$$

Where;

H = Height above water surface [m]

p = Laser pulse power [mJ].

It is not clear whether it is possible to generate the required laser pulse power with a TLS device and if it exceeds the limit for eye-safety. Again these values are rather hypothetical and serve only as a first orientation, since there is no prove that it is sufficient to simply scale up the laser power to provide a working measurement.

Atmosphere

In the experiments (section 3.2) no influence of lighting on the measurements could be observed. This is in line with the observations of Irish et al. (2006).

It is assumed that rain will deteriorate the measured reflections.

	TLS 1	TLS 2	TLS 3	TLS 4	TLS 5
Height above water [m]	3.6	4.1	5.6	8.6	12.6
Offset on water surface [m]	0.63	0.72	0.99	1.52	2.22
Laser pulse power [J]	0.14	0.18	0.33	0.77	1.65
Footprint [m]	0.10	0.11	0.15	0.22	0.31
FoV [m]	9.59	10.92	14.92	22.91	33.56

Tab. 8: Overview of possible TLS location in the Delta Flume

5.1.3 Water Parameter

Turbidity

The need of turbid water (section 2.3.2) is essential for TLS based range measurements from water waves. With clear water and no reflecting particles inside, only a very limited FoV about 0.2 m was obtained (section 4.2.2) with the SICK and Riegl TLS devices.

In section 4.1.3 it is shown that for turbidities above 40 NTU a relative constant range standard deviation is obtained with the SICK device. Lower turbidities lead to larger scatter in the range standard deviation.

Different additives were used during experiments to guarantee for the required turbidity of the water. Mainly the additive Kaolinit ($\rho = 2.65$ g/cm³, $D50 = 20$ µm) was used. As an experiment also Magnesium powder ("Moon Dust", $\rho = 1.738$ g/cm³) was tested. Since it has a lower density it sank slower allowing for a longer measurement time. It was difficult to dissolve the magnesium powder in water, it was sticking together in larger clumps. Hence, Kaolinit is the preferred additive.

Still water, Green water, Run-up zone

It was observed in the experiments (section 3.1.3) that breaking waves could be detected from distances up to 20 m with a TLS device. Breaking waves and produced foam in the wave run-up zone of the Delta Flume will improve the reflectivity of the water surface.

The measurements in the green water with unbroken waves will be comparably difficult to obtain. Here, the turbidity must exceed 40 NTU (section 4.1.3) to enable TLS based range measurements from the water surface.

It will be even more challenging to receive a reflection from the still water surface over increasing distances.

Water depth

In section 4.1.4 the distance the laser beam travels under water before being reflected by any particle is derived. Distances between 0.01 m and 0.18 m were found. Hence, it is recommended to use water depths higher than 0.18 m to guarantee that no points from the bottom, but only from the water itself are measured.

5.2 Workflow

The set-up and the calibration of the device (determine the distance between TLS and water surface and position of zero-angle by scanning a still water surface), the recording of the experiments and the instantaneous visualization of the obtained signal is part of the measurement itself.

In a second step the recorded signal must be exported with the specified TLS software before the post processing steps to reconstruct a wave from the signal are applied. The methods suggested in section 4.1 are: transformation from polar to cartesian coordinates, geometrical filtering, definition of a FoV with 95% reflecting points, interpolation as well as temporal and spatial averaging. Finally the refraction correction is applied.

In a last step the required wave parameter (Height, Period, Length) are derived and ideally validated to single wave gauges along the flume. The obtained wave profile allows for a detailed study of the shape and its characteristics over time.

The basic workflow for TLS based range measurements from water waves is given in Fig. 37.

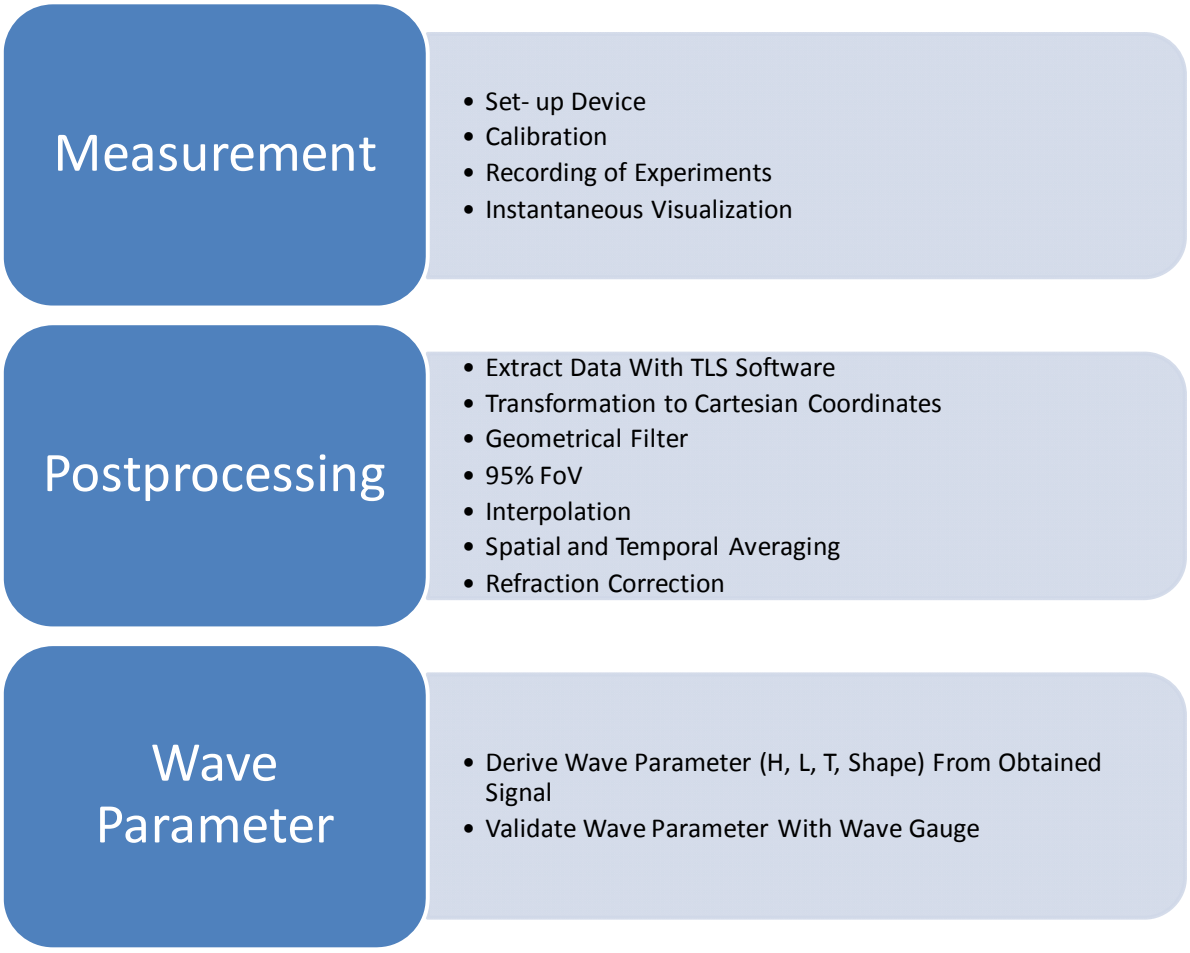

Fig. 37: Workflow TLS based range measurement from water waves

5.3 Validation Methods

It is necessary to validate the measurements of water waves, obtained with a TLS device, to prove that they are reliable and in a reasonable range. In section 5.3.1 methods are outlined to determine the still water surface as it is important for refraction correction (section 4.1.4). Also for calibration purpose a first identification of the still water surface is necessary.

In section 5.3.2 the validation of the derived wave parameters is discussed.

5.3.1 Water Surface Identification

Dry flume

A scan of the empty flume could be taken before testing. Then the flume will be watered and the water height measured manually. The distance between the scan points of the empty flume and the watered flume should be the same as the manually measured water height. The disadvantage of this method is that before each use of the TLS the flume has to be empty for cali-

bration. Unless a fixed position of the scanner is arranged, so that the distance to the bottom is the same every time.

Fixed target

Another possibility is to use a fixed target within the flume, above the water surface and within the scan line. It should be easy to recognize from the scan data. The distance between this target and the water surface could be determined manually and added to the vertical distance between target and TLS.

Object on the surface

In this case a highly reflective, floating object is placed on the water surface within the scan line. From the scan data this object will be easy to recognize since it is slightly higher than the surrounding points (the laser beam penetrates the water before being reflected by any particles). Also a change in Intensity (between the highly reflective floating object and the surrounding low reflective water particles) should be visible from the obtained scan data.

A white piece of paper was used during the experiments (section 3.2) to determine the still water surface.

5.3.2 Wave Parameter Validation

Input wave parameter

The measured wave height, length and period are compared to the input parameter of the wave maker. This gives a first and very rough validation if the measurements are in a reasonable range.

Water Wave Measurement Devices

The wave parameters derived from the TLS based range measurements from the water waves are compared to standard water wave measurement devices used in hydraulic modeling (section 2.4) at single locations along the flume. Capacitance and resistance type of wave probes (section 2.4.2) are reported to give accurate and reliable results and are therefore adequate for validation.

To prevent influences of the peak in nadir (section 4.1.2) an optimum location for the wave gauges is above 10° incidence angle (if no slant angle implemented). Locations with large incidence angles should be prevented to avoid a deteriorated signal due to an elongated footprint (Soudarissanane et al. 2009).

6 Summary and Conclusions

It is stated that a suitable and ready to use TLS based range measurement of water waves in the Delta Flume has not been applied yet. However, some important steps to reach this ultimate goal are presented in this work.

A parameter inventory identifying and summarizing the influencing parameters on TLS based range measurement of water waves was derived (section 2.7). Such a table was not available yet. The parameters were roughly divided into TLS, water and atmosphere/geometry parameter as well as combined parameters resulting from at least two of the above mentioned categories.

Available data sets from TLS based range measurements of water waves were analyzed with the focus on a quality assessment of the reconstructed wave field. A Riegl VZ-400 device (in green water of Deltares Scheldegoot flume) and a SICK LMS511 (in the wave run-up zone of Delta Flume) were found to give the most promising results (section 3.1).

Additionally, a SICK LMS511 device was applied in the small scale wave flume facility of the TU Delft (section 3.2). It was the purpose to implement a working measurement set-up, which can later be adapted to a measurement set-up in the large scale Delta Flume. Different wavelengths were visible from the reconstructed wave signal. It was considered the most promising data set and used for further analysis. The experienced problems (e.g. the peak in nadir, upwards bending of the profile edges, scatter and bias in the measurements) were analyzed for still water conditions in section 4.1 and methods to finally reconstruct the wave field were described.

First of all the coordinates were transformed from polar to cartesian, a geometrical filter applied, a 95% Field of View (FoV) defined, the obtained profile interpolated as well as temporally and spatially averaged (section 4.1.1). To correct for the upwards bending of the edges a correction method was proposed. The correction is based on the physical phenomena of refraction and a difference in velocity when the laser beam enters the water- air boundary (section 4.1.4). To correct for the peak in nadir a slant angle was suggested.

The scatter in range standard deviation was lowest for turbidities above 40 NTU (section 4.1.3). Also, the bias in range standard deviation was high for incidence angles between 0° and 10°. Hence, in an optimized measurement set-up water turbidities above 40 NTU and a slant angle of 10° were recommended.

In section 4.2.2 the analysis was extended to water wave conditions and a Field of View (FoV) with 95% reflecting points defined. For water turbidities above 40 NTU a minimum FoV of 3.2 m was present in each test. The height of the TLS above the water was 1.2 m and the according incidence angle was 53.1°. The tests were conducted for wave steepness (H/L_0) of 0.03.

The error due to parallel movement of TLS device and water wave was calculated in section 4.2.3. With a scanning frequency of 50Hz, the resulting error was typically much less than 1% related to the wavelength. Hence, the scanning frequency of 50Hz was sufficient to keep the error negligible. A SICK LMS511 device was compared to a Riegl VZ-400 device. It was found that the Riegl VZ-400 was still able to receive a signal from the water surface for larger

ranges. Hence, the Riegl VZ-400 is the preferred device for measurements in the Delta Flume with larger ranges. Also, when using the SICK LMS511 device in the green water of the Delta Flume no good results were obtained.

Although no ready to use TLS based measurement set-up for the Delta Flume was presented, the gained knowledge from section 2 to section 4 was transferred to a possible TLS based measurement set-up of water waves in the new Delta Flume. A desirable list of parameters to enable an optimized measurement in the Delta Flume was derived and presented in Tab. 9.

TLS	Scanning Frequency	50Hz
	Sampling Frequency	50 Hz
	Receiver	very sensitive
	Filter/threshold	off
	Measurement principle	pulsed ToF
	Spectral resolution	800nm - 1500nm (2500nm - 4000nm)
	TLS location	TLS 4 (section 5)
Water	Turbidity	>40 NTU
	Water depth	> 0.18m
	Surface roughness	high
Geometry	Height	27m above surface (to see one full wave)
	Location	Above area of interest
	Slant angle	10°

Tab. 9: Desirable parameter for TLS based measurement set-up of water waves in Delta Flume

7 Recommendations

TLS based range measurements of water waves in hydraulic modeling is a new measurement technique. Improvements in the choice of TLS, water and geometrical parameters are required for advanced measurements. The following recommendations are given:

- Tests in the small flume with ranges between 1m and 4m are recommended to prove the suggested refraction correction method (section 4.1.4). Finally the distance B, the laser beam travels under water, is assumed to be dependent on the water turbidity and the water turbidity might be measured using the recorded intensities of the reflected laser beam signal. Hence, a TLS setting to record the intensities of the reflected signal should be implemented. An advanced measurement set-up should include the possibility to determine the true water surface from the scan data as outlined in section (5.3.1). This way an estimation of the distance B, the laser beam travels through the water, before being reflected can be determined more accurately.
- The recorded intensities could serve to distinguish the water- land boundary, to point out foamy parts on the wave (no refraction correction here) and to increase the understanding of water reflection characteristics (whether it is a sediment particle giving the reflection or if also Raman- and Mie scattering are present). In this context it would be helpful to determine the relative size of the reflecting particle compared to the laser beam wavelength.
- The optimized footprint size of the laser beam enabling the best results for TLS based range measurements of water waves needs to be investigated.
- Although Kaolinit served well in current experiments, an optimized additive based on the size, sinking velocity, its ability to dissolve, reflection properties, safety, costs and the possibility to be removed after testing should be further investigated. It is very important for the analysis of the scan data, that the additive is equally distributed over the total length of the measured profile. An advanced additive steering approach is required for additional experiments.
- If they exist, laser beam wavelengths in the highly reflective part of the seawater spectral reflectance curves (2600nm - 4000nm) should be investigated (section 2.5.3).
- To find a TLS device suitable for the Delta Flume dimension, tests in large flume dimensions are required. Especially the laser power and the influence of an increased and elongated footprint when measuring in large flume dimensions should be investigated.
- Regarding the post processing the presented, averaging, interpolation and refraction correction methods should be adapted for wave conditions in order to create a continuous, precise and accurate signal.

8 References

Allis, M.J.; Peirson, W.L.; Banner, M.l. (2011): Application of LIDAR as a Measurement Tool for Waves. *International Offshore and Polar Engineering Conference*, Maui, Hawaii.

Alonso, J.I.S.J.; Rubio, J.M.; Martín, J.J.F.; Fernández, J.G. (2011): Comparing Time- of-Flight and Phase- Shift. The Survey of the Royal Pantheon in the Basilica of san Isidoro Léon. *International Society for Photogrammetry and Remote Sensing*, Trento.

Baltsavias, E.P. (1999): A comparison Between Photogrammetry and Laser Scanning. *ISPRS Journal of Photogrammetry and Remote Sensing*, 54.

Belmont, M.R.; Horwood, J.M.K.; Thurley, R.W.F.; Baker, J. (2006): Shallow Angle Wave Profiling LIDAR. *Journal of Atmospheric and Oceanic Technology*, 24.

Bendat, J.S. (1986): Random data. Analysis and measurements procedures. New York, USA: John Wiley & Sons., 2nd edition, revised and expanded, 566 p.

Bishop, C.T.; Donelan, M.A. (1987): Measuring Waves With Pressure Transducers. *Coastal Engineering*, 11.

Blenkinsopp, C.E.; Mole, M.A.; Turner, I.L.; Peirson, W.L. (2010): Measurements of the Time- Varying Free- Surface Profile Across the Swash Zone Obtained Using an Industrial LIDAR. *Coastal Engineering*, 57.

Blenkinsopp, C.E.; Turner, I.L.; Allis, M.J.; Peirson, W.L.; Garde, L.E. (2012): Application of LiDAR technology for Measurement of Time- Varying Free- Surface Profiles in Laboratory Wave Flume. *Coastal Engineering*, 68.

Brock, J.C.; Purkis, S.J. (2009): The Emerging Role of Lidar Remote Sensing in Coastal Research and Resource Management. *Journal of Coastal Research*, 53.

Bruckner, M.Z. (2012): Measuring Lake Turbidity Using a Secchi Disk.

Daimon, M.; Masumura, A. (2007): Measurement of the refractive index of distilled water from the near- infrared region to the ultraviolet region. *Applied Optics*, 46.

EAK (2002): Empfehlungen für Küstenschutzwerke. Heide i. Holst., Germany: *Die Küste. Archiv für Forschung und Technik an der Nord- und Ostsee*, Heft 65, Boyens & Co., 589 S.

Evans, A.J. (2010): Laser Scanning Applied to Hydraulic Modeling. International Archives of Photogrammetry, Remote Sensing and Spatial Information Sciences, Newcastle.

Fadeev, V.V.; Komitsas, M.; Reuter, R. (1999): System (complex) for Optical Monitoring of Coastal Marine Water Areas: Concept and Methods. Environmental Sensing and Applications, Munich.

Fingas, M.F.; Brown, C.E.; Mullin, J.V. (1997): Review of Oil Spill Remote Sensing. *Spill Science and Technology Bulletin*, 4.

Foote, M.; Horn, D. (2002): Using Video and GIS to Measure Two- Dimensional Water Surface Elevations in the Swash Zone. *Transactions in GIS*, 6.

Frouin, R.; Schwindling, M.; Deschamps, P.-Y. (1996): Spectral Reflectance of Sea Foam in the Visible and Near- Infrared: In Situ Measurements and Remote Sensing Implications. *Journal of Geophysical Research*, 101.

Gillespie, A.B.; Deighton, M.O.; Pike, R.B.; Watkins, R.D. (1982): A new Ultrasonic Technique for the Measurement of Liquid Level.

Guenther, G.C.; Cunningham, A.G.; LaRocque, P.e.; Reid, D.J. (2000): Meeting the Accuracy Challenge in Airborne Lidar Bathymetry.

Harry, M.; Zhang, H.; Lemckert, C.; Colleter, G. (2010): 3D Spatial Definition of a Water Surface. *Pacific/Asia Offshore Mechanics Symposium*, Busan, Korea.

Heritage, G.L.; Large, A.R.G. (2009): Laser Scanning for the Environmental Science. *Principles of 3D Laser Scanning*, Oxford.

Höfle, B.; Vetter, M.; Pfeifer, N.; Mandlburger, G.; Stätter, J. (2009): Water Surface Mapping From Airborne Laser Scanning Using Signal Intensity and Elevation Data. *Earth Surface Processes and Landforms*, §$.

Holthuijsen, L.H. (1983): Stereophotography of ocean waves. *Applied Ocean Research*, 5.

Houser, C.; Barrett, G. (2009): Bed Elevation Changes in the Upper- Swash Zone. *Journal of Coastal Research*, 56.

Hwang, P.A.; Walsh, E.J.; Krabill, W.B.; Swift, R.N.; Manizade, S.S.; Scott, J.F.; Earle, M.D. (1998): Airborne Remote Sensing Applications to Coastal Wave Research. *Journal of Geophysical Research*, 103.

Irish, J.L.; Wozencraft, J.M.; Cunningham, A.G.; Giroud, C. (2006): Nonintrusive Measurement of Ocean Waves: Lidar Wave Gauge. *Journal of Atmospheric and Oceanic Technology*, 23.

Koepke, P. (1984): Effective Reflectance of Oceanic Whitecaps. *Applied Optics*, 23.

Kusterle, T. (2007): Surf Zone Hydrodynamics.

Lange, P.A.; Jähne, B.; Tschiersch, J.; Ilmberger, I. (1982): Comparison Between an Amplitudemeasuring Wire and a Slopemeasuring Laser Water Wave Gauge. *Revie of Scientific Instruments*, 53.

Long, B.F.; Aucoin, F.; Montreuil, S.; Robitaille, V.; Charedé, R. (2010): Airborne Lidar Bathymetry Applied to Coastal Hydrodynamic Processes. *Coastal Engineering*

Maiman, T.H. (1960): Stimulated Optical Radiation in Ruby. *Nature*, 187.

Maslov, D.V.; Fadeev, V.V.; Lyashenko, A.I. (2000): A Shore- Based LIDAR for Coastal Seawater Monitoring. *EARSeL- SIG Workshop LIDAR*, Dresden.

Masselink, G.; Turner, I.; Conley, D.; Ruessink, G.; Matias, A.; Thompson, C.; Castelle, B.; Wolters, G. (2013): BARDEX II: bringing the beach to the laboratory - again! *Journal of Coastal Research*, 65.

Miche, M.R. (1944): Mouvements ondulatoires de la mer en profondeur constante ou décroissante. Paris, France: *Annales des Ponts et Chaussées*, vol. 114, no. 2, pp. 25-78.

Misra, S.K.; Thomas, M.; Kambhamettu, C.; Kirby, J.T.; Veron, F.; Brocchini, M. (2006): Estimation of Complex Air- Water Interfaces From Particle Image Velocimetry Images. *Experiments in Fluids*, 40.

Park, H.S.; Sim, J.S.; yoo, J.; Lee, D.Y. (2011): Breaking Wave Measurement Using Terrestrial LIDAR: Validation With Field Experiment on the Mallipo Beach. *Journal of Coastal Research*, 64.

Peirson, W.L. (1997): Measurement of Surface Velocities and Shears at a Wavy Air- Water Interface Using Particle Image Velocimetry. *Experiments in Fluids*, 23.

Piepmeier, J.A.; Waters, J. (2004): Analysis of Stereo Vision- Based Measurements of Laboratory Water Waves. IEEE International Geoscience and Remote Sensing Symposium, Alaska.

Raffel, M.; Willert, C.E.; Werely, S.T.; Kompenhans, J. (2007): Particle Image Velocimetry A Practical Guide.

Rees, W.G.; P.Pellika (2010): Principles of Remote Sensing. *Remote Sensing of Glaciers*, London.

Reuter, R.; Diebel, D.; Hemgstermann, T. (1993): Oceanographic Laser Remote Sensing: Measurement of Hydrographic Fronts in the German Bight and in the Northern Adriatic Sea. *International Journal of Remote Sensing*, 14.

Sadar, M. (2002): Turbidity Instrumentation- An Overview of Todays Available Technology. Turbidity and Other Sediment Surrogates Workshop, Reno.

Schimmels, S.; Santel, F.; Zielke, W.; Heipke, C. (2002): Wavescan- Automatisierte Erfassung udn Modellierung von Brandunszonen auf Basis Digitaler Bildsequenzen.

Shepherd, I.E. (1997): Wave measurement methods in laboratory experiments. *Ocean Wave Measurement and Analysis, Waves '97 Proceedings of International Symposium*, no. 3, Virginia, USA, pp. 1155-1166.

Soudarissanane, S.; Lindenbergh, R.; Menenti, M.; Teunisse, P. (2009): Incidence Angle Influence on the Quality of Terrestrial Laser Scanning Points. *isprs*.

Stansberg, C.T.; Frechou, D.; Henn, R.; Hennig, J.; Bouvy, A.; Borleteau, J.-P.; Ollivier, M.; Ran, H. (2011): Investigation of Techniques for 3D Wave Surface Measurements and Analysis. The 2nd International Conference on Advanced Model Measurement Technology for the EU Maritime Industry (AMT'11), Newcastle.

Stokes, G.G. (1880): On the Theory of Oscillatory Waves. *Mathematical and Physical Papers by Stoke*, 1.

Strybny, J.; Wegmann, H.; Santel, F. (2001): Combining Phase- Resolving Wave Models With Photogrammetric Measurement Techniques. *Ocean Waves Measurement and Analysis*, San Francisco.

Swanson, H.A.; Baldwin, H.L. (1965): A Primer on Water Quality.

Vosselmann, G.; Maas, H.G. (2010): Airborne and Terrestrial Laser Scanning. *Laser Scanning Technology*, Dunbeath.

Vousdoukas, M.I.; Wübbold, F.; Hentschel, M.; Wagner, B. (2011): Towards Autonomous Coastal Monitoring Using 3D Laser Range Scanners and Camera Vision.

Vries, S.d.; Hill, D.F.; Schipper, M.A.d.; Stive, M.J.F. (2011): Remote Sensing of Surf Zone Waves Using Stereo Imaging. *Coastal Engineering*, 58.

Wang, Y.; Mingotaud, C.; Patterson, L.K. (1991): Noncontact Monitoring of Liquid Surface Levels With a Precision of 10 Micrometers: A Simple Ultrasound Device. *Review of Scientific Instruments*, 62.

Whitlock, C.H.; Bartlett, D.S.; Gurganus, E.A. (1982): Sea Foam Reflectance and Influence on Optimum Wavelength for Remote Sensing of Ocean Aerosols. *Geophysical Research Letters*, 9, 719- 722.

Whittenbury, C.G.; Huber, E.A.; Newell, G.S. (1959): Instrument for Measuring Water Waves. *The Review of Scientific Instruments*, 30.

Williamson, M. (2010): Golden Age of Lasers. *Engineering and Technology*.

Appendices

A. Refraction Corrected Water Surface Plots

No refraction correction for Test 1 (no 95% FoV), Test 9 (no measurement), Test 20 (particles on the water) and Test 23 (no measurement) available.

Test 2 (11 NTU)

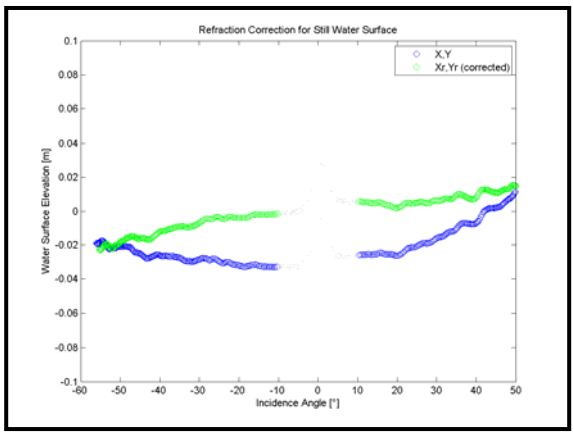

Test 3 (25 NTU)

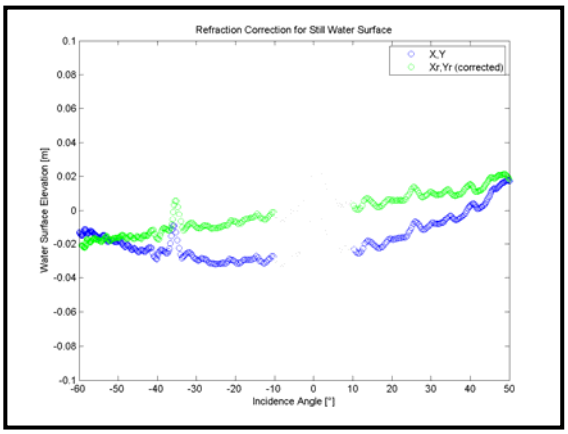

Test 4 (35 NTU)

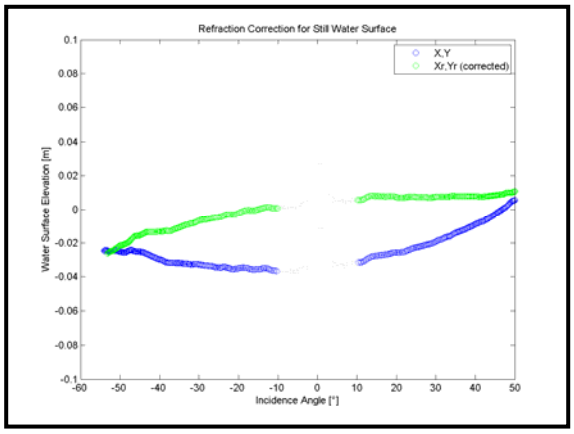

Test 5 (33 NTU)

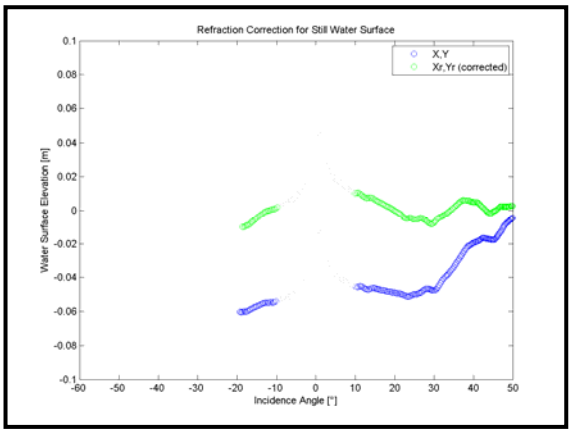

Test 6 (45 NTU)

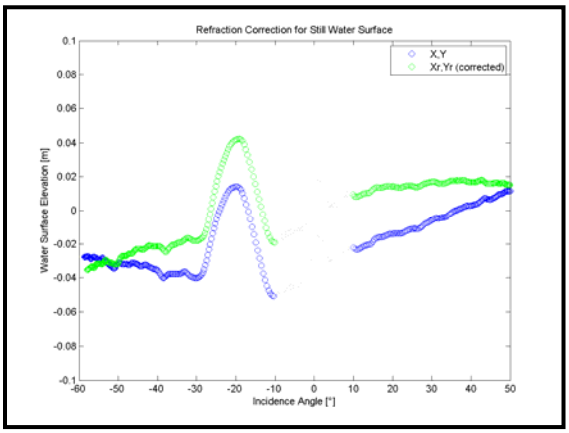

Test 7 (89 NTU)

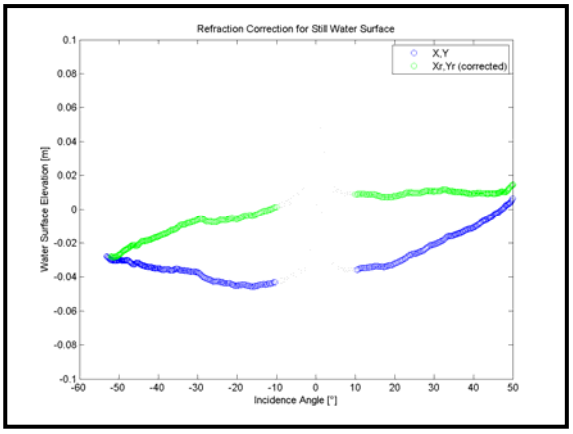

Test 8 (no turbidity available)

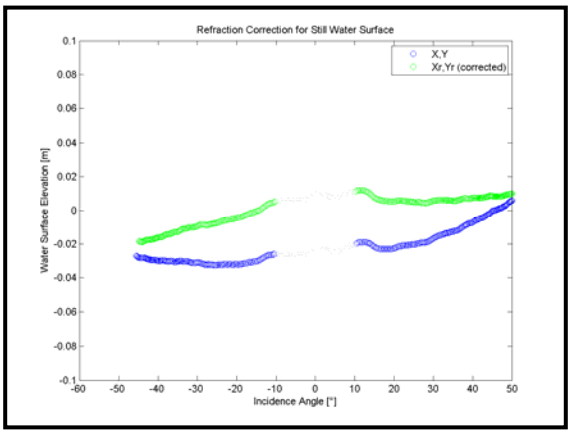

Test 10 (22 NTU)

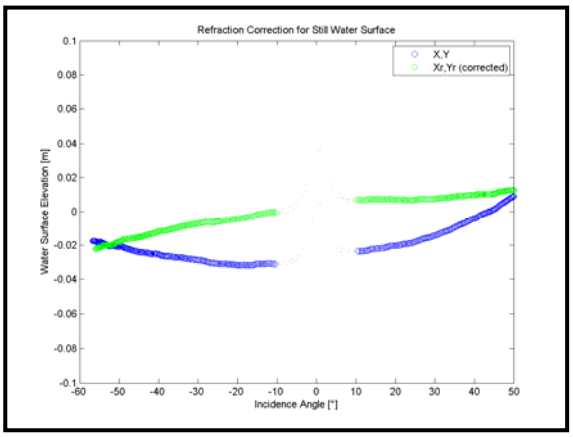

Test 11 (33 NTU)

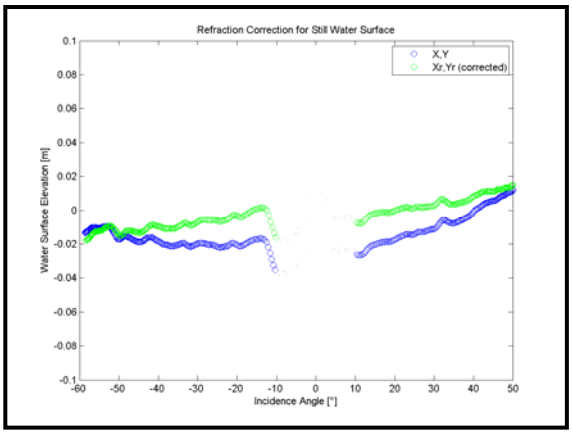

Test 12 (64 NTU)

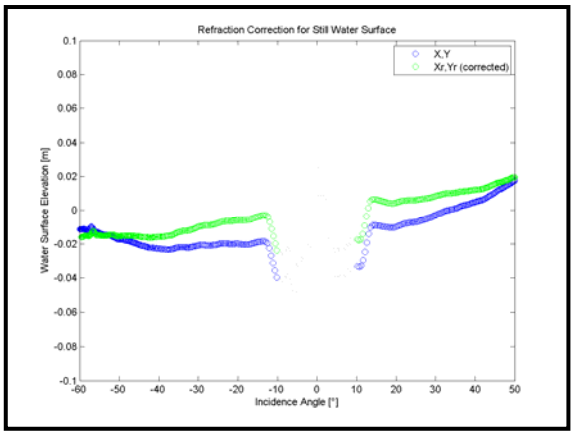

Test 13 (42 NTU)

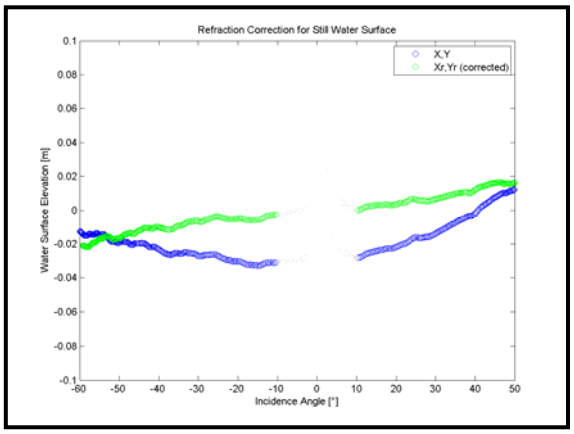

Test 14 (53 NTU)

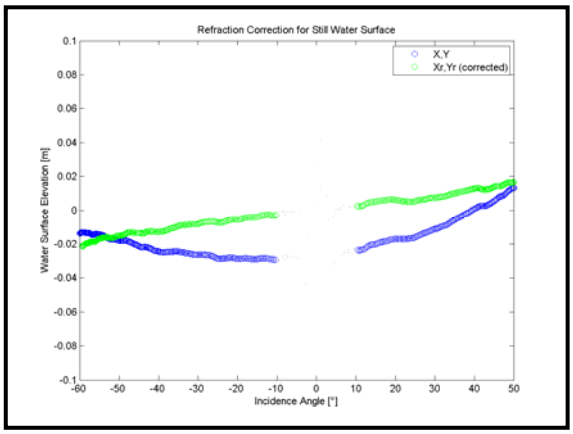

Test 15 (11 NTU)

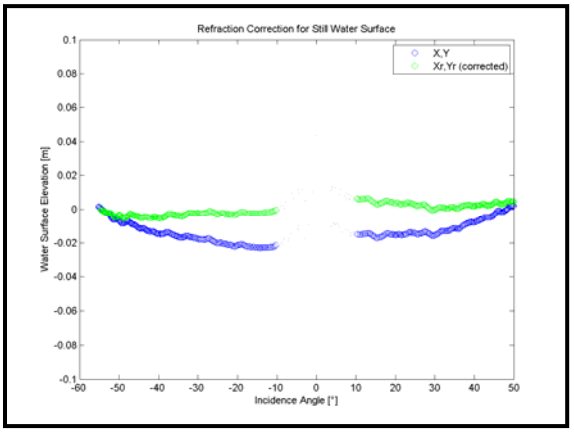

Test 16 (20 NTU)

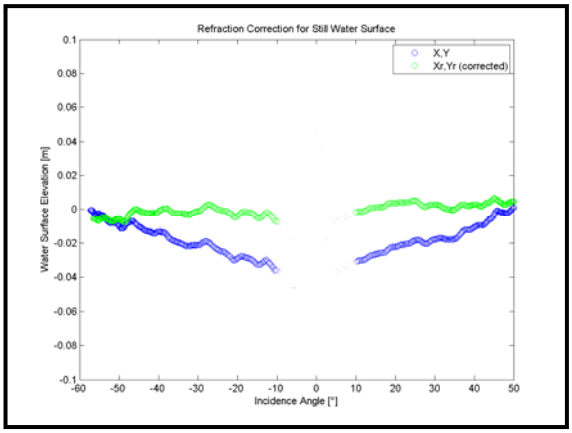

Test 17 (46 NTU)

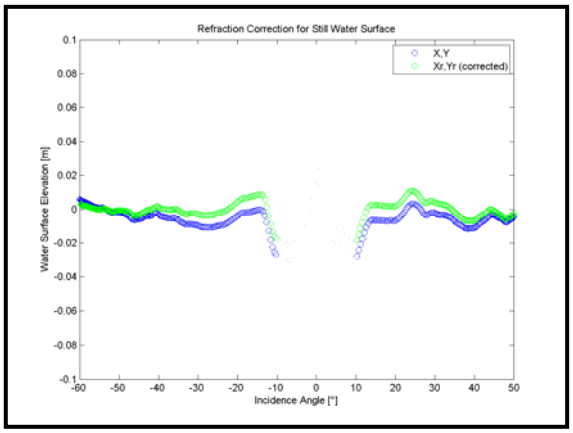

Test 18 (66 NTU)

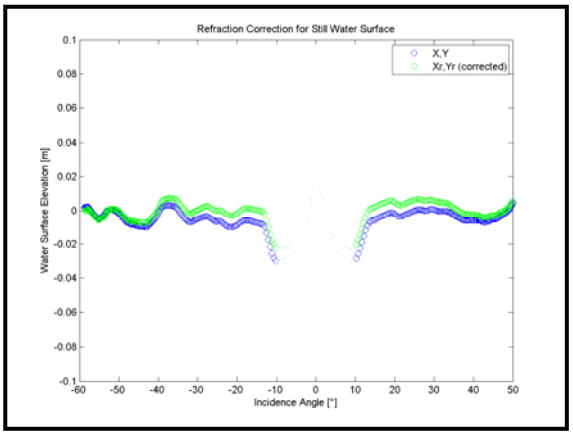

Test 19 (69 NTU)

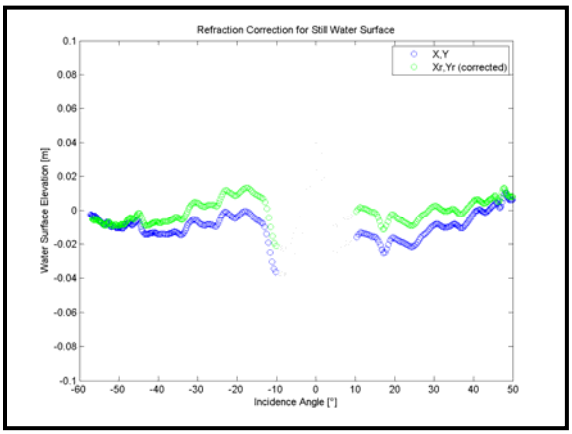

Test 21 (35 NTU)

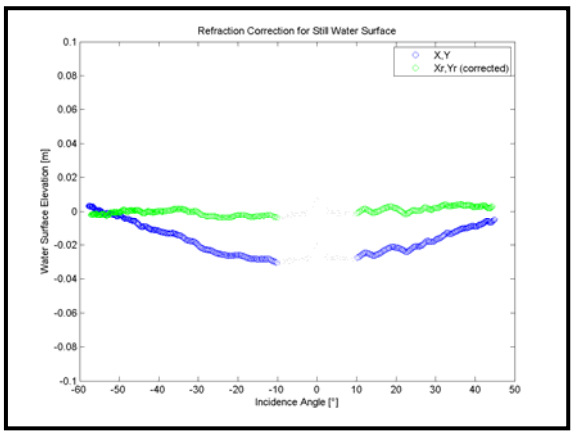

Test 22 (29 NTU)

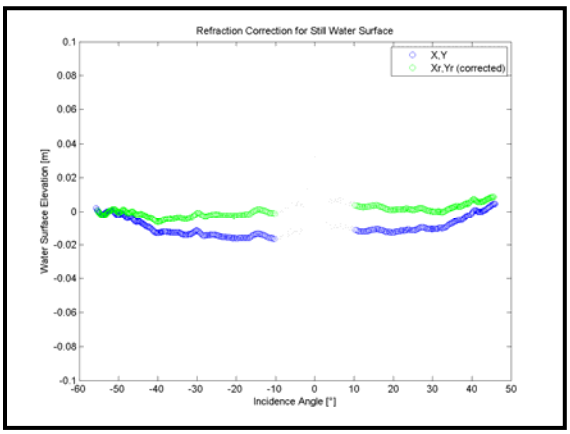

Test 24 (19 NTU)

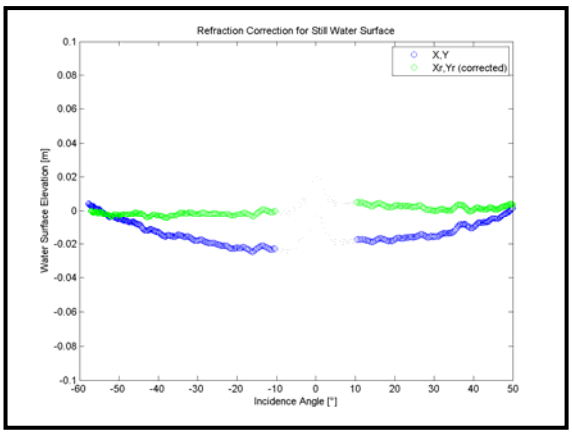

Test 25 (18 NTU)

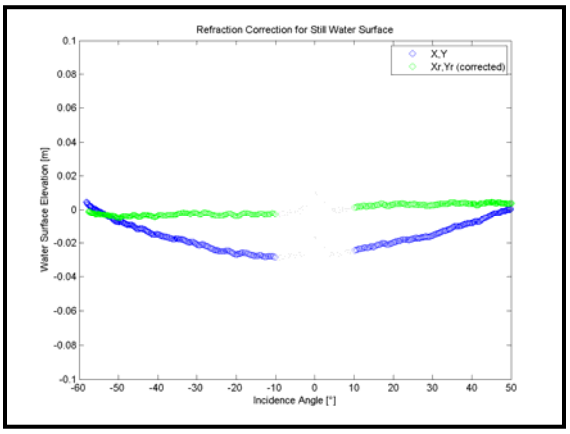

Test 26 (16 NTU)

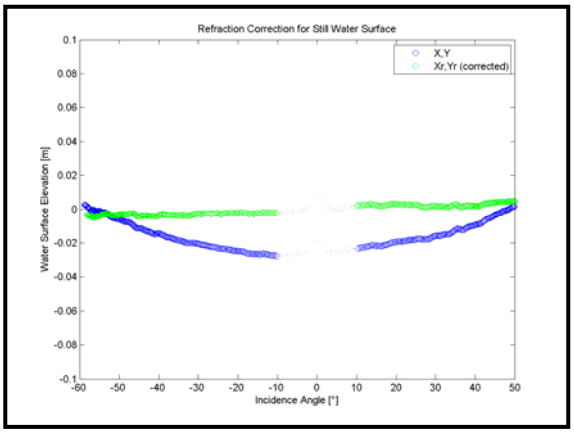

B. Technical Specification Sheets

1. SICK LMS511 Pro SR

Detailed technical data

Features

	LMS500	LMS511	LMS531
Field of application	Indoor	Outdoor	Outdoor, Security
Type	Mid Range		
Version	Lite / PRO (depending on type)		Lite
Resolution power	High Resolution	Standard Resolution, High Resolution (depending on type)	Standard Resolution
Light source	Infrared (905 nm)		
Laser class	1, eye-safe (IEC 60825-1 (2007-6))		
Field of view	190°		
Scanning frequency			
Lite	25 Hz / 35 Hz / 50 Hz / 75 Hz		25 Hz / 35 Hz / 50 Hz / 75 Hz
PRO	25 Hz / 35 Hz / 50 Hz / 75 Hz / 100 Hz		–
Angular resolution			
Lite	0.25°, 0.5°, 1°		0.25°, 0.5°, 1°
PRO	0.167°, 0.25°, 0.333°, 0.5°, 0.667°, 1°		–
Heating	–	Yes	
Operating range	0 m ... 80 m		
Max. range with 10 % reflectivity	26 m	40 m / 26 m (depending on type)	40 m
Spot size			
High Resolution	4.7 mrad	4.7 mrad	–
Standard Resolution	–	11.9 mrad	11.9 mrad
Amount of evaluated echoes			
Lite	2		2
PRO	5		–
Fog correction	No	Yes	

Performance

	LMS500	LMS511	LMS531
Response time			
Lite	≥ 13 ms		≥ 13 ms
PRO	≥ 10 ms		–
Detectable object shape	Almost any		
Systematic error			
High Resolution	± 25 mm (1 m ... 10 m) ± 35 mm (10 m ... 20 m)	± 25 mm (1 m ... 10 m) ± 35 mm (10 m ... 20 m)	–
Standard Resolution	–	± 25 mm (1 m ... 10 m) ± 35 mm (10 m ... 20 m) ± 50 mm (20 m ... 30 m)	± 25 mm (1 m ... 10 m) ± 35 mm (10 m ... 20 m) ± 50 mm (20 m ... 30 m)
Statistical error			
High Resolution	± 7 mm (1 m ... 10 m) ± 9 mm (10 m ... 20 m)	± 7 mm (1 m ... 10 m) ± 9 mm (10 m ... 20 m)	–
Standard Resolution	–	± 6 mm (1 m ... 10 m) ± 8 mm (10 m ... 20 m) ± 14 mm (20 m ... 30 m)	± 6 mm (1 m ... 10 m) ± 8 mm (10 m ... 20 m) ± 14 mm (20 m ... 30 m)
Integrated application	Field evaluation		
Number of field sets			
Lite	4 fields		4 fields
PRO	10 fields		–
Simultaneous processing cases			
Lite	4		4
PRO	10		–

Interfaces

	LMS500	LMS511	LMS531
Serial (RS-232, RS-422)	✔		
Function	Host		
Data transmission rate	9.6 kBaud ... 500 kBaud		
Ethernet	✔		
Function	Host		
Data transmission rate	10/100 Mbit		
Protocol	TCP/IP, OPC		
CAN bus	– / ✔ (depending on type)		–
Function	Outputs extension		
USB	✔, mini USB		
Function	AUX		
Data transmission rate	9.6 kBaud ... 500 kBaud		
Switching inputs			
Lite	2		2
PRO	4 (Encoder)		–
Switching outputs			
Lite	3		3 (2 relay, 1 digital)
PRO	6		–
Optical indicators	5 LEDs (additional 7-segment display)		

Mechanics/electronics

	LMS500	LMS511	LMS531
Electrical connection	1 system plug with screw terminal block	1 M12 4-pin plug-in connector	
Operating voltage	24 V DC		
Power consumption	22 W	22 W, + 43 W heating (typical)	
Housing color	Light blue (RAL 5012)	Gray (RAL 7032)	
Enclosure rating	IP 65 (EN 60529, Section 14.2.7)	IP 67 (EN 60529, Section 14.2.7)	
Protection class	III (EN 60529, Section 14.2.7)		
Weight	3.7 kg		
Dimensions	160 mm x 155 mm x 185 mm		

Ambient data

	LMS500	LMS511	LMS531
Object remission	2 % ... > 1,000 % (reflectors)		
Electromagnetic compatibility (EMC)	EN 61000-6-2:2005 / EN 61000-6-3 (2001-10)		
Vibration resistance	EN 60068-2-6 (1995-04)		
Shock resistance	EN 60068-2-27 (1993-03), EN 60068-2-29 (1993-04)		
Ambient operating temperature	0 °C ... +50 °C	–30 °C ... +50 °C	
Storage temperature	–12 °C ... +50 °C	–30 °C ... +70 °C	
Ambient light safety	70,000 lx		

Ordering information

- **Type:** Mid Range
- **Object remission:** 2 % ... > 1,000 %, reflectors

Sub product family	Field of application	Version	Resolution power	Model name	Part no.
LMS500	Indoor	Lite	High Resolution	LMS500-21000 Lite	1054153
		PRO	High Resolution	LMS500-20000 PRO	1047468
LMS511	Outdoor	Lite	Standard Resolution	LMS511-11100 Lite	1054155
			High Resolution	LMS511-21100 Lite	1054154
		PRO	Standard Resolution	LMS511-10100 PRO	1046135
			High Resolution	LMS511-20100 PRO	1047782
LMS531	Outdoor	Lite	Standard Resolution	LMS531-11100 Lite	1055376

Operating range diagram

LMS5xx High Resolution

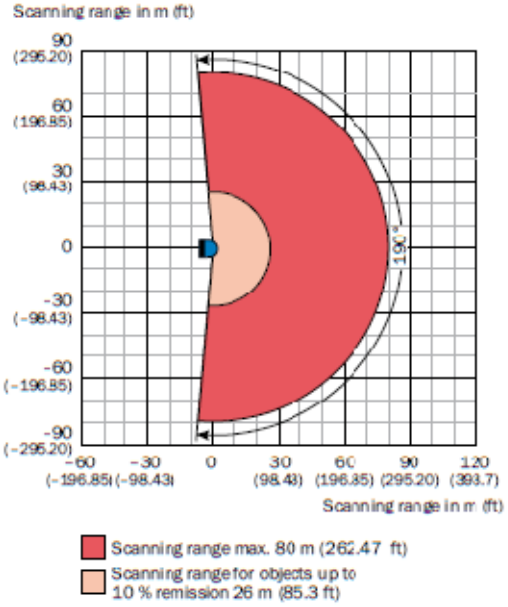

LMS5xx Standard Resolution

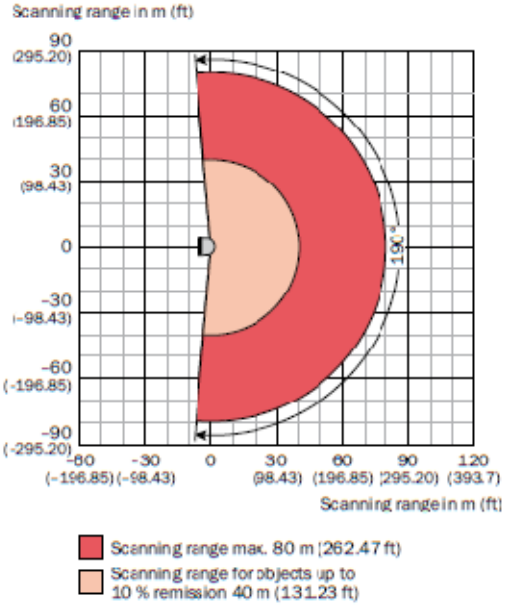

2. Riegl VZ-400

Technical Data 3D Scanner Hardware *RIEGL* VZ®-400

Laser Product Classification	Class 1 Laser Product according to IEC60825-1:2007 The following clause applies for instruments delivered into the United States: Complies with 21 CFR 1040.10 and 1040.11 except for deviations pursuant to Laser Notice No. 50, dated June 24, 2007.
Physical Data	temperature range 0°C to +40°C (operation), -10°C to +50°C (storage) protection class IP64 (dust and splash-proof) weight approx. 9.6 kg

CLASS 1 LASER PRODUCT

Range Performance[1]

	Long Range Mode	High Speed Mode
Laser PRR (Peak) [2]	100 kHz	300 kHz
Effective Measurement Rate [2]	42 000 meas./sec	122 000 meas./sec
Max. Measurement Range [3] for natural targets ρ ≥ 90% for natural targets ρ ≥ 20%	 600 m 280 m	 350 m 160 m
Max. Number of Targets per Pulse	practically unlimited [4]	
Accuracy [5] [7]	5 mm	
Precision [6] [7]	3 mm	

Minimum Range	1.5 m
Laser Wavelength	near infrared
Beam Divergence [8]	0.3 mrad

1) with online waveform processing
2) rounded values
3) Typical values for average conditions. Maximum range is specified for flat targets with size in excess of the laser beam diameter, perpendicular angle of incidence, and for atmospheric visibility of 23 km. In bright sunlight, the max. range is shorter than under an overcast sky.
4) details on request
5) Accuracy is the degree of conformity of a measured quantity to its actual (true) value.
6) Precision, also called reproducibility or repeatability, is the degree to which further measurements show the same result.
7) One sigma @ 100 m range under *RIEGL* test conditions.
8) 0.3 mrad correspond to 30 mm increase of beamwidth per 100 m of range.

Scan Performance

	Vertical (Line) Scan	Horizontal (Frame) Scan
Scan Angle Range	total 100° (+60° / -40°)	max. 360°
Scanning Mechanism	rotating multi-facet mirror	rotating head
Scan Speed	3 lines/sec to 120 lines/sec	0°/sec to 60°/sec [10]
Angular Stepwidth Δ ϑ (vertical), Δ φ (horizontal)	0.0024° ≤ Δ ϑ ≤ 0.288° [9]	0.0024° ≤ Δ φ ≤ 0.5° [9]
Angle Measurement Resolution	between consecutive laser shots better 0.0005° (1.8 arcsec)	between consecutive scan lines better 0.0005° (1.8 arcsec)

Inclination Sensors	integrated, for vertical scanner setup position, details see page 2
GPS receiver	integrated, L1 antenna
Compass	optional, for vertical scanner setup position, details see page 2
Internal Sync Timer	integrated real-time synchronized time stamping of scan data
Scan Sync (optional)	scanner rotation synchronization

9) selectable
10) frame scan can be disabled, providing 2D operation

Max. Measurement Range

The following conditions are assumed:
Flat target larger than footprint of laser beam, perpendicular angle of incidence, average brightness

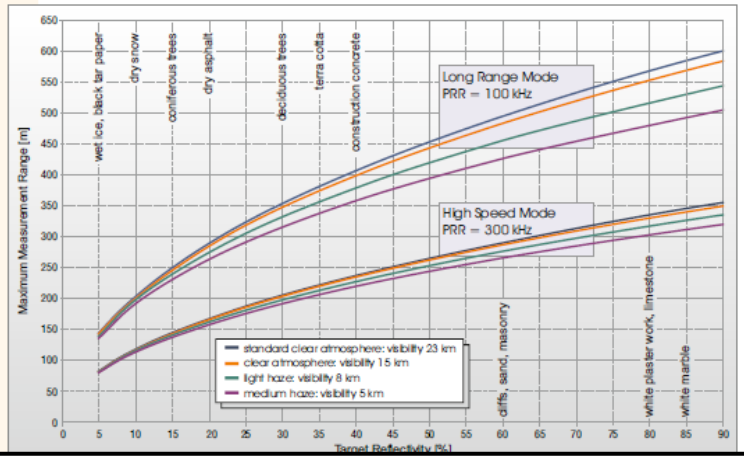

3. Faro Photon 120

Specifications

Ranging unit
Unambiguity interval: 153.49m (503.58ft)
Range[2]: 0.6m - 153m indoor or outdoor with low ambient light on 90% reflective surface, 0.6m - 120m in outdoor cloudy environments on 90% reflective surface
Range (Photon 20[2]): 0.6m - 20m on >2% matt reflective surface
Range resolution: 0.07mm
Measurement speed: 122,000 / 244,000 / 488,000 / 976,000 points/sec
Systematical distance error: ±2mm at 25m
Repeatability: noise compressed[3] / raw data
@10m: 0.4mm/0.8mm rms @ 90% refl. | 0.7mm/1.4mm rms @ 10% refl.
@25m: 0.5mm/1.0mm rms @ 90% refl. | 1.35mm/2.7mm rms @ 10% refl.

Deflection unit
Vertical field of view: 320°
Horizontal field of view: 360°
Vertical resolution: 0.009° (40,000 3D pixel on 360°)
Horizontal resolution: 0.00076° (470,000 3D pixel on 360°)
Angular resolution (hor./vert.): ±0.009°
Max. vertical scan speed: 2,880 rpm

Laser (Optical transmitter)
Laserpower (cw Ø): 20 mW (Laser class 3R)
Wavelength: 785 nm
Beam divergence: Typical 0.16 mrad (0.009°)
Beam diameter at exit: 3.3 mm, circular

Handling of data
Internal PC: Intel Celeron-M 600MHz, 512 MB RAM, 80 GB HD
Data storage: Local: on internal hard disk drive (for most resolutions)
Remote: via Ethernet on external PC or laptop
Scanner control: via Ethernet or WLAN by PC or PDA, on local network, internet or independent operation

[1] All specifications for range and accuracy apply to the Photon 120 unless otherwise noted.
*[2] **Depends on ambient light**, which can act as a source of noise. Bright sunshine may shorten the actual range of the scanner to lesser distances. Measured on a non moving orthogonal 90%/10% reflectivity reference paper in averaging mode.*
[3] Noise compression algorithm.
More details upon request at www.faro.com
Subject to change without prior notice.

General

Power supply voltage: 24 V DC (Battery pack or AC converter)
Power consumption: ~60 W
Ambient temperature: 5° - 40° C
Humidity: Non condensing
Inclination sensor: Accuracy 0.02°; Resolution 0.001°; Range ±15°
Weight: 14.5 kg (31.97lb)

Size (LxWxH): 410 mm x 160 mm x 280 mm
Maintenance calibration: Once a year
Exchange modules: Distance sensor / mirror axis / PC
Georeferencing: Yes
Cable connector: Located in scanner mount
Parallax-free: Yes

SOPAS Software Manual for Use of SICK LMS511 Pro

Installation of SOPAS

- Find on www.mysick.com the latest version of SOPAS software
- Download exe and start installation
- Choose for typical set-up
- Choose for launch SOPAS and install SDDs (SOPAS Device Description)

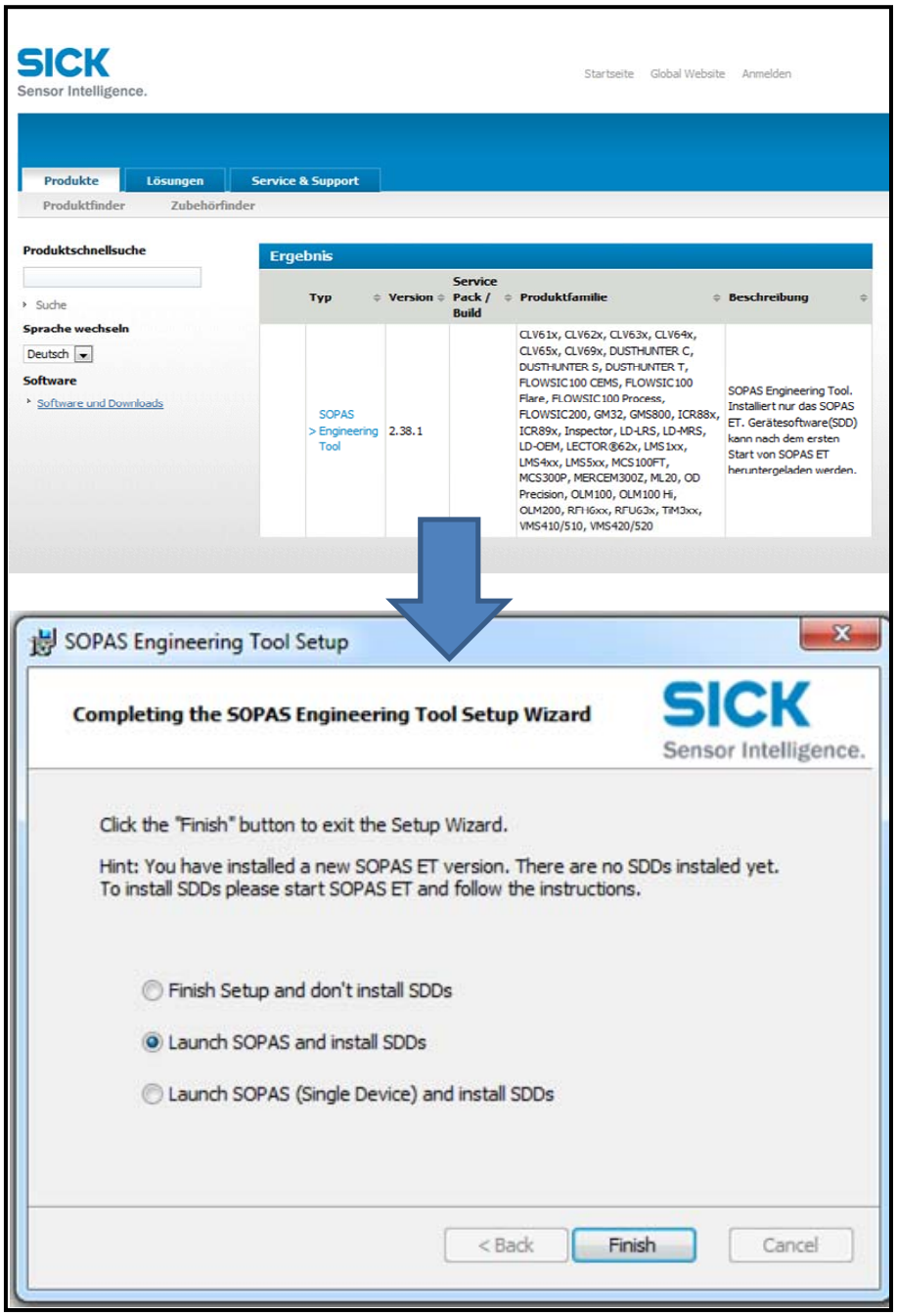

- Being asked to download SDD files click yes
- Choose the appropriate SDD file (in case of SICK LMS511 Pro SR the correct files are highlighted in red circle)

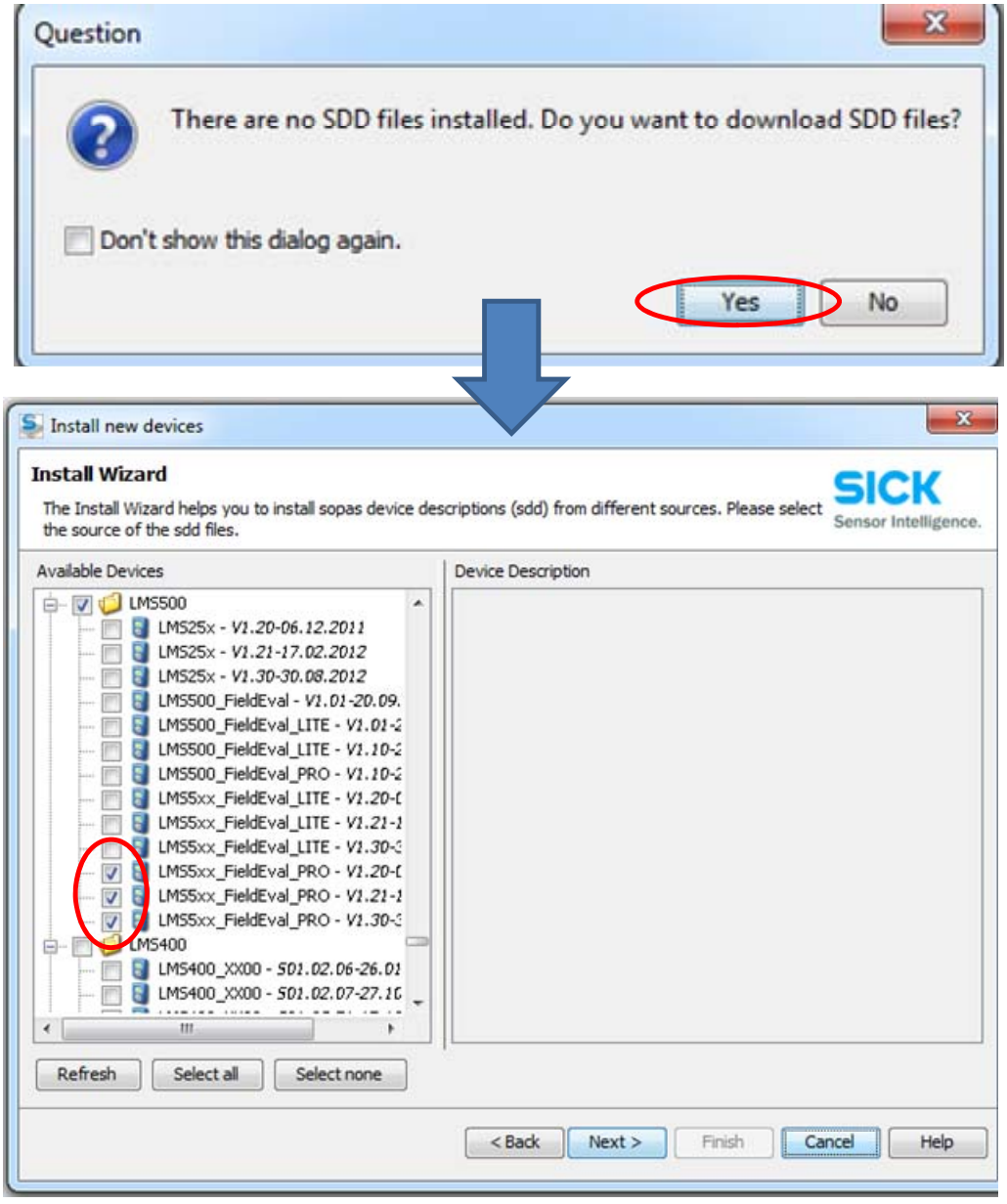

Scanning with SOPAS

- When opening SOPAS you are asked to either connect to device, create a new project, open existing project or open last project. In our case create a new project is chosen.

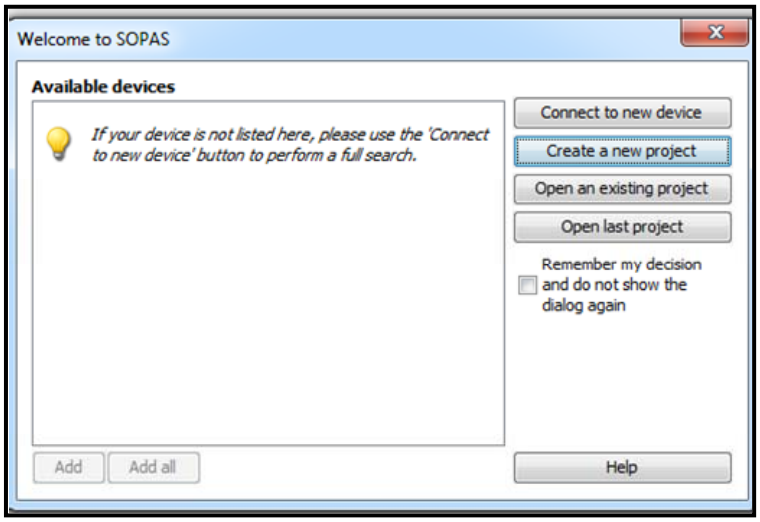

- Open the header "Device catalog" (red circle) and with drag and drop move the appropriate SDD in the project tree
- The latest SDD version for the SICK LMS511 is used

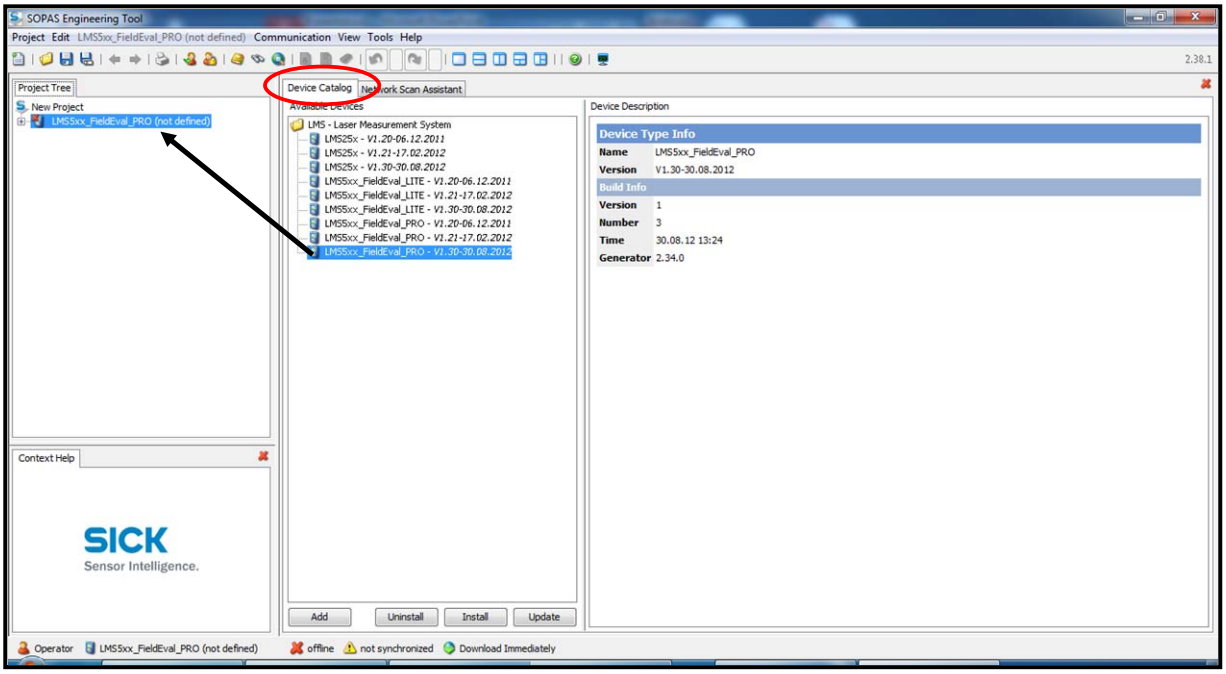

- Connect the Scanner to your laptop and click on network scan (lower red circle) to automatically search for connected devices
- In some cases it is necessary to synchronize the IP address of scanner and laptop
- Sometimes it was also necessary to right click on the SDD in the project tree and enter the command "Go Online" (upper red circle) to be able to connect to device and start the measurements

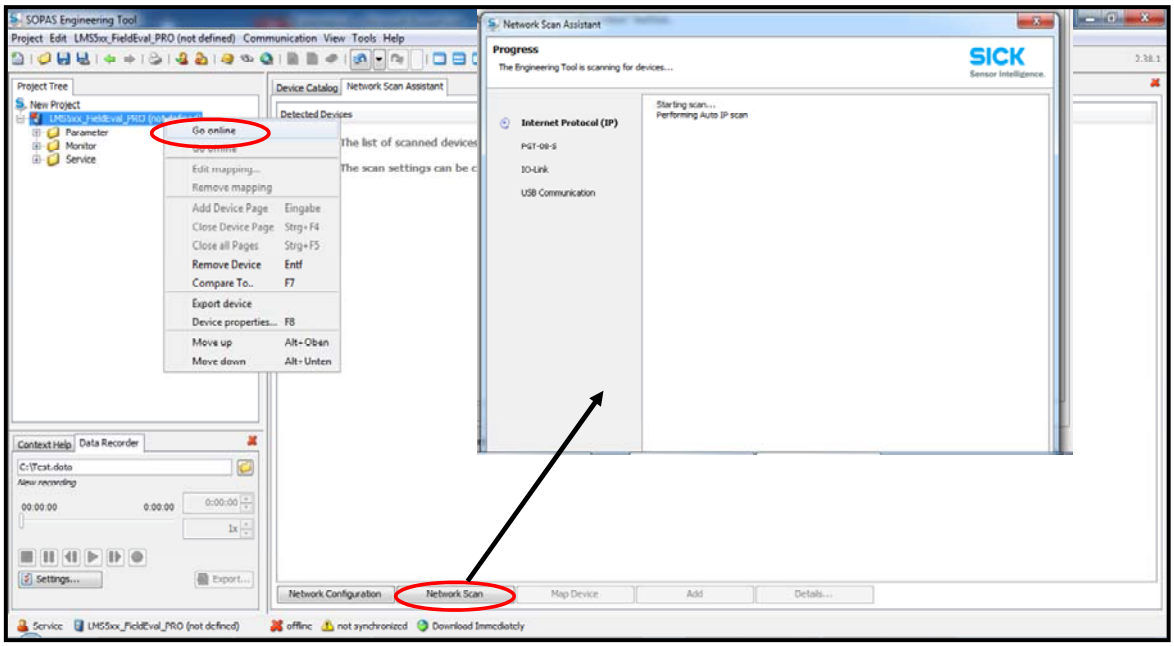

- Open Tools and click on "Login device". The Userlevel is "Service" and the password "servicelevel"
- Click on "Data Recorder" to open the recording platform in the lower left corner

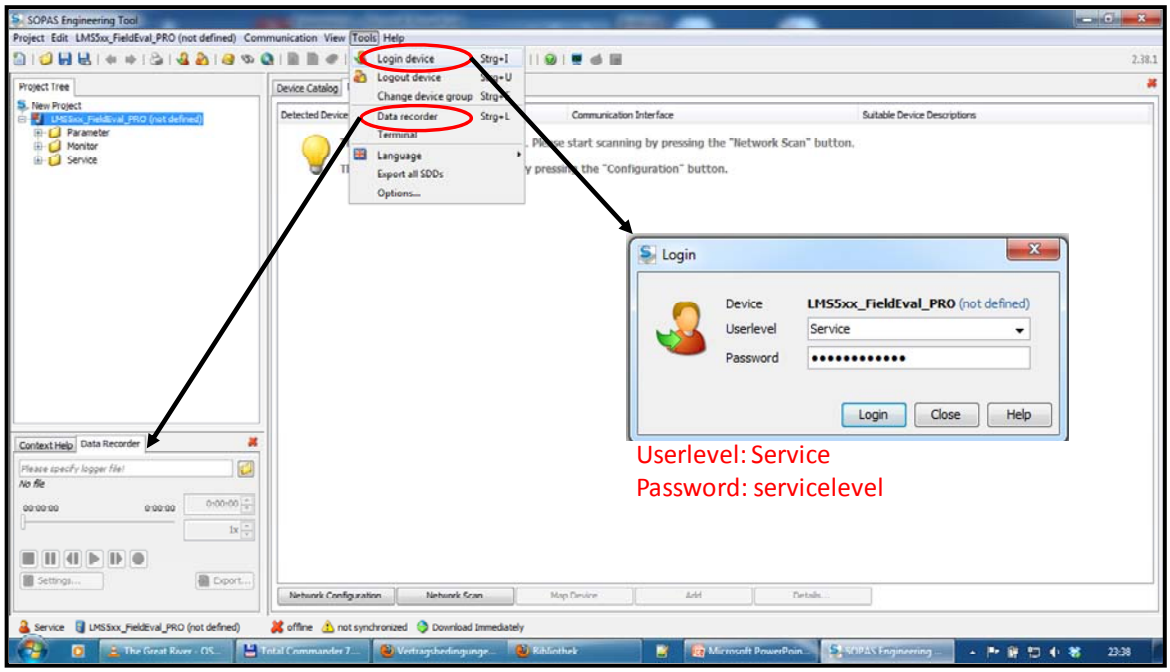

- In the project tree set scanning frequency/ angular resolution under "Basic Settings"
- Switch off the fog filter and chose for an echo (in our case most of the time first echo used) under "Filter"
- Determine a predefined scanning area under "Data Processing"
- With "Scan View" you can instantaneously visualize the measurements

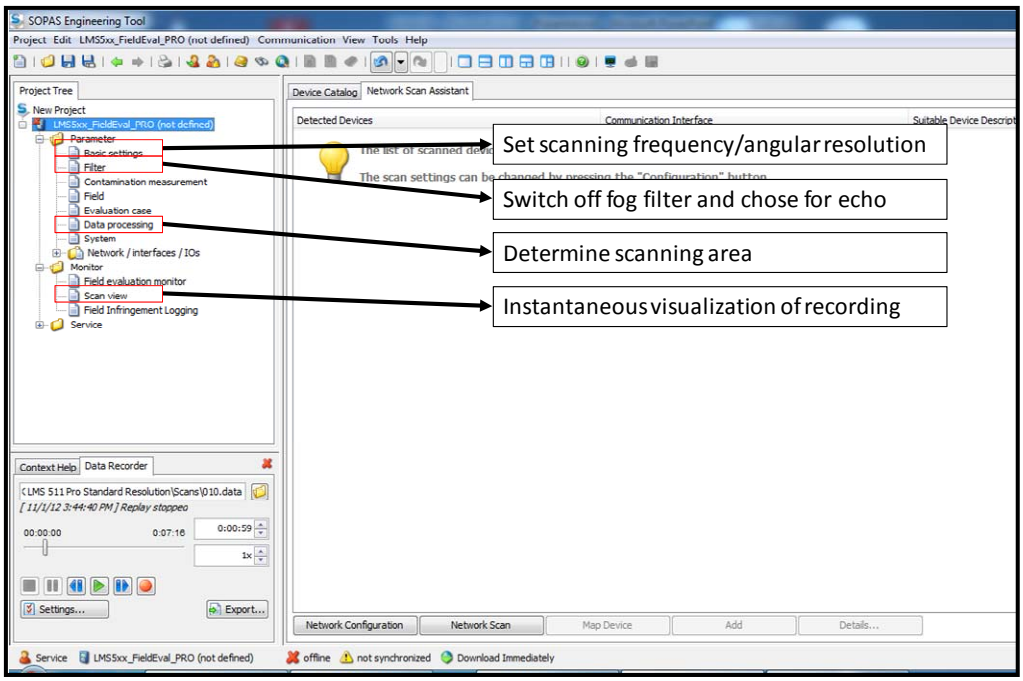

- Click on "Settings" in the data recorder. Here you can choose for "ScanDataMonitor" to record the measured ranges (no intensities)
- Synchronize sampling rate and scanning rate in the same box
- Specify a file location where the test should be saved
- Start the measurement by clicking on the red button
- Stop the recording by clicking on the blue stop button, the measurement is saved

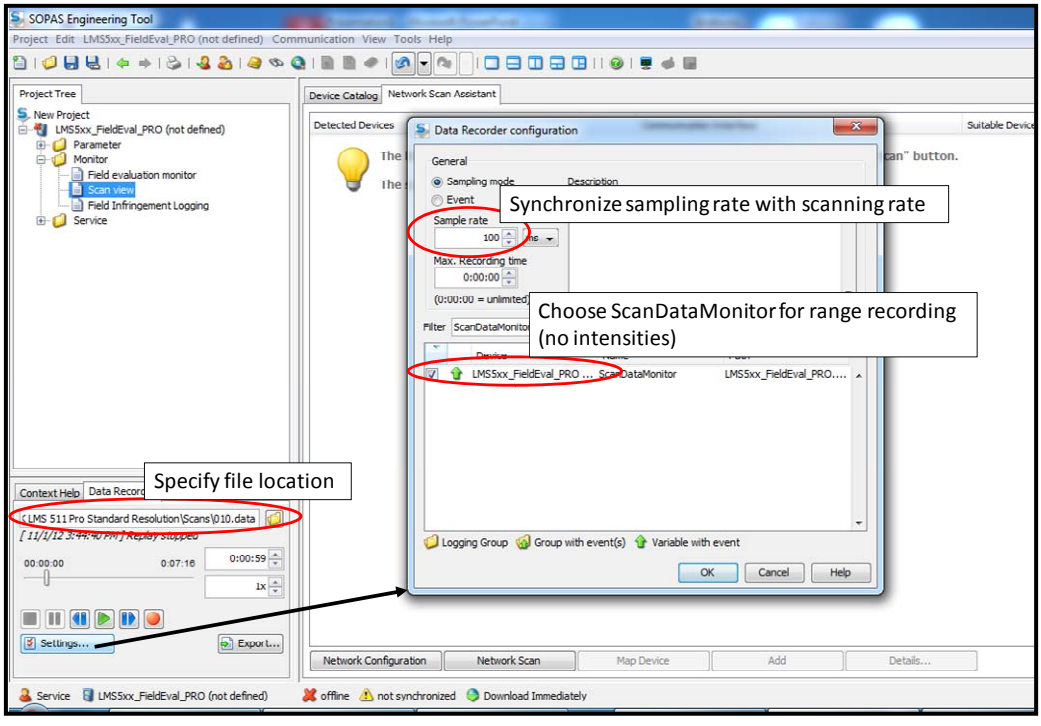

- you can have a look at the measurement by loading the requested file and click on play
- Open the Field evaluation monitor and switch on the two buttons in the red circle

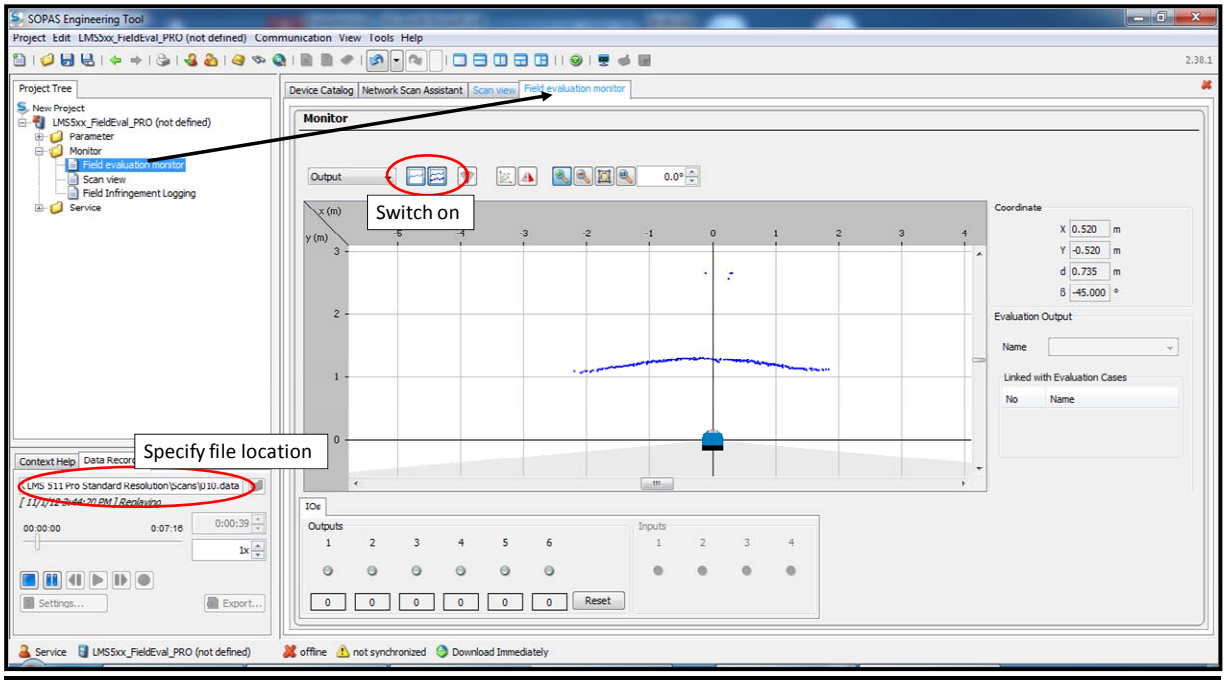

- Export the measurements by clicking on "Export" in the Data Recorder and specify the variable or a timeframe for export
- Then specify a file extension (mostly csv file used, because xls not large enough)

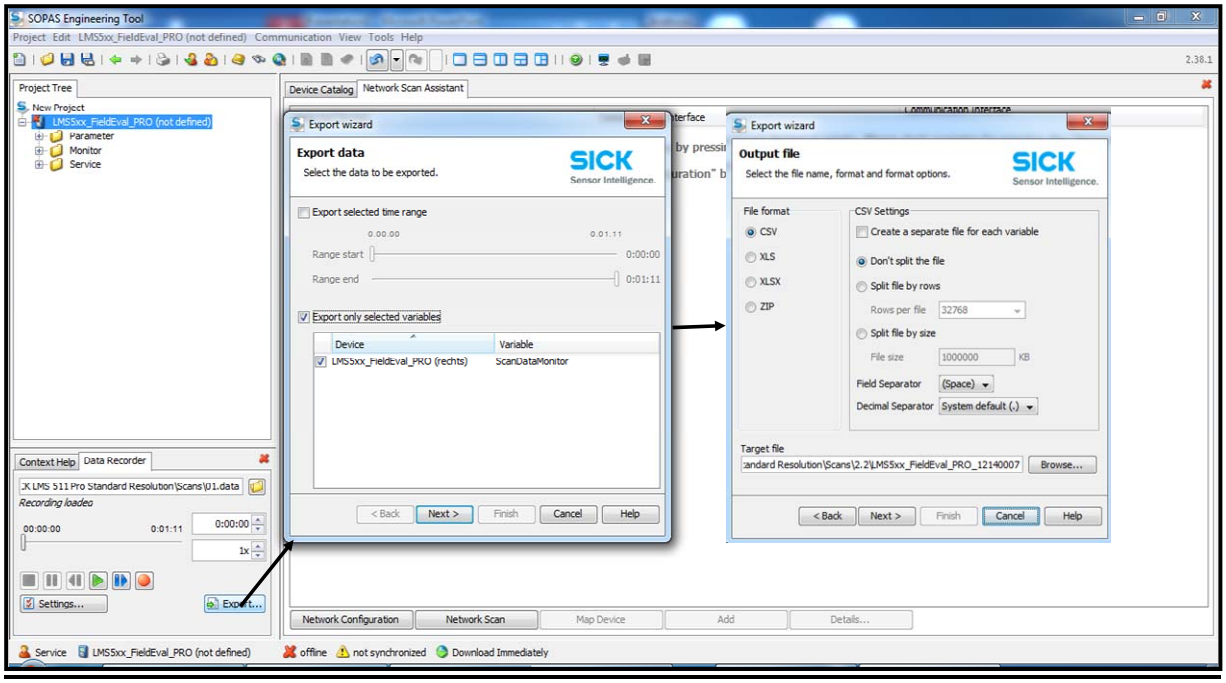

Eidesstattliche Erklärung

Ich erkläre hiermit an Eides statt, dass ich die vorstehende Masterarbeit selbstständig angefertigt und die benutzten Hilfsmittle sowie die befragten Personen und Institutionen vollständig angegeben habe.

Braunschweig, den 30.04.2013

Maximilian Streicher